

## 7. Storm Surges Generated by Extra-Tropical Cyclones – Case Studies

### 7.1 North America

Earlier we mentioned that there appears to have been a decrease in the frequency of tropical cyclones (TC's) during the second half of the 20<sup>th</sup> century. For the frequency of extra-tropical cyclones (ETC's) the opposite might be true as can be seen from Fig. 7.1.

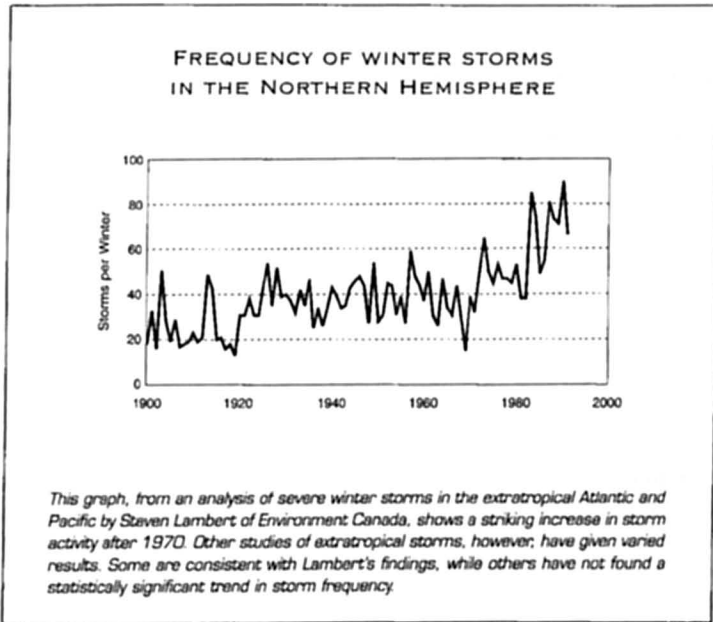


Fig. 7.1: Frequency of winter storms in the Northern Hemisphere (LAMBERT, 1995)

BODE and HARDY (1997) made some interesting observations on the development of research in storm surge modelling (SSM). We quote a few sentences below from their work.

“The storm surge phenomenon has long been characterised by a geographic divide. Surges tend to be associated either with mid-latitude storms or, often more disastrously with tropical cyclones. This divide has also extended, somewhat artificially into the modelling area. The efforts of various modelling groups are usually concentrated in one geographic region or the other. This separation of effort is reflected in recent research, in which many of the noteworthy developments have occurred in Europe, leading to the development of operational mid-latitude operational storm surge warning systems.

However, little corresponding development appears to have been supported in recent times for hurricane surge prediction. Presumably, this is a reflection of the magnitude and difficulty of the problem, but also of relative funding levels allocated for such purposes. A logical starting point is the review of HEAPS (1983), which concentrated on midlatitude storm surges. At that stage, European models have advanced to the point where NWP (Numerical

Weather Prediction) models of National Meteorological Services were being coupled to storm surges models to provide routine operational storm surge forecasts.

The foremost requirement for SSM is an accurate wind field model and the divide between the midlatitude and tropical cases is most pronounced here. Midlatitude models take their wind (and pressure) fields from operational NWP models, which generally perform well. (Although exceptions arise, such as the great storm of 1987 in U. K. for which forecasts largely failed.

### 7.1.1 Errors in the Specification of Wind Fields

CARDONE et al. (1980) discussed errors in the techniques, which are generally in use for the specification of wind fields for ETC's. They make the important point that the accuracy of specifications of extrapolated marine surface winds is limited basically by the sparsity of observations of surface wind and sea-level pressure from ships rather than by intrinsic shortcomings in the technique of analysis. However, it should be noted that during these past two decades subsequent to 1980 when CARDONE et al. (1980), published their paper, there is progressively less reliance on ships for marine winds and more reliance on ocean buoys and remote sensing through satellites.

According to these authors, three basic methods are available for elaborating surface marine wind fields in historical storms: (a) Use of parametric wind models (b) Objective analysis and (c) Direct Kinematic analysis. Parametric wind models have been successfully applied for tropical cyclones, but are not appropriate for the complex patterns of surface winds associated with ETC's.

Objective analysis methods were developed in the 1960's to satisfy the need for fast production, in real time, of fields of meteorological variables on grids for use in numerical forecast models. Objective analysis schemes for surface marine wind fields usually include (1) an initial guess at the surface wind on a regular grid, (2) a method for automatically screening a collection of wind reports from ships to eliminate highly discrepant and presumably erroneous winds, and (3) a method for blending the ship reports into the initial guess. Such schemes usually exploit the relation between the surface marine wind and the local pressure gradient by calculating the initial-guess winds from a marine sea-level pressure field, which in turn derives from an objective analysis of surface pressure measurements on land and sea.

CARDONE (1969) described an objective analysis scheme that included the application of a model of the wind profile in the planetary boundary layer (PBL) that related the surface marine wind velocity to the local pressure gradient, the air/sea temperature difference, and the atmospheric thermal advection. Winds derived from the PBL model, and reduced to a standard height of 19.5 m, are blended with winds from ship reports after the latter are ranked in order of presumed accuracy.

Kinematic analysis is a tedious, time-consuming, entirely manual procedure that only experienced analysts can execute successfully. The basic steps involved are (1) plot all synoptic ship reports on suitable meteorological base maps for the entire storm event, (2) standardize wind measurements to 19.5 m, using a marine-wind-profile model for measured winds where the ship's anemometer height is on file, and using the Beaufort conversion procedure described earlier for estimated winds, (3) identify and reject erroneous and unrepresentative reports so far as possible, (4) construct a continuity chart containing the "solution" for the storm event in terms of the movement of major discontinuities, singularities and other features of the surface wind field, and (5) construct streamlines and isotachs.

### 7.1.2 Great Lakes

Several finite element models are now available which have been referred to in chapter three. Here we will give a few more general references for the application of the impulse response method for storm surge computation, see SIMONS and SCHERTZER (1989). This method will be successful for those situations where there is linear dynamics for storm surge generation.

SCHWAB (1982) showed that this method could be inverted to provide an estimate of Overlake wind fields from observations of water level fluctuations around the shore of the lake. HAMBLIN (1987) provided a review of lake Erie storm surge computation techniques.

SCHWAB and LYNN (1987) developed a simple computer program for estimating the maximum and minimum storm surge amplitudes for the Great Lakes. The user has to provide a mean lakewater level, a wind speed and a wind direction. The program then lists maximum and minimum expected water level at several points on the shoreline of the selected area. The program covers the U. S. Shoreline only, (not Canadian) separately for the following water bodies: Lake Ontario, Central and Eastern Lake Erie, Western Lake Erie, Lake St. Clair, Lake Huron, Saginaw Bay, the Eastern Shore of Lake Michigan, the western shore of Lake Michigan, Green Bay and Lake Superior.

### 7.1.3 East Coast of Canada

PARKES et al. (1997) discussed storm surge events in the Maritime (eastern) provinces of Canada. MURTY et al. (1994) reviewed storm surges in Canadian waters. GRAY et al. (1984) used numerical models to simulate storm surges on the Nova Scotia Coast (Table 7.1). Fig. 7.2 shows the area of study. Here CMC refers to the Canadian Meteorological Center Fig. 7.3 shows the grid used in the numerical model.

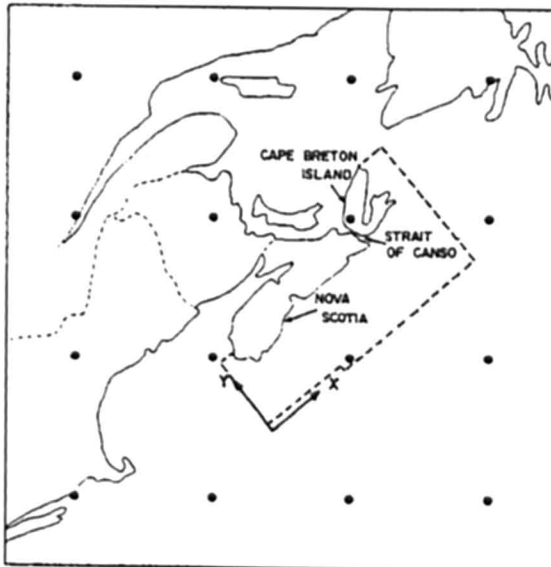


Fig. 7.2: Orientation of CMC and storm surge model grids showing the array of 4 x 4 CMC grid points (dots), and the computational domain of the storm surge model (dashed line) (GRAY et al., 1984)

Table 7.1: Comparison between computed and observed amplitudes (cm) and phases (deg.) of the  $M_2$  tide (observed values taken from the Admiralty Tide Tables, except where indicated) (GRAY et al., 1984)

Grid Numbers*	Port	Observed		Computed	
		Amp.	Phase	Amp.	Phase
1	Yarmouth	163	63	163	63
2	Lower E. Pubnico	127	39	134	38
3	Sea Island	120	52	127	43
4	Clark Harbour	106	27	110	22
5	Lockeport	70	359	71	357
6	Liverpool	65	353	64	355
7	Lunenburg	60	353	64	354
8	Boutilier Point	64	352	66	353
9	Halifax	62	352	64	353
10	Jeddore Harbour	65	352	64	352
11	Sheet Harbour	62	347	64	351
12	Sonora	62	351	64	349
13	Isaac's Harbour	56	352	65	348
14	White Head	54	347	63	347
15	Canso Harbour	59	347	62	346
16	Point Tupper	59	344	66	345
17	Cannes	56	351	62	344
18	Loudibourg	50	344	52	344
19	North Sydney	38	355	43	350
20	Dingwall	27	11	32	354
21	St. Paul Island	31	6	31	6
22	Sable Island	52	352	57	350
23	T1**	48	351	48	353
24	1.2.23	49	350	50	354
25	T21**	49	357	48	355

\* See Fig. 7.21

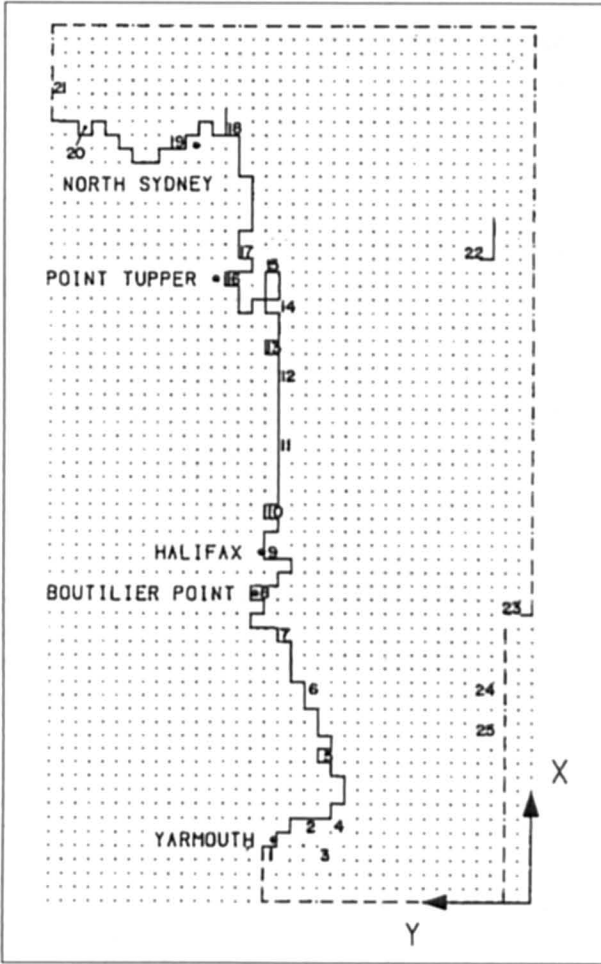


Fig. 7.3: Nova Scotia storm surge grid showing the coastline (solid line) and open – sea radiating boundary (dashed line). Numbers indicate the tidal stations listed in Table 7.1 (GRAY et al., 1984)

Fig. 7.4 shows the track of the Ground Hog Day storm of February 1976. The sea-level pressure map for 2<sup>nd</sup> February 1976 is shown in Fig. 7.5. Figs. 7.6 and 7.7 respectively show the wind stress computed on two grid spacings.

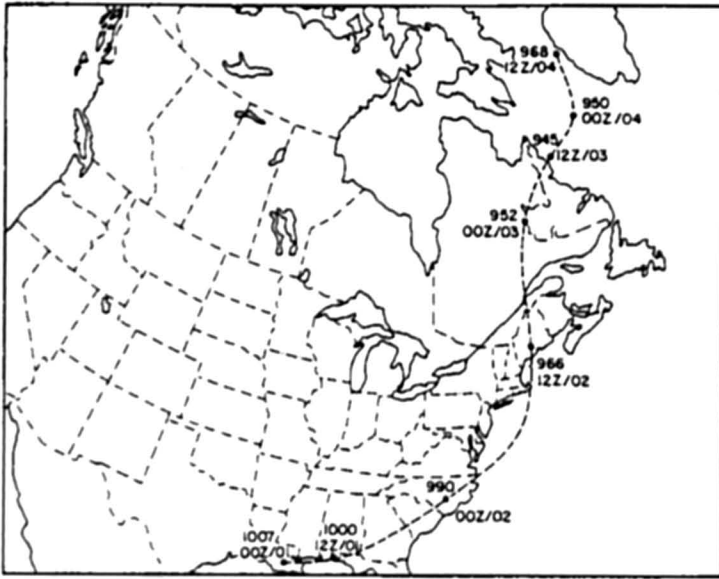


Fig. 7.4: Observed track and central sea-level pressures (mb) of the low center from 0000 GMT 1 February (00Z/01) to 1200 GMT 4 February (12 Z/04) 1976 (GRAY et al., 1984)

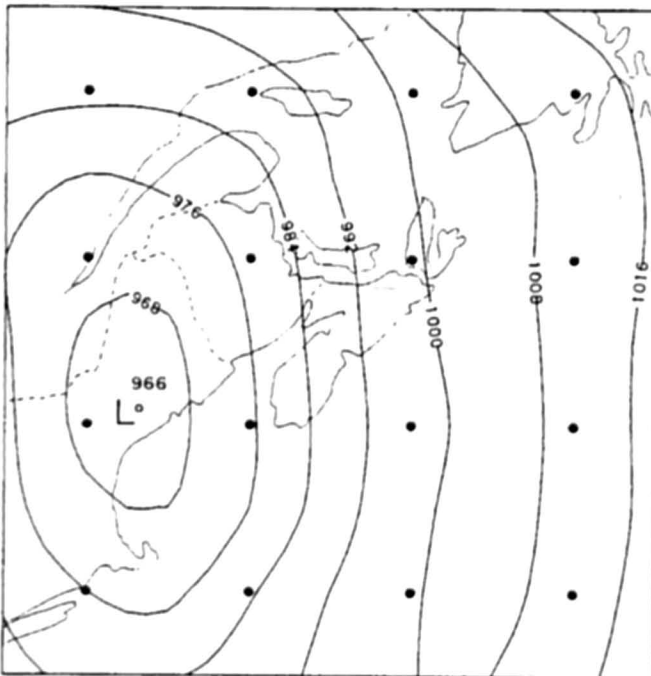


Fig. 7.5: Sea-level pressures (mb) at 1200 GMT 2 February 1976 (GRAY et al., 1984)

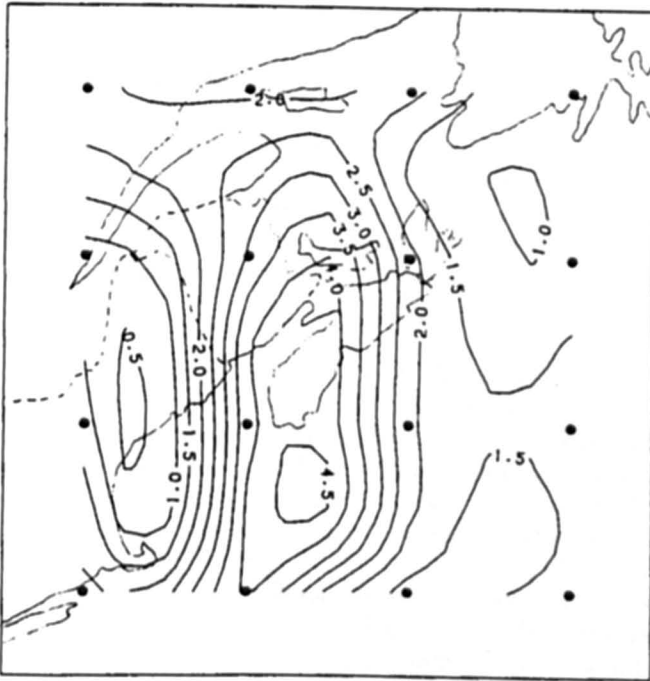


Fig. 7.6: Wind stress (Pa) at 1200 GMT 2 February 1976 computed from subjectively analysed sea-level pressures (190-km grid spacing) (GRAY et al., 1984)



Fig. 7.7: Wind stress (Pa) at 1200 GMT 2 February 1976 computed from CMC analyzed 1000-mb heights (38-km grid spacing) (GRAY et al., 1984)

The model is designed to be run, using CMC (Canadian Meteorological Center) prognostic data. The model incorporates a quadratic bottom friction term and is capable of including advective, topographic and tidal effects. It can simulate a moving land-sea boundary approximately.

The model is applied to the East Coast of Nova Scotia for the "Ground Hog Day" storm of February 1976. Meteorological forcing is calculated using subjectively analysed sea-level pressures. Away from open boundaries, the agreement with observed surge residuals is generally good. However, the results are less satisfactory near the boundaries. CMC meteorological data are found to underestimate the surface wind stress during this period.

## 7.2 South America

The Rio de la Plata estuary is located on the Atlantic Coast of South America, with the cities of Buenos Aires (Argentina) and Montevideo (Uruguay) along its shores (O'CONNOR, 1991). The length of the estuary is about 270 km and its width varies from about 230 km at its mouth to 25 km at its head where the Parana and Uruguay rivers meet. The depth of the estuary at its mouth is 20 m.

GAGLIARDINI et al. (1984) divided the estuary into three regions: (a) Upper region (Playahonda) leads from the river delta and is less than 5 m deep (b) Intermediate region stretches from Buenos Aires to Montevideo and has several shallow banks (c) the outer region is wide and extends to the ocean. Here the continental shelf has a width of about 200 km.

The tidal range in the estuary is about 2 m. Storm surges due to south easterly winds from a stationary cyclone over the estuary can generate storm surges with amplitudes greater than 3 m. Historically, surges up to 4 m in amplitude have occurred over periods of several hours to several days.

The largest surges are along the coast of Argentina near Buenos Aires. This is due to the shallowing and narrowing of the estuary, the long fetch over which the wind acts on the water surface and the effect of the Coriolis Force (O'CONNOR, 1991). According to BALAY (1959) surges with amplitudes greater than 3 m have occurred in the years - 1914, 1922, 1923, 1940, 1958 and 1959. During the 27-28 July 1958 event, the flood depths were 3 to 4 m along the Buenos Aires shore for 100 km, but there was little flooding along the coast of Uruguay.

On the other hand during the storm of 10-12 July 1923, southerly winds lasted two days and surges up to 6 m in amplitude occurred on the coast of Uruguay, east of Montevideo. O'CONNOR (1991) numerically simulated the tides and storm surges in Rio de la Plata estuary and his results agreed reasonably well with those shown in Fig. 7.8.

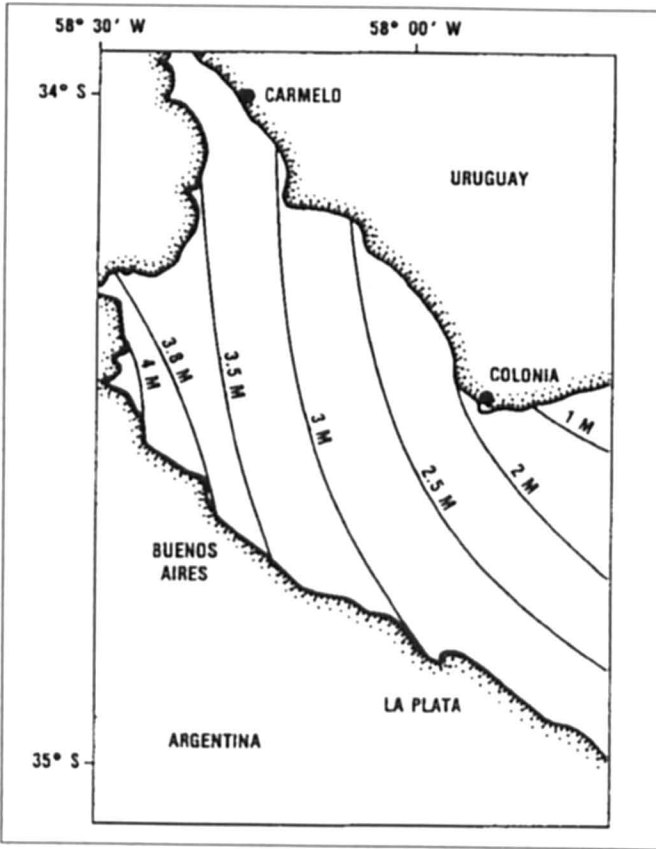


Fig. 7.8: The sea level in meters at the time of maximum surge, 27 July 1958 (BALAY, 1959)

### 7.3 Storm Surges in Europe

In section 5.1.2 the meteorological problems associated with storm surges in European waters were introduced. Here, case studies of storm surges in several water bodies in Europe and environs will be considered.

#### 7.3.1 North Sea

The North Sea is a border sea of the Atlantic. The oscillation of the Atlantic effects the North Sea from the north through the channel. The shape of the basin, the depth and coriolis force influence the tide. The tide runs along the Scottish and English coastline with a mean tidal range of 4.20 m at Aberdeen and 7.20 m at Immingham and reaches the Dutch coast after crossing the Strait of Dover. There the tidal range increases from 1.50 m at Den Helder (135 cm at Texel) to 2.28 m at Borkum and 3.00 m at Cuxhaven, is the same till Pellworm and decreases from there to the Danish coast with 1.83 m at Sylt and 1.70 m at Rømø. The tidal range increases again from the islands to the continental coast.

The counterclockwise rotation of the tide can be seen in the progression of a storm surge from Aberdeen over Southend, Dover, Newhaven Hoek van Holland, Cuxhaven to Bergen. Fig. 7.9A shows the surge profiles along the western side of the North Sea during January 6–10, 1949, beginning at Aberdeen and ending at Newhaven. The surge profiles along the eastern boundary of the North Sea during the same period are given in Fig. 7.9B. One can see first a counterclockwise progression of the disturbance with about the same propagation velocity as that of the diurnal tide (Fig. 7.10). The interaction between the tide and surge appears to be small (note that in the Thames Estuary the tide-surge interaction is significant). Second, one can see the progression of the surge height, which rises from Aberdeen to Southend and falls in the Strait of Dover from Dover to Newhaven. The increase of water level height at Grimsby, Kings Lynn and London Bridge is influenced by the topography of the locations of these gauges in an estuary or small basin like the Wash. But in general it can be stated that there is a level increase, because at Felixstone and Dover it is higher than at Hartlepool. In this storm event at the eastern boundary of the North Sea the water level increases a little from the Dutch coast to the German coast till Cuxhaven and decreases from there to Norway (Bergen). As the storm surge of April 2–6, 1973, DAVIES and FLATHER (1977) compared the calculated and observed surges at five locations along the south and west coasts of the North Sea, which confirm this. A change of the wind direction can modify this development at the eastern boundary of the North Sea.

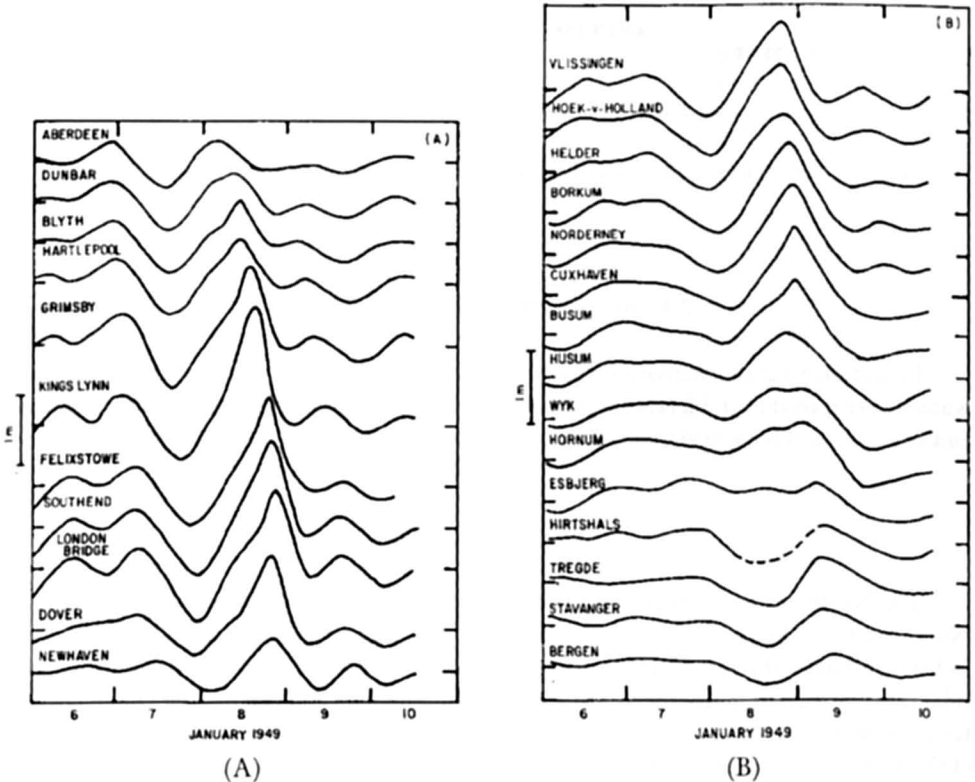


Fig. 7.9: Storm surge profiles at stations along the (A) western boundary of the North Sea and the (B) eastern boundary of the North Sea during January 6–10, 1949 (CHARNOCK and CREASE, 1957)

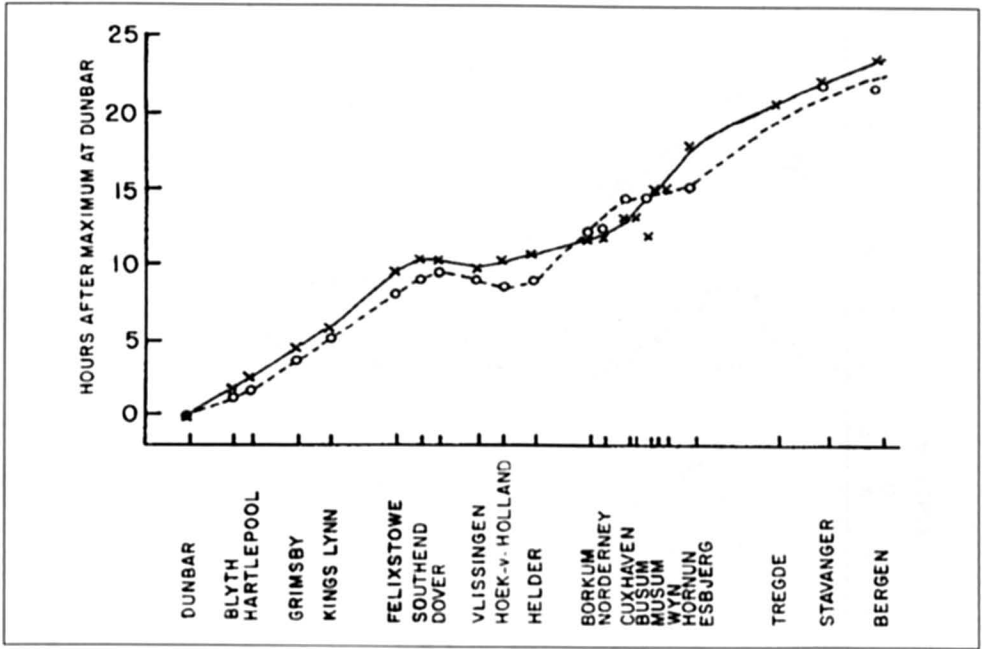


Fig. 7.10: Progression of storm surge and diurnal tide around the North Sea (CHARNOCK and CREASE, 1957)

During the storm surge on January 31–February 1, 1953 the situation at the southeastern and eastern boundary of the North sea was different to the situation on January 6–10, 1949. The track of the storm that produced this major surge is shown in chapter 5, Fig. 5.28. This depression caused a wind situation over the North Sea that produced very high storm surge levels at the British coast with rising level from Tyne over Immingham and Southend to London Bridge and falling levels to Dover and Newhaven (Fig. 7.12a & b.). Afterwards however, the surge reaches Ostende not with a lower level than in Dover; the level increased and reached a level there which was higher than at the British coast. At the German coast the high water level has become lower. A clear decrease of the water level can be seen from Esbjerg to Hornstholm (Denmark).

The horizontal distribution of the storm surge amplitudes during three different periods is summarized in Fig. 7.13. Maximum amplitudes up to 3 m occurred at the Belgian and Netherlands coasts. Amplitudes up to 2.5 m occurred at the coast of France, whereas amplitudes up to 2 m were found in the German Bight. At the Danish coast the maximum amplitudes were about 1 m. So the general principle has been lost since the wind direction and the surge do not increase anymore from the Dutch to the German coast. It must be stated that each location has its special wind direction in which the maximum surge can occur.

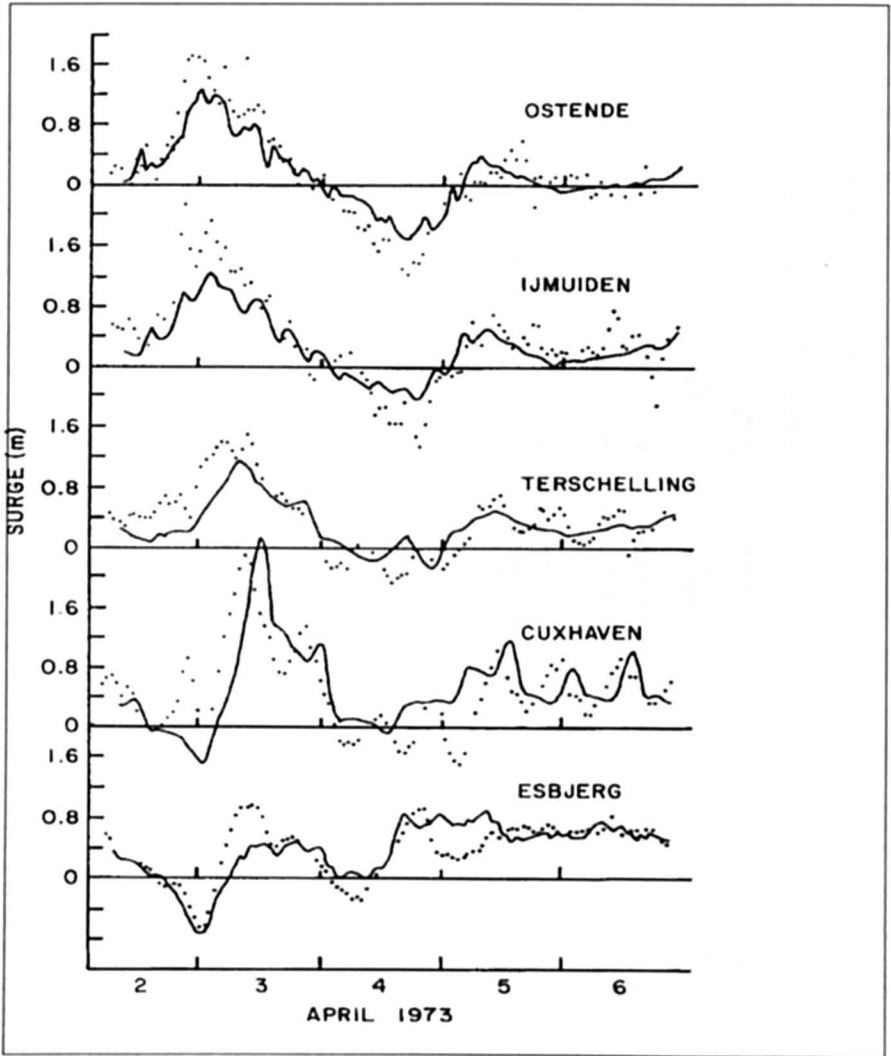


Fig. 7.11: Computed (solid line) and observed (dotted line) storm surges at five locations on the south and west coasts of the North Sea during April 2-6, 1973 (DAVIES and FLATHER, 1977)

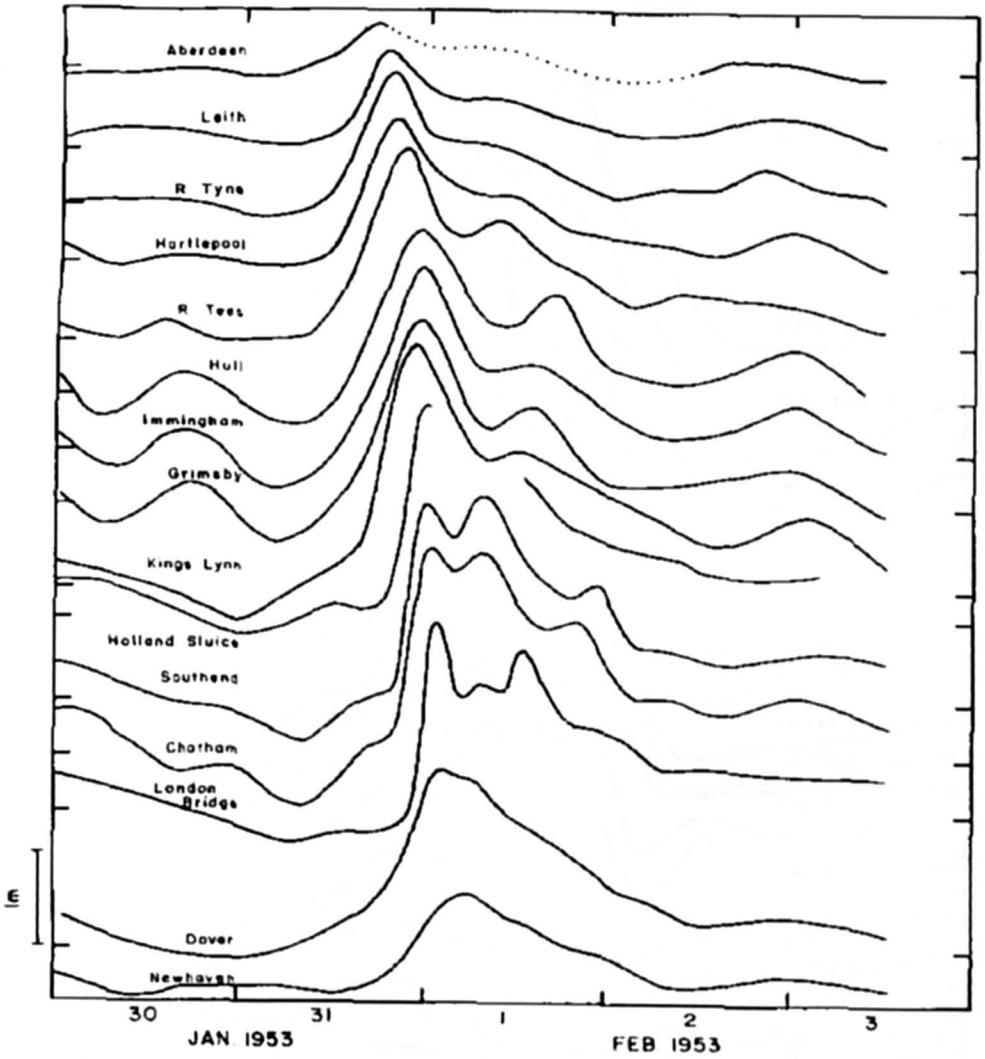


Fig. 7.12a: Storm surges at various locations around the North Sea during January 30–February 3, 1953 (ROSSITER, 1954)

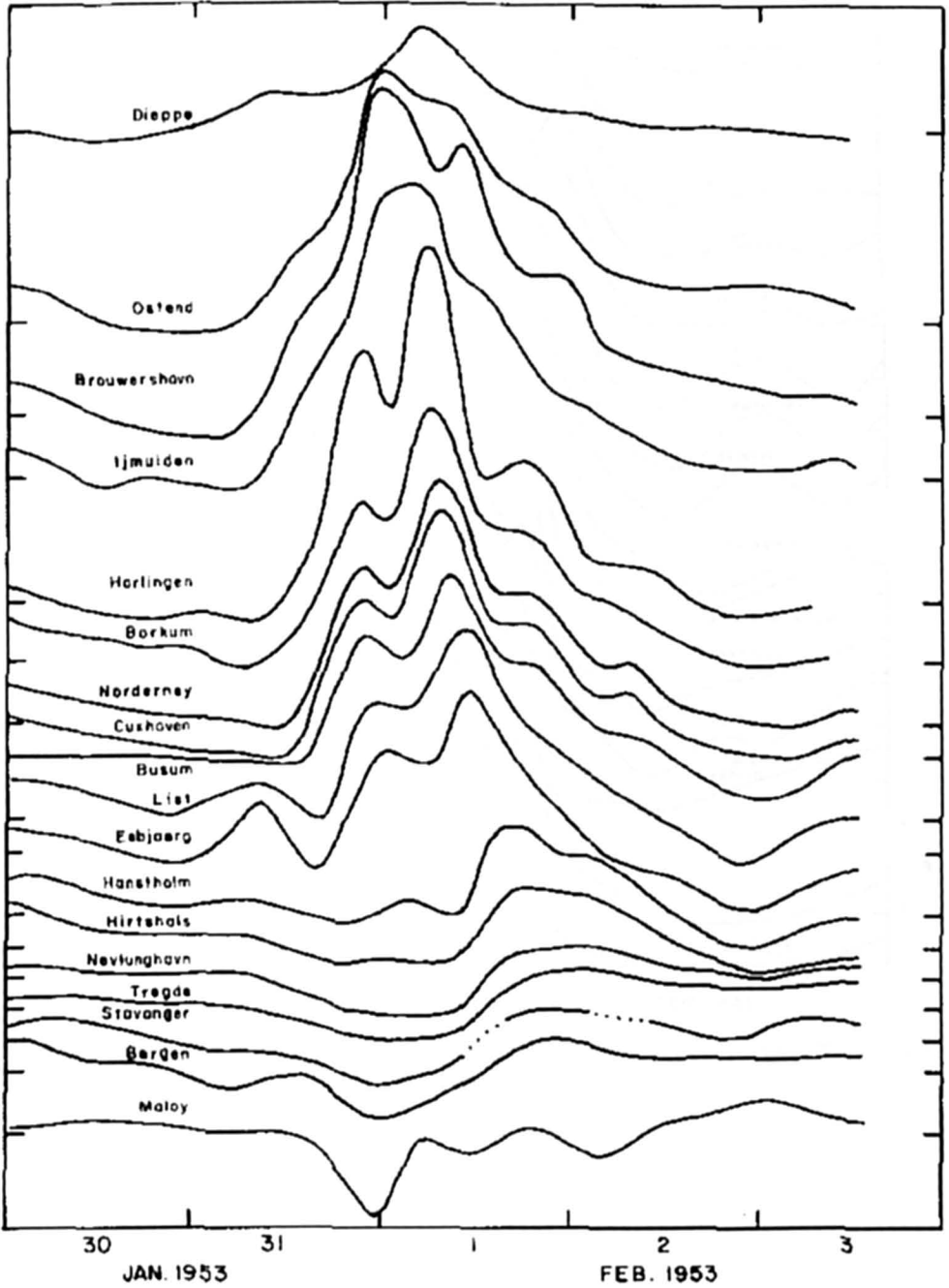


Fig. 7.12b: Storm surges at various locations around the North Sea during January 30–February 3, 1953 (ROSSITER, 1954)

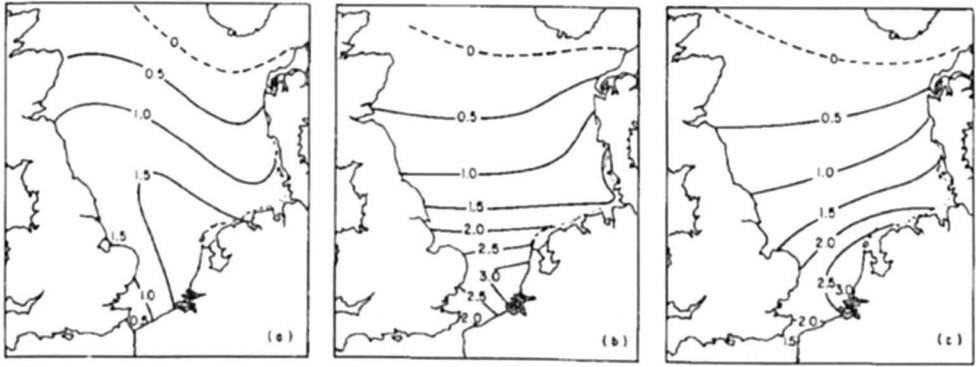


Fig. 7.13: Distribution of storm surge amplitudes (meters) in the North Sea during January 31–February 1, 1953, at (a) 18:00 (GMT) on January 31, (b) 00:00 (GMT) on February 1, and (c) 06:00 (GMT) on February 1

As described before in the English Channel the storm surge heights become smaller. The propagation of the surge through the English Channel from the North Sea is shown in Fig. 7.14.

BOWDEN (1957) mentioned that, in the southern part of the North Sea, the greatest elevation tends to occur along a line from Harwich to Flushing. The surface then slopes downward towards the Strait of Dover due to the flow of water into the English Channel.

LUNDBAK (1956) studied the storm surge of January 31–February 2, 1953, on the west coast of Denmark. He mentioned that one of the worst storm surges on the Danish coast occurred November 12–14, 1872, in which there was great damage and loss of life on the island of Lolland. The storm surge of October 10–11, 1634, was supposed to have killed more than 6000 people. This surge cut the German island, Nordstrand, into two separate islands, which were later named Pellworm and Nordstrand.

The question if the storm surge is the highest at any given instant or not depends first on the location and second on the time scale that one considers. For the coast of the United Kingdom, PETERS (1954) mentioned that a series of surges occurred during the period between 1086–99. A surge in the year 1099 killed 100 000 people. During the twelfth century, there were more surges. Another period of great surges was 1218–23. Other periods when the death toll exceeded 100,000 were in the years 1421 and 1446. Great surges also occurred (though the death toll was much smaller) on November 15, 1875, January 2, 1877, January 18, 1881, and November 29, 1897. After this period, the next comparable surge occurred in 1928 and then in 1953.

For the Netherlands VAN MALDE (1995) used the highest water level as the storm surge level. According to the official storm surge table of the Rijkswaterstaat; starting in 1825, the highest tidal-water levels recorded were those of the storm surge of February 4, 1825. But the question is, whether higher storm surge levels occurred in the past. VAN MALDE (1995) named the surges of 1421, 1446, 1468 and those from 1539 and 1552 as large, but shows that the conversion of such deceptive levels to centimeters is not a simple matter. He shows that the oldest reliable storm surge event was the All Saints Flood of 1570, one of the most disastrous floods that ever ravaged the Netherlands and summarizes that “the storm surges caused along the Dutch coast between Scheveningen and Den Helder were among the highest storm surge levels ever known”. Off the northern provinces and the adjacent German coast the storm surge levels were very close to the highest ones having occurred ever

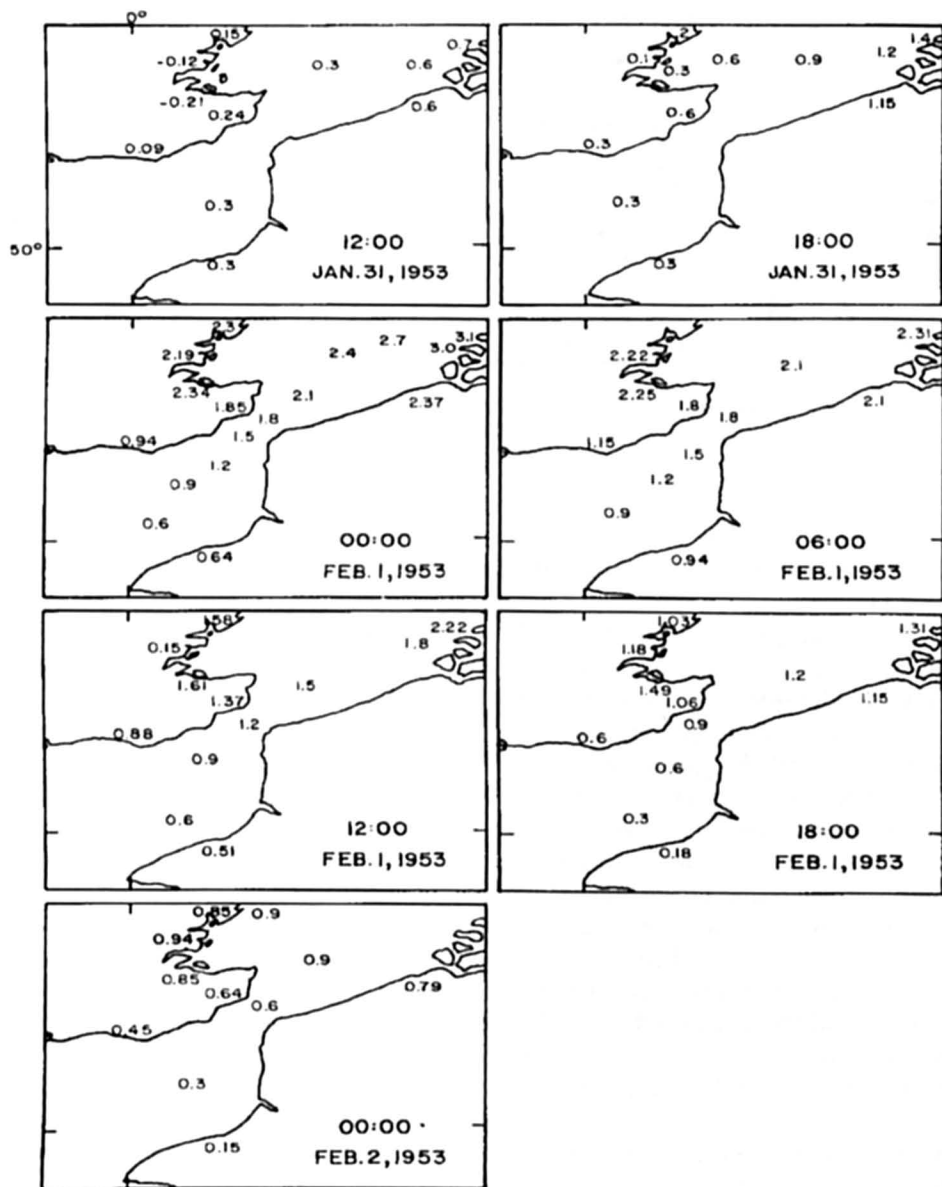


Fig. 7.14: Storm surge heights (meters) in the English Channel during January 31–Feb 2, 1953 (ROSSITER 1954)

since...” (meaning the storm surges of 1570, 1717, 1775, 1776, 1825 and 1953). The conclusion about the German coast is based on the research of ROHDE (1977), who did derive four historical storm surge levels at Emden with the following result:

- November 1, 1570:  $\geq$  NN + 470 cm    NN = Normal Null = mean sea level
- December 14, 1717:    NN + 475 cm
- November 15, 1775:    NN + 388 cm
- November 21, 1776:    NN + 451 cm
- February 3–4, 1825:    NN + 465 cm

To these results the following storm surge levels in the German Bight can be added. The highest storm surge level in the German Bight was reached in 1976 with a level of 370 cm over mean high tide level and 1010 cm NN. The storm surge of February 16–17, 1962, when a lot of people died was 355 cm over mean high tide level at Cuxhaven. This level has been reached during the flood of February 3–4, 1825, with 355 cm at Cuxhaven (GÖNNERT, 1999a). Therefore it can be stated that in recent years cause the storm surge level in the German Bight only a little increased and is compared to mean high tide level increase.

While the flood of 1825 caused high water levels along the Dutch and German Coast, the storm surge of 1962 was very high only in the German Bight and especially along the rivers Ems, Weser and Elbe within the cities of Emden, Bremen and Hamburg. The reason is the character of the storm and the location of the island in the deep water area of the North Sea. After the storm surge of 1962 coastal protection has been developed so that the higher storm surge of 1976 did not cause much damage.

A major storm surge occurred in the southern part of the North Sea and in the Thames Estuary during January 31–February 1, 1983, exactly 30 years after the surge of 1953. The meteorological conditions were somewhat different in these two cases. The surge of 1983 was potentially as destructive as the one of 1953. However, because of considerable improvement in storm surge warning services and the development of coastal protection works and the Thames Estuary barrier, loss of life and damage to property were considerably less than in 1953.

### *Negative Surges in the North Sea*

ROSSITER (1971) drew attention to the navigational hazard posed to large ships in the southern North Sea due to negative storm surges. DOODSON (1947) mentioned that negative surges occurred at Dunbar and Southend during the storms of November 10–13, 1929, January 1–3, 1928, and October 17–21, 1935.

Table 7.2: Frequency of negative storm surges in the southern part of the North Sea (GELHOED, 1973)

Location	Amplitude (cm) of negative surge that can occur (at the time of low water) with the frequency per year of			Amplitude (cm) of negative surge that can occur (at the time of high water) with the frequency per year of		
	10	1	10 <sup>-1</sup>	10	1	10 <sup>-1</sup>
Hook of Holland	50	83	117	50	80	111
Flushing	46	75	103	47	80	113
Dunkerque	44	68	92	46	75	105
Dover	43	69	96	47	79	111

GELHOED (1973) studied negative storm surges in the southern part of the North Sea, with particular attention to the Sandettie Bank and the Brand Ridge areas because of the shallow water depths there. The data source consisted of 50 years of data for the stations of Hook of Holland and Flushing, 4.7 years of data for Dunkerque, and 20.1 years of data for Dover. The results of a frequency analysis are summarized in Table 7.2. This table must be interpreted as follows. For example, at Hook of Holland, negative surges of amplitudes up to

50 cm occur on the average about 10 times per year; negative surges with amplitudes up to 83 cm occur once a year and negative surges of amplitudes up to 117 cm occur only once in 10 years. The differences between the negative surges at low and at high waters are not significant.

Negative surges predominantly occur in winter. Southerly to westerly winds produce negative surges at Dover whereas at Hook of Holland, southerly to easterly winds cause negative surges. Largest negative surges occur at Southend (up to 2.3 m) and at Tilbury (up to 2.8 m). At other stations, negative surges with amplitudes of 1.0–1.5 m occur. GEELHOED (1973) attributed the differences in the amplitudes of the negative surges at various locations to topographic differences.

Table 7.3: Calculated amplitudes (m) of storm surges at three locations in the southern part of the North Sea for three different wind fields. (GEELHOED, 1973)

Type of wind field (83 km·h <sup>-1</sup> )	Amplitude (m) of surge at		
	Sandettie	Brown Ridge	Hook of Holland
Easterly	-0.8	-0.7	-1.3
Westerly	+0.8	+0.7	-
Southerly	-1.9	-1.8	-2.1

Westerly winds appear to cause negative surges exclusively on the east coast of the United Kingdom whereas easterly winds could cause negative surges exclusively on the coast of the Netherlands. On the other hand, southerly winds can cause negative surges on both coasts simultaneously (and indeed in the whole southern part of the North Sea). The calculated negative surges at three locations for three different wind fields are summarized in Table 7.3.

Negative surges in rivers are a special problem for navigation for the example of the Elbe river (German Bight) this has been investigated by RUDOLPH (1999). The following is based on RUDOLPH (1999) and also on personal communication.

The estuaries along the German Bight are well exposed to storms coming over the North Sea from westerly direction. In the Elbe estuary which is orientated from West to East, high water levels at the mouth in combination with strong westerly winds can result in high water levels along the whole estuary, which reaches inland more than 100 km. Even the harbor of Hamburg, which is situated about 120 km upstream of the mouth of the Elbe estuary is endangered by storm surges coming from the North Sea.

There are indeed situations too, where strong winds cause a decrease in water level. This might be called a negative storm surge. In the Elbe estuary for example strong easterly winds blowing for several days can lower high as well as low water levels significantly.

An example of a negative storm surge is found in the first week of October 1992. This period was preceded by a low fresh water discharge of only appr. 200 m<sup>3</sup>/s while the mean fresh water discharge of the last 50 years was 712 m<sup>3</sup>/s. During the end of September 1992 the wind over the Elbe estuary had easterly direction with wind speeds between 5 m/s and 10 m/s (Bft 4 to 5). In the first week of October 1992 the wind speed increased and reached up to 15 m/s (Bft 7) from April 10, 1992 until June 10, 1992.

For the period January 10, 1992 until July 10, 1992 the astronomical tide for Cuxhaven at the mouth of the Elbe estuary was calculated from harmonic tidal constants. Fig. 7.15a

shows the comparison between observed and predicted water levels at Cuxhaven. In addition the measured wind speed and wind direction in this area is given.

The difference between these water levels can be interpreted as surge. Fig. 7.15b shows the observed water level, the predicted astronomical tide and the surge during the period of strong easterly wind. In fact, a negative storm surge of up to one meter can be found.

Inside the estuary e.g. close to the harbour of Hamburg the difference between predicted and observed water levels is even higher. In this part of the estuary the effects of the low fresh water discharge and the strong easterly winds add up to differences in the high water level of 110 cm and in the low water level of 80 cm (Table 7.4).

Table 7.4: Measured and predicted water levels in [mNN] as well as the differences at Cuxhaven and Hamburg St. Pauli in the Elbe estuary during negative storm surges

Date		Cuxhaven			Hamburg St. Pauli		
		measured	predicted	difference	measured	predicted	difference
10/03/1992	HW	+ 1.13 m	+ 1.15 m	- 2 m	+ 1.49 m	- 2.00 m	- 51 cm
	LW	- 1.79 m	- 1.40 m	- 39 cm	- 2.01 m	- 1.40 m	- 61 cm
	HW	+ 0.70 m	+ 1.30 m	- 60 cm	+ 1.07 m	+ 1.80 m	- 73 cm
	LW	- 1.64 m	- 1.20 m	- 44 cm	- 1.97 m	- 1.30 m	- 67 cm
10/04/1992	HW	+ 1.71 m	+ 1.40 m	- 31 cm	+ 1.05 m	+ 1.90 m	- 85 cm
	LW	- 1.80 m	- 1.30 m	- 50 cm	- 2.13 m	- 1.40 m	- 73 cm
	HW	+ 0.09 m	+ 1.10 m	+ 101 cm	+ 0.43 m	+ 1.60 m	- 117 cm
10/05/1992	LW	- 1.67 m	- 1.10 m	- 57 cm	- 2.11 m	- 1.30 m	- 81 cm
	HW	+ 0.40 m	+ 1.20 m	- 80 cm	+ 0.77 m	+ 1.80 m	- 103 cm
	LW	- 1.61 m	- 1.20 m	- 41 cm	- 2.08 m	- 1.40 m	- 68 cm
	HW	- 0.02 m	+ 0.90 m	- 92 cm	+ 0.44 m	+ 1.50 m	- 106 cm
10/06/1992	LW	- 1.26 m	- 1.00 m	- 26 cm	- 1.72 m	- 1.30 m	- 42 cm
	HW	+ 0.37 m	+ 1.20 m	- 83 cm	+ 0.83 m	+ 1.80 m	- 97 cm
	LW	- 1.40 m	- 1.20 m	- 20 cm	- 1.84 m	- 1.40 m	- 44 cm
	HW	+ 0.26 m	+ 0.90 m	- 64 cm	+ 0.77 m	+ 1.50 m	- 73 cm

Investigations with a numerical model of the Elbe estuary showed, that not only the low water levels at the mouth of the Elbe caused the low water levels inside the estuary, but also the strong local wind over the Elbe estuary helped to lower the water level along the Elbe estuary during ebb tide (increasing ebb current) and to keep the water levels low during flood (decreasing flood current).

The processes described here, low fresh water discharge and continuous high easterly winds, resulted in a decrease in low and high water levels along the whole Elbe estuary. This negative storm surge lasted for more than four days. On July 10, 1992, the wind direction changed to North, the wind speed decreased and so the water levels finally reached their normal height again.

In contrast to storm surges these negative storm surges do not endanger the life of the inhabitants of the coastal areas. Nevertheless they are a problem for the traffic on e.g. the navigation channel Elbe, as the navigable depth is reduced significantly in comparison to the usually occurring tide.

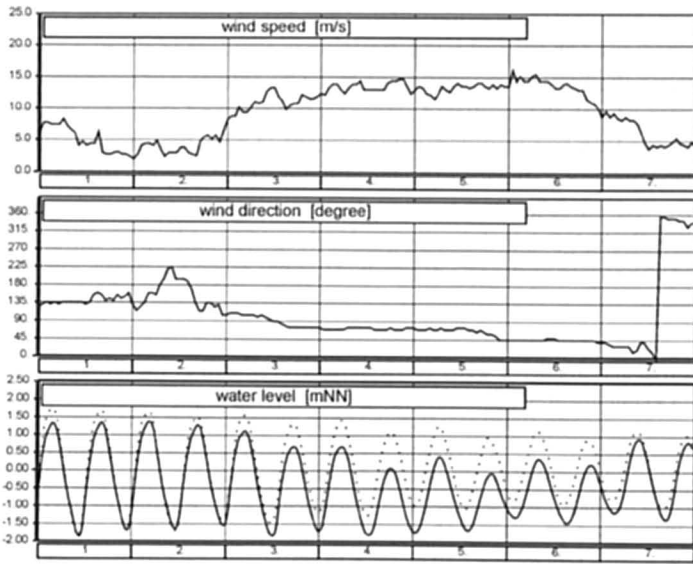


Fig. 7.15a: Negative Surge Elbe: Wind speed and wind direction at the island of Scharhörn in the mouth of the Elbe estuary and measured (dotted) and predicted (solid) water levels at Cuxhaven for the period 10/01/1992 until 10/07/1992. With increasing wind speed the difference between observed and predicted water level also increases

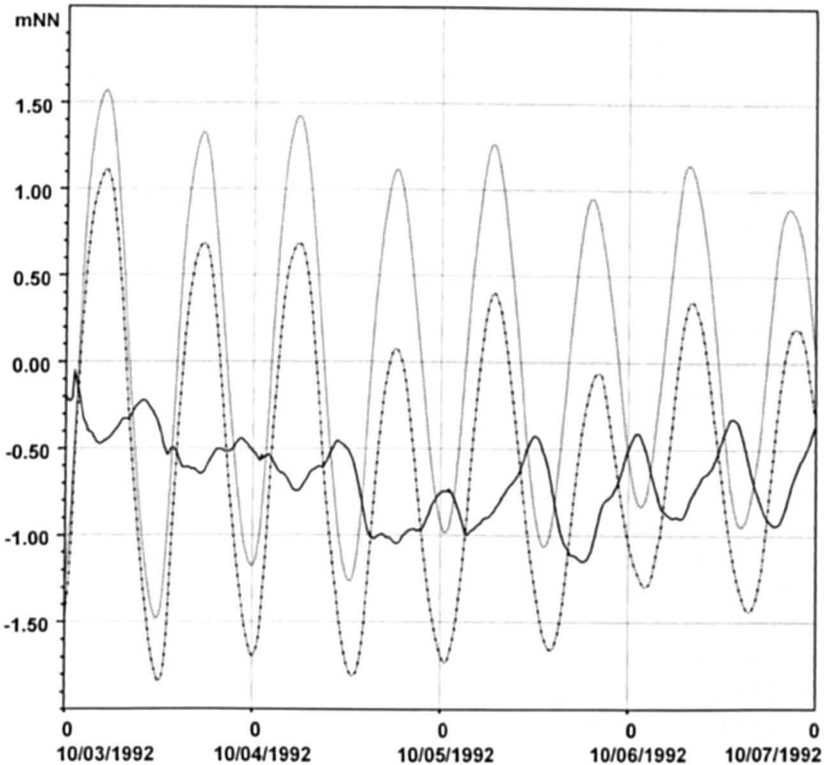


Fig. 7.15b: Negative Surge Elbe: Measured water level (dashed), astronomical tide (dotted) and surge (solid) at Cuxhaven during October 1992

*The Netherlands*

Earlier, the works of GALLÉ (1915) and SCHALKWIJF (1947) were discussed. The storm surge amplitudes along the coast of the Netherlands during the major storm surge of January 31–February 1, 1953, were greater than those at the east coast of the United Kingdom (UFFORD, 1953). Surge amplitudes up to 9 ft (2.74 m) occurred along the coasts of the provinces of Zeeland and Zuid-Holland, with a peak surge of 9.6 ft (2.93 m) occurring at Hellevoetsluis. In the Scheldt Estuary the amplitudes were even greater. At Berger op Zoom the amplitude was about 11 ft (3.35 m).

The water level rose above the dykes, and about 50 dykes collapsed and at least 1800 people died. The damage exceeded £ 100 million (at 1953 prices). UFFORD (1953) mentioned that this was the biggest surge since the one on November 18, 1421, when at least 10 000 people died. Since the time tide gauges were set up in 1890, the surge of 1953 was 2 ft higher on the average than any other surge during the period 1890–1953. The extent of the flooding on the coast of the Netherlands is shown in Fig. 7.16.

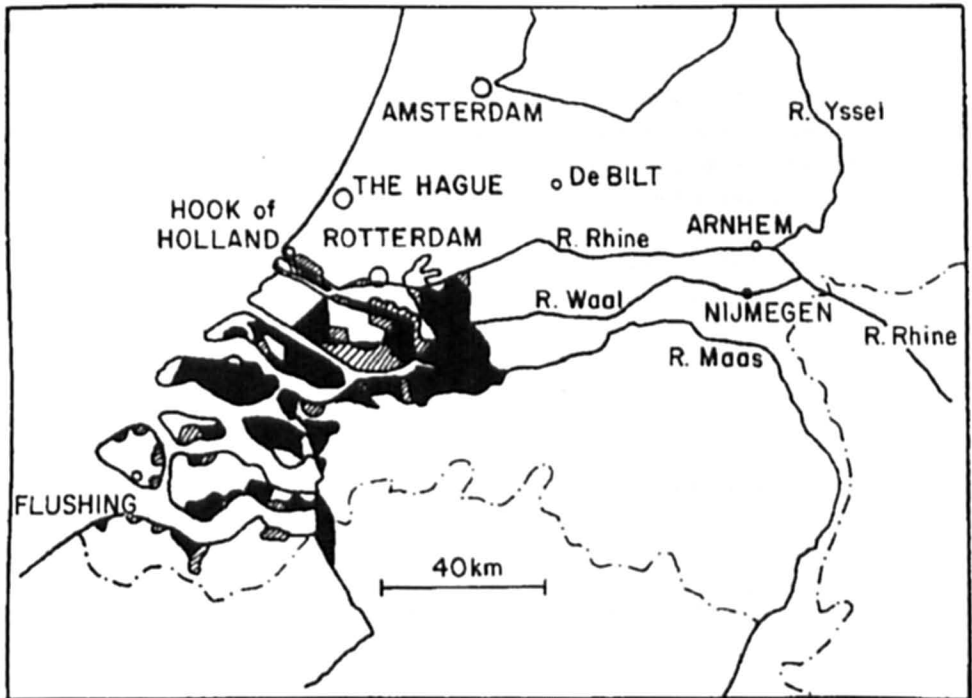


Fig. 7.16: Extent of flooding on the coast of the Netherlands due to the storm surge of January 31–February 1, 1953. Dark areas show regions that were flooded until March 1953. Hatched areas are those that were reclaimed after the flooding (UFFORD, 1953)

WEENINK (1956) studied the so-called twin storm surges that occurred on December 21 and 24, 1954. The observed surge and that computed through an equilibrium wind assumption are shown in Fig. 7.17.

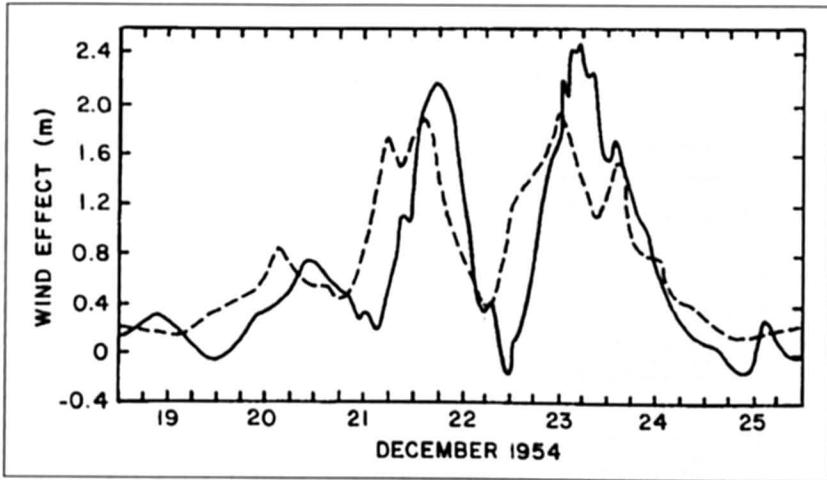


Fig. 7.17: Twin surges of the North Sea in December 1954 as recorded at the Hook of Holland (solid line). Broken line shows the computed surge using the equilibrium wind effect (WEENINK, 1956)

TIMMERMAN (1971) showed that moving cold fronts over the southern part of the North Sea could produce a sudden increase of water levels at the Netherlands coast (he uses the rather inappropriate term “gust bump” to refer to these water level increases). These increases in the water level occur only when the speed of propagation of the cold front lies between 29 and 36 knots (54–67 km/h). This suggests resonance between the traveling atmospheric disturbance and the long surface gravity waves in the water body. He numerically simulated the event of December 13, 1956. One can obtain some idea of the time scale and amplitudes of the gust bumps from Fig. 7.18. One can clearly see the bump at Katwuk at 11 a.m. on March 27, 1966. The locations of these stations can be seen in Fig. 7.19. Similar sudden water level increases for the event of December 13, 1956, are shown in Fig. 7.20.

After the storm surge of 1953 in the Netherlands it was decided to set new safety standards and perform extreme value statistics. It was agreed that the central, and most important, part of Netherlands was given a safety standard with a return period of 10,000 years (...) (RONDE et al., 1995). The wadden islands have a return period of 2000 years and the remaining coastal areas have a return period of 4000 years. With respect to the central coastal part, this gives a reduction of about 40 cm for most coastal areas.

RONDE et al. (1995) describe the extreme value water level as follows. At first the storm surge data were selected by use of depression storm tracks to obtain a homogeneous data set. Only one value per storm was taken to get un-correlated data. This is comparable with the method to calculate a storm surge curve and take only the highest water level. A so called “Peak over Threshold Method” was fitted to choose the extreme value distribution. “Finally a design level of about 5 m + NAP was designated for the Hook of Holland as the event with a return period of 10,000 years.” RONDE et al. (1995) described the method to calculate the design level of other stations with help of the design level of Hook van Holland.

Using statistical methods, RONDE et al. (1995) took into account a sea level rise of about 15 to 20 cm and the return period was re-calculated.

For real time forecasting of storm surges the CSM model with a grid size of 8 km is used at the KNMI (Royal Netherlands Meteorological Institute).

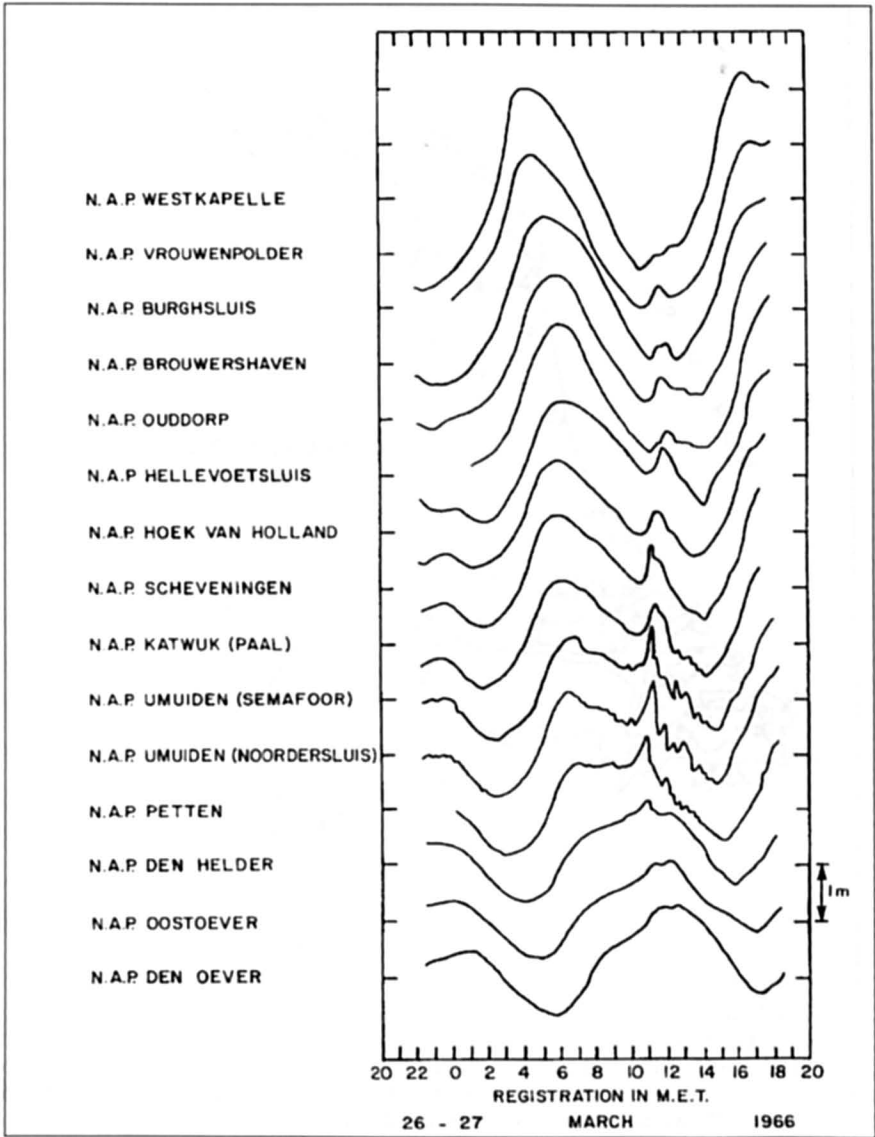


Fig. 7.18: Sudden water level changes (gust bumps) during March 27, 1966, at several locations on the Netherlands coast (TIMMERMAN, 1971)

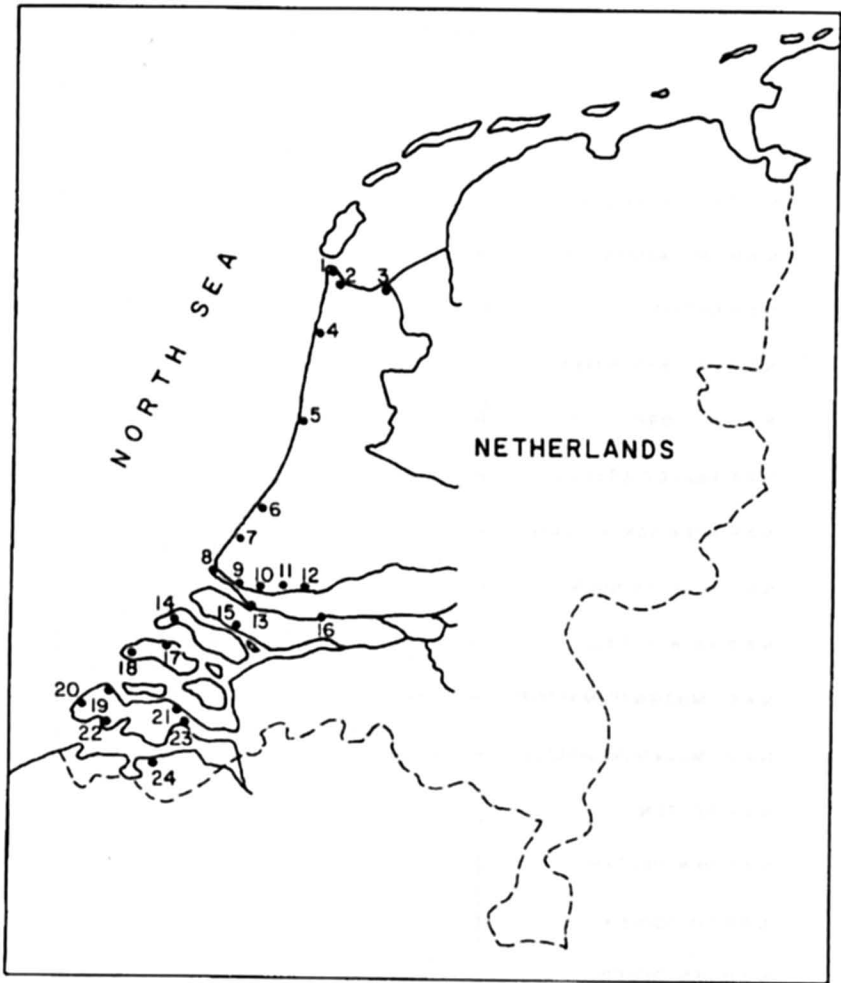


Fig. 7.19: Netherlands coast showing the locations of the tide gauge stations used in the storm surge study, 1, Den Helder; 2, Oostoever; 3, Den Oever; 4, Petten; 5, Urnuiden; 6, Katwuk aan Zee; 7, Scheveningen; 8, Hoek van Holland; 9, Maassluis; 10, Vlaardingen; 11, Rotterdam; 12, Krimpen aan den Lek; 13, Spukenisse; 14, Ouddorp; 15, Hellevoetsluis; 16, Dordrecht; 17, Brouwershaven; 18, Burghsluis; 19, Vrouwenpolder; 20, Westkapelle; 21, Wemeldinge; 22, Vlissingen; 23, Hansweert; 24, Temeuzen (TIMMERMAN, 1971)

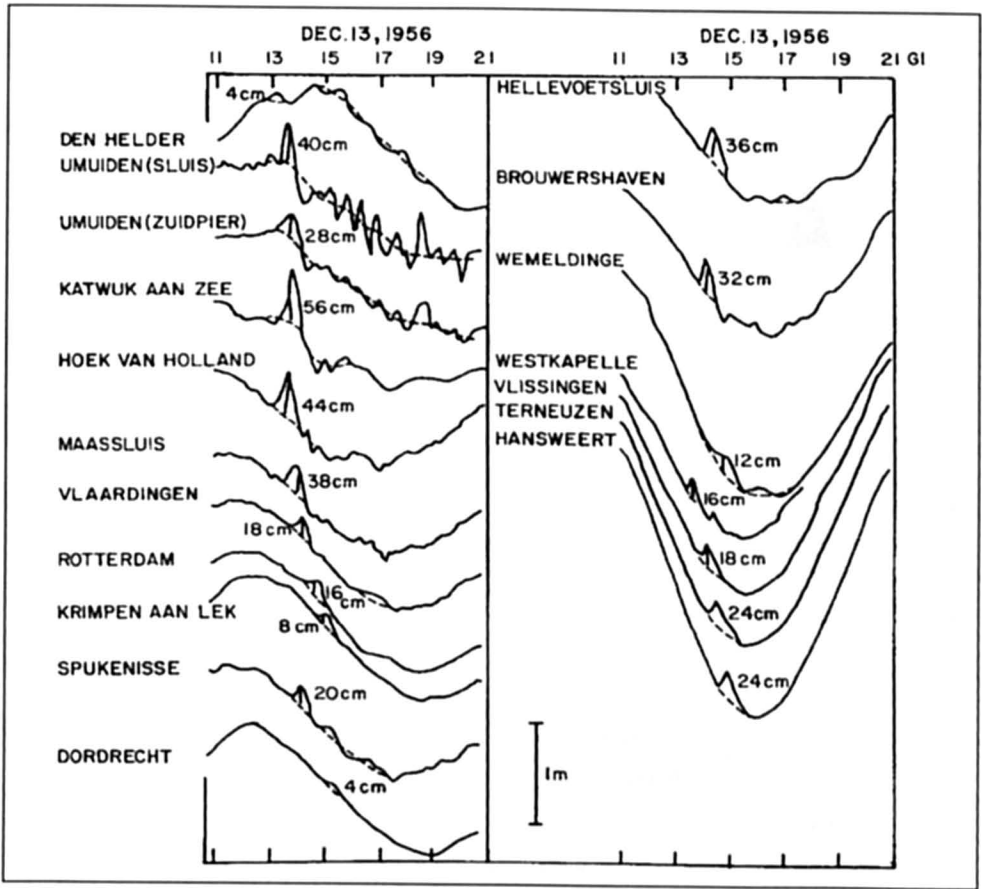


Fig. 7.20: Sudden water level changes (gust bumps) at several locations on the Netherlands coast on December 13, 1956 (TIMMERMAN, 1971)

### German Bight

Storm surges occur in the German Bight when wind blows over the North Sea from N to NW. To reach a very high water level the duration of a high wind speed must be a minimum of 3 h. The so called critical wind direction for each location is different. For example the critical wind direction for Cuxhaven for very high storm surges lies between  $280^{\circ}$ – $310^{\circ}$ , for Helgoland between  $265^{\circ}$ – $280^{\circ}$  and for Norderney between  $255^{\circ}$ – $290^{\circ}$  (GÖNNERT, 1999b).

In the North Sea near the Amphidromic point the water levels rise only slightly and increase towards the coast.

TOMCZAK (1950) discussed the storm surge of February 9–10, 1949, in the North Sea. The greatest effect of the surge was on the coast of Northern Friesland. One interesting feature was that the storm center remained almost stationary off the island of Sylt on February 9<sup>th</sup> and blocked the outflow of water from the German Bight northwards. The maximum amplitudes of the water level at several locations are listed in Table 7.5.

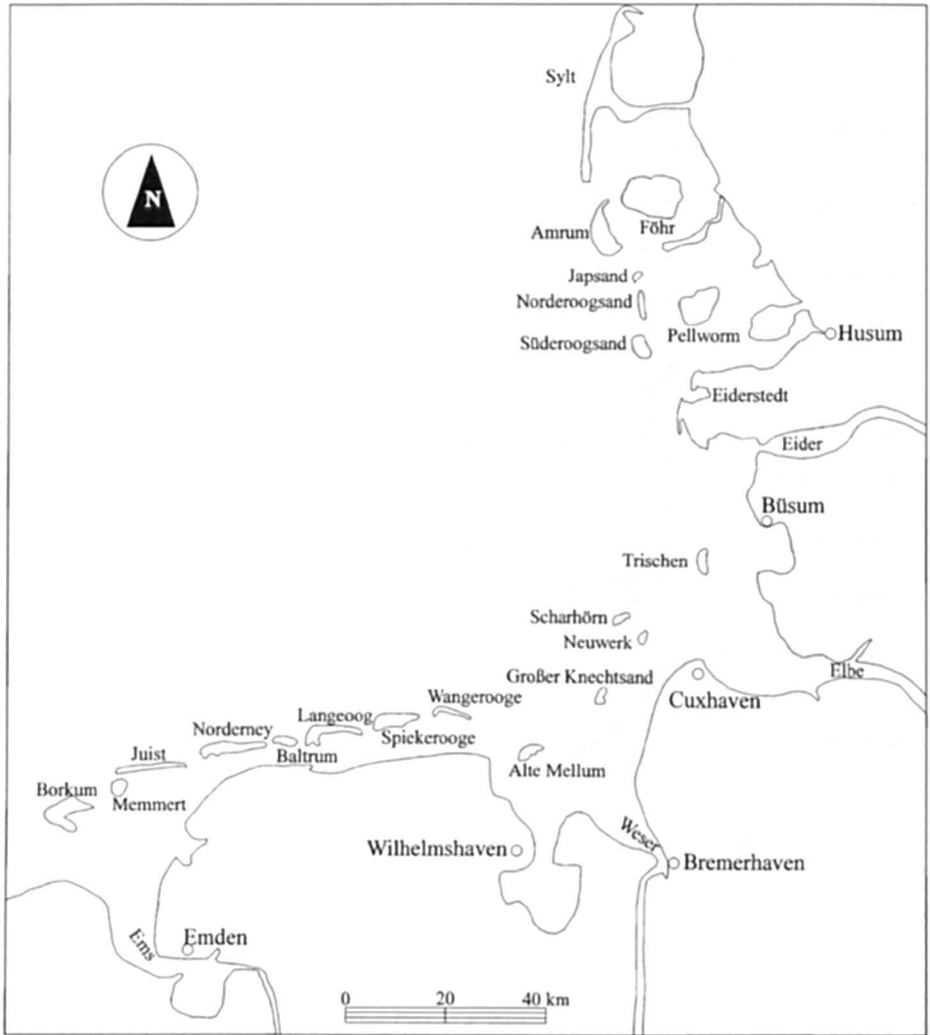


Fig. 7.21: The German Bight

Table 7.5: Maximum water levels during the storm surge of Feb. 9–10, 1949, at the German North Sea Coast (TOMCZAK, 1950)

Station	Amplitude (m)	Station	Amplitude (m)
Borkum	2.4	Bremerhaven	3.9
Norderney	3.0	Cuxhaven	4.2
Emden	3.3	Büsum	4.8
Wilhelmshaven	3.4	Husum	5.6

Other examples are shown in Table 7.6, indicating that the level depends on wind direction and location with each special topography.

Table 7.6: Storm surge level over NN (Normal Zero) in the German Bight

Storm surge	Feb. 16, 1962	Jan. 3, 1976	Feb. 26–28, 1990	Jan. 10, 1995
Cuxhaven	495 cm NN	5010 cm NN	434 cm NN	448 cm NN
Norderney	410 cm NN	386 cm NN	366 cm NN	346 cm NN
Wittdün	360 cm NN	327 cm NN	324 cm NN	266 cm NN
Helgoland	414 cm NN	405 cm NN	384 cm NN	301 cm NN

SIEFERT (1968, 1978, 1982, 1988a, 1988b, 1990), SIEFERT and LASSEN (1985) and GÖNNERT and SIEFERT (1997) studied storm surges in Cuxhaven and the Elbe River. The studies involved a total of 153 storm surges, which included 192 high tide water levels for the period of 1901–1995 (GÖNNERT and SIEFERT, 1998). Only events that generated a surge of 2 m or more between low water time and four hours after high water time are considered for the analysis (SIEFERT and LASSEN, 1985). During low tide the surge reaches a higher level than during high tide. Therefore the data record is restricted to storm tides with a surge level lower than 1.50 m at high tide. To analyze the change of storm tides in the last century utilization of the surge curve (Fig. 7.23) – which is the difference between the storm tide and the astronomical or mean tide curve – is the best approach, because it includes the meteorological factors. With this approach GÖNNERT (1999a & b) studied the 20th century storm tides (level, number, duration and character) in the German Bight (Fig. 7.21). The results showed an increase in the number of storm surges, but no significant increase in the level. The increase in frequency is mainly true for the small events, but the average storm surge curve is longer and there are more events with long duration (GÖNNERT, 1999a & b). For example, during the storm surge of February 26–28, 1990 one storm surge curve includes five height water peaks for Cuxhaven (Fig. 7.22).

In the German Bight the character of very high storm surges is different. At the coast very high crests are associated with a fast increase of wind speed. Since wind fields cannot be reliably predicted too far ahead, storm surges also cannot be predicted reliably for more than 12 hours ahead. But at the islands very high crests are associated with the slow increase of wind speed.

Investigations into the change of storm surge level and frequency by focusing on the tidal crest have been done for example by LÜDERS (1974), PETTERSON and ROHDE (1991), NASNER and PARTENSKY (1977), FÜHRBÖTER et al. (1988), FÜHRBÖTER (1989), FÜHRBÖTER and TÖPPE (1991), JENSEN (1987), NIEMEYER et al. (1995) and STORCH et al. (1998).

GÖHREN (1976) studied currents on the tidal flats in the German Bight. Note that these tidal flats could be as wide as 20 km. He showed that the currents can increase from an average 30 cm/s to as much as 120 cm/s during storm surges. The destructive storm surges at the North Sea coast of Germany during February 16–17, 1962, December 6–7, 1973, and January 3, 1976, prompted ZSCHAU et al. (1978) to develop a storm surge forecasting technique by measuring the inland crustal tilt and the deflection of the local vertical due to the buildup of the surge. These authors, using a vertical pendulum, measured such tilts with precision. According to them there is advance information about the storm surge in these tilt measurements. The rationale for this is explained below.

There is an indirect effect of tides on tidal gravity, tilt, and strain measurements. Since this effect depends on the elasticity of the crust and the upper mantle, this effect has been used to determine their elastic properties. However, in the regions where the elastic properties are known better than the tides, the inverse problem of determining the tides from measurements

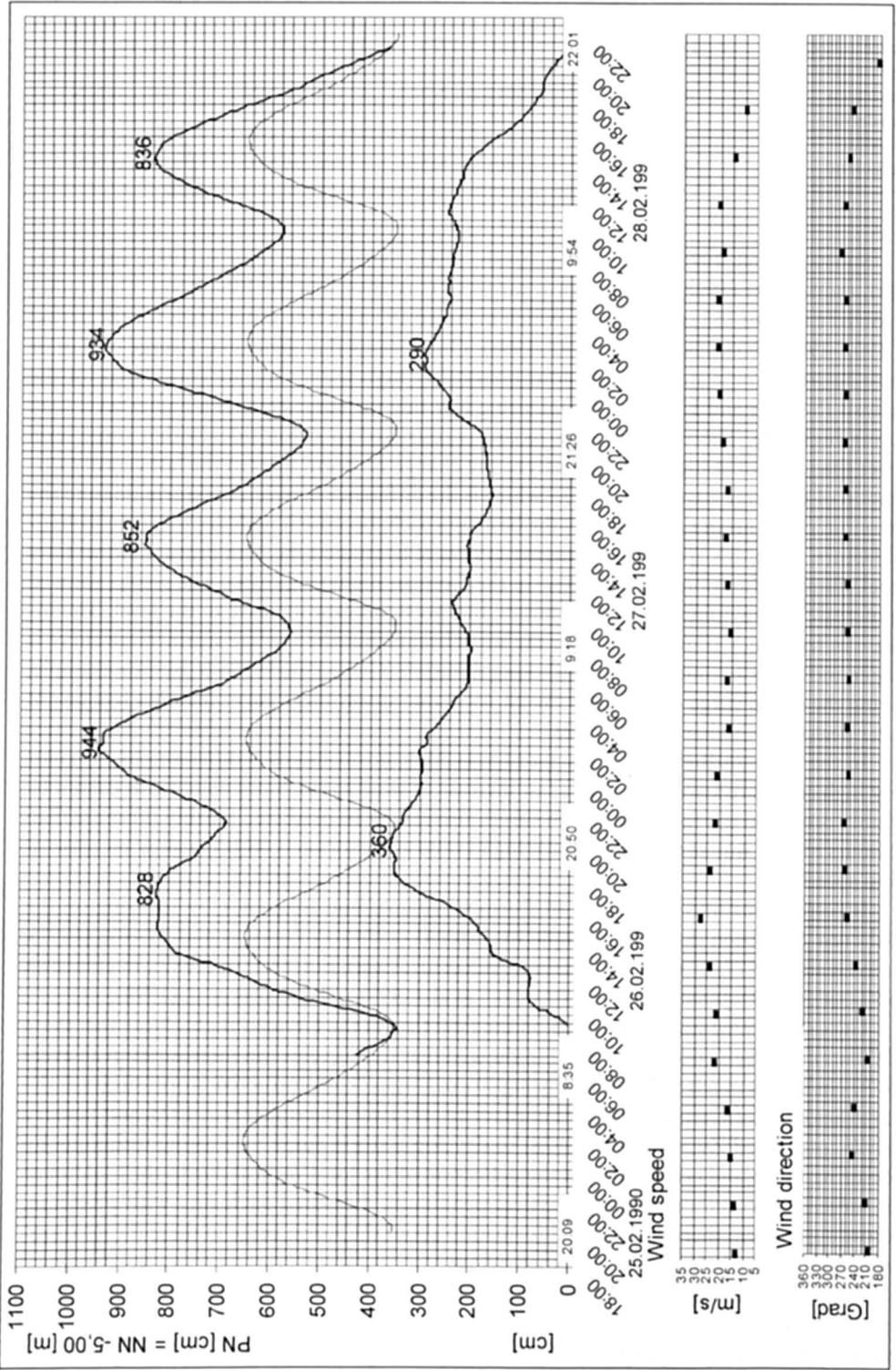


Fig. 7.22: Storm Surge at Cuxhaven February 26-28, 1990 (GONNERT and SIEFERT, 1998)

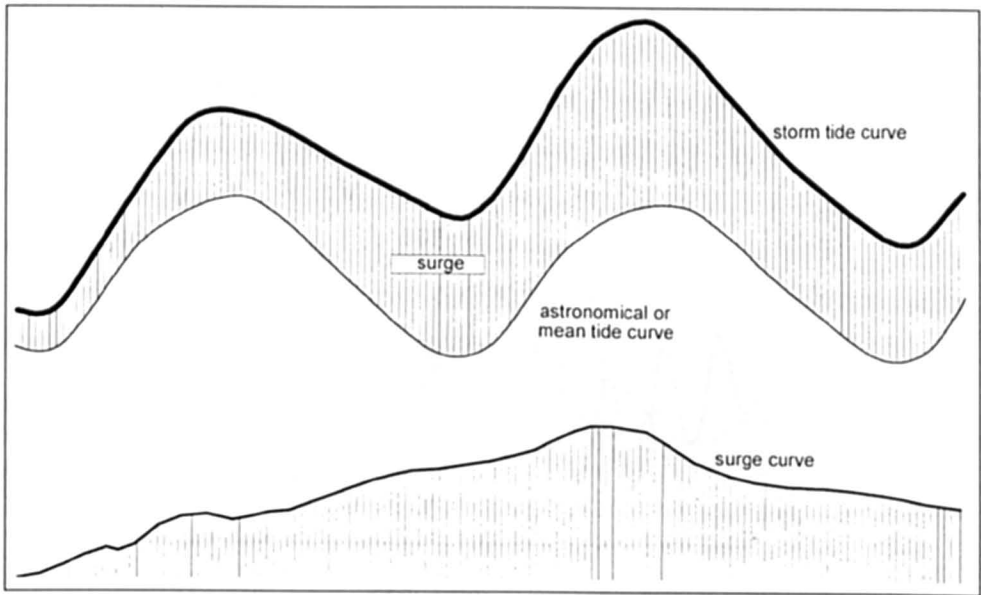


Fig. 7.23: The storm surge curve

of tidal gravity on the land has been used. ZSCHAU et al. (1978) used this inverse approach of determining the storm surge from tilt measurements made inland. According to them, the additional water mass of the surge has three different effects on these measurements: (1) the deflection of the vertical due to the gravitational attraction of the water mass, called the Newtonian tilt; (2) the tilt of the surface due to the loading and unloading of the sea floor, called the primary loading tilt; (3) the secondary deflection of the vertical due to the redistributions of mass caused by the loading and unloading, called the secondary loading tilt.

The secondary loading tilt, generally, is small compared with the primary tilt and it can be combined with the loading tilt. Note that the Newtonian tilt and the primary tilt cause a deflection of a vertical pendulum tilt meter and also tilt its casing.

The storm surge at Büsum on the west coast of Schleswig Holstein of December 6–7, 1973, is shown in Fig. 7.24. A maximum amplitude of about 3 m was attained. The measured tilt at Kiel-Rehmsberg and also the astronomical tide are shown. It can be seen that the tilt curve matches the storm surge curve except for a 12-h phase advance. This phase advance is explained as due to the amphidromic component of the North Sea surge, which takes roughly a day to propagate in a counterclockwise direction from Scotland along the coasts of the United Kingdom, Belgium, the Netherlands, Germany, and Denmark to Norway.

This same technique was used to simulate four major, two moderate, and three minor surges during November–December 1973. The predictions (Fig. 7.25) 9, 6, and 3 h ahead had average errors of 29, 18, and 11 cm, respectively, in the maximum storm surge amplitudes.

FÜHRBÖTER (1979), JENSEN (1985), FÜHRBÖTER and TÖPPE (1991) studied the frequencies of extreme storm surges on the North Sea coast of Germany. They suggested that the classical extrapolation techniques for return periods might not be applicable in this situation because the time series (representing the storm surge data) are not stationary but changing with time continuing. JENSEN (1999) summarized their work:

The current approaches for estimating a storm surge defence level can be classified into empirical and statistical methods. Statistical methods are mostly based on the consideration

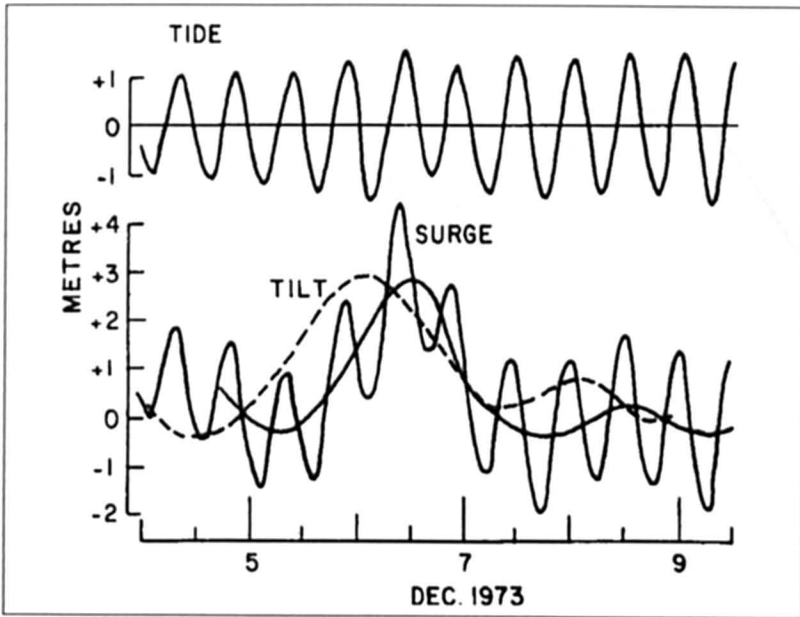


Fig. 7.24: Tide and surge at the coast of Germany during December 6-7, 1973. Top: tide at Büsum; bottom: solid curve shows the surge at Büsum and the broken curve shows the tilt at Kiel-Rehmsberg (ZSCHAU, 1977)

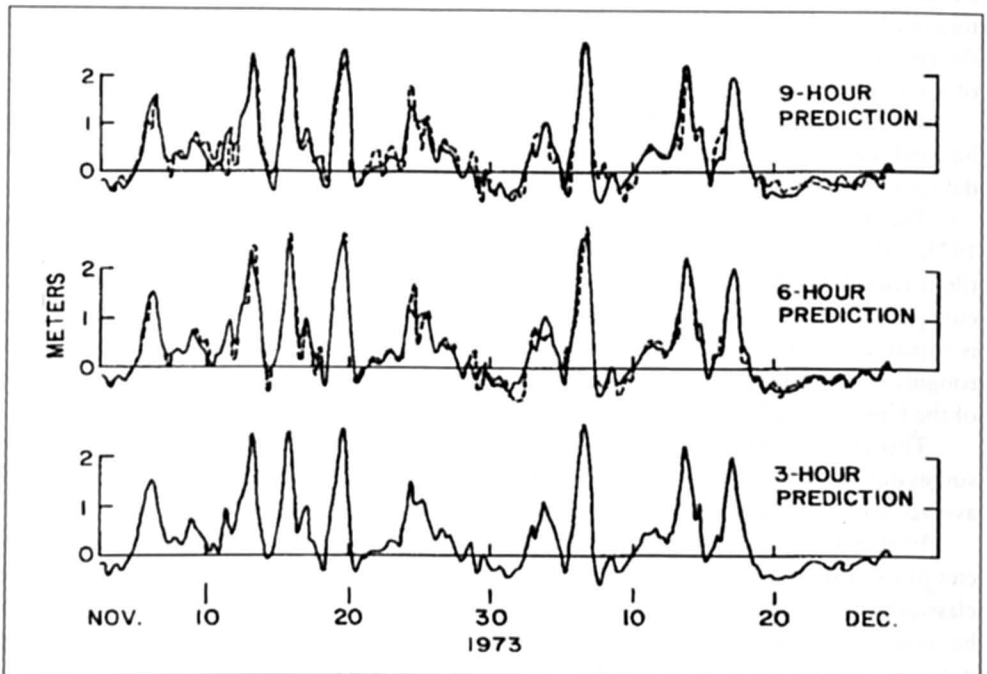


Fig. 7.25: Hindcast of storm surges for Büsum from tilt measurements at Kiel-Rehmsberg 9, 6, and 3 h in advance. Solid line: observed surge; broken line: hindcasted surge (ZSCHAU and KUMPEL, 1979)

of high water levels (HW) of an equidistant period (e.g. yearly maximum). The basic requirements of any data set are consistency, homogeneity and stationarity of the data.

Before further processing, time series should be checked and analysed very carefully for observation errors and inherent defectiveness. If mean values (mean tidal high water) are available, extreme values  $HW$  of the gauge should be homogenized using the linear trend  $s_T$  of the respective mean values as follows (if the year 2000 is the reference year):

$$BHW_i = HW + (2000 - i) \cdot s_T.$$

For the German Bight, a rise  $s_T$  of 25 cm to 50 cm for the mean tidal high water (MHW) has to be used for homogenisation of the extreme water levels. In order to estimate water levels that occur with a given probability or return period, usually some distribution functions are fitted to the observed values and a best-fitting function is selected. The most commonly used distribution functions for extreme water levels in the German Bight are: (LOG) Pearson III, Jenkinson (several procedures) and a linear regression procedure based on empirical return periods. In such an approach, the physical conditions that lead to an extreme water level are ignored.

A more reliable method of estimating extreme water levels is based on the separation of as many as possible single components from the total water level.

Examples of such components are wind set up, external surges, other astronomical influences, local wind set up, oscillations and others. Such a concept requires a continuous record of water levels as well a continuous computation of astronomical tides.

In general, as many components as possible should be regarded separately, but since such data is not yet available for the gauges in the German Bight, the only way of considering single components of the total water level is to analyse storm surge curves has done in SIEFERT (1999) and GÖNNERT (1999).

In doing so, the probabilities of a storm surge of a given level and the probability of that wind set up to occur during a high water period can be combined. Hence, the estimation of storm surge levels with a very low probability of exceedance is more reliable than of those obtained with a "classical statistical method", in particular for extreme water levels.

BARTHEL (1979) showed that significant wind wave activity could occur in the German Bight. One must include this in predicting the total water level.

## Norway

GJEVIK and ROED (1974) mentioned that catastrophic surges occurred at the island of Grip (a small island on the west coast of Norway) and were discussed by HELLAND (1911). Major surges occur also at the Island of Ona. JOHANSEN (1959) studied the surge along the southeast coast of Norway. GJEVIK and ROED (1974) studied the following three surges on the Norwegian west coast: November 2, 1971, December 30, 1972, and December 31, 1972. The surge curves at three locations for the three cases together are shown in Fig. 7.26 and 7.27, respectively. The peak surge amplitudes at six locations for the first case are given in Table 7.65.

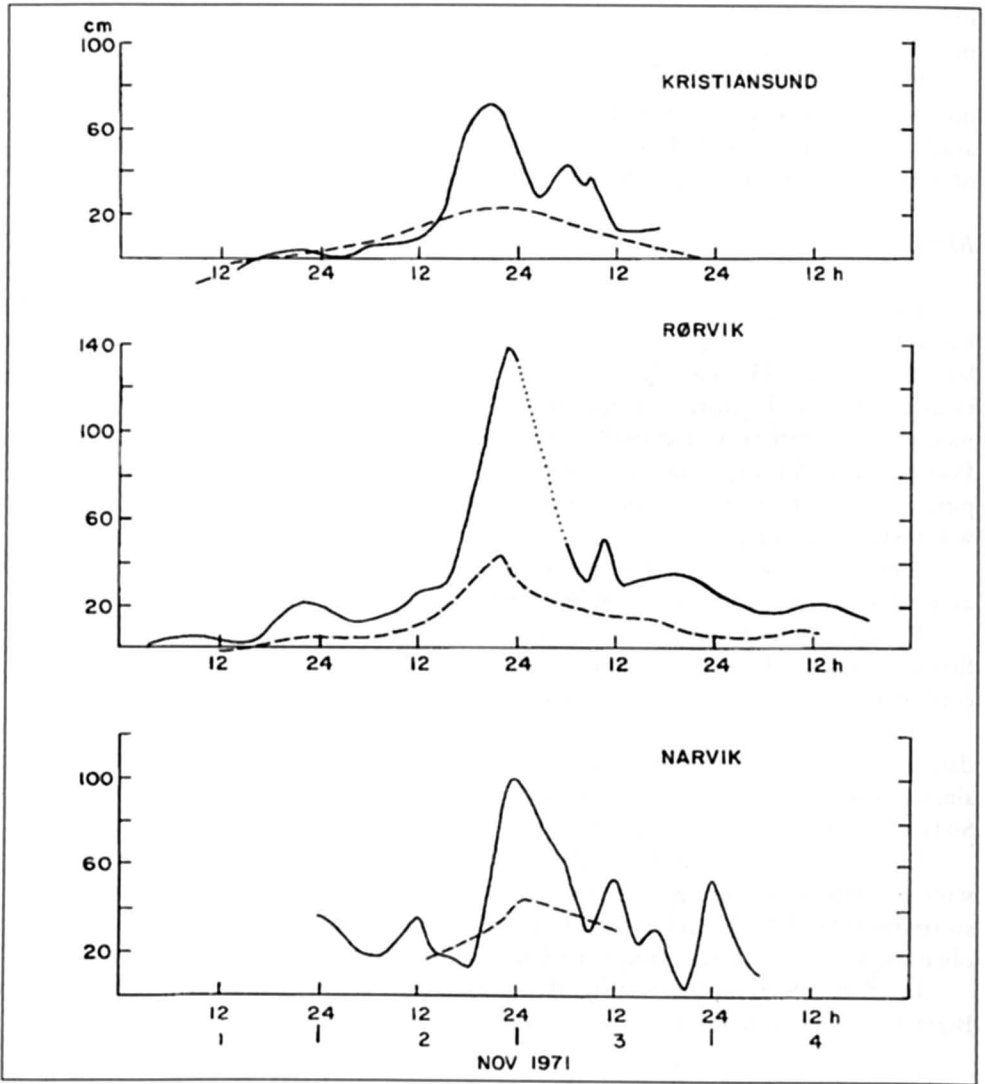


Fig. 7.26: Observed storm surges on the west coast of Norway during November 1–4, 1971. Dots denote missing observations. Broken curve represents the theoretical surge due to the atmospheric pressure gradient only (GJEVIK and ROED, 1974)

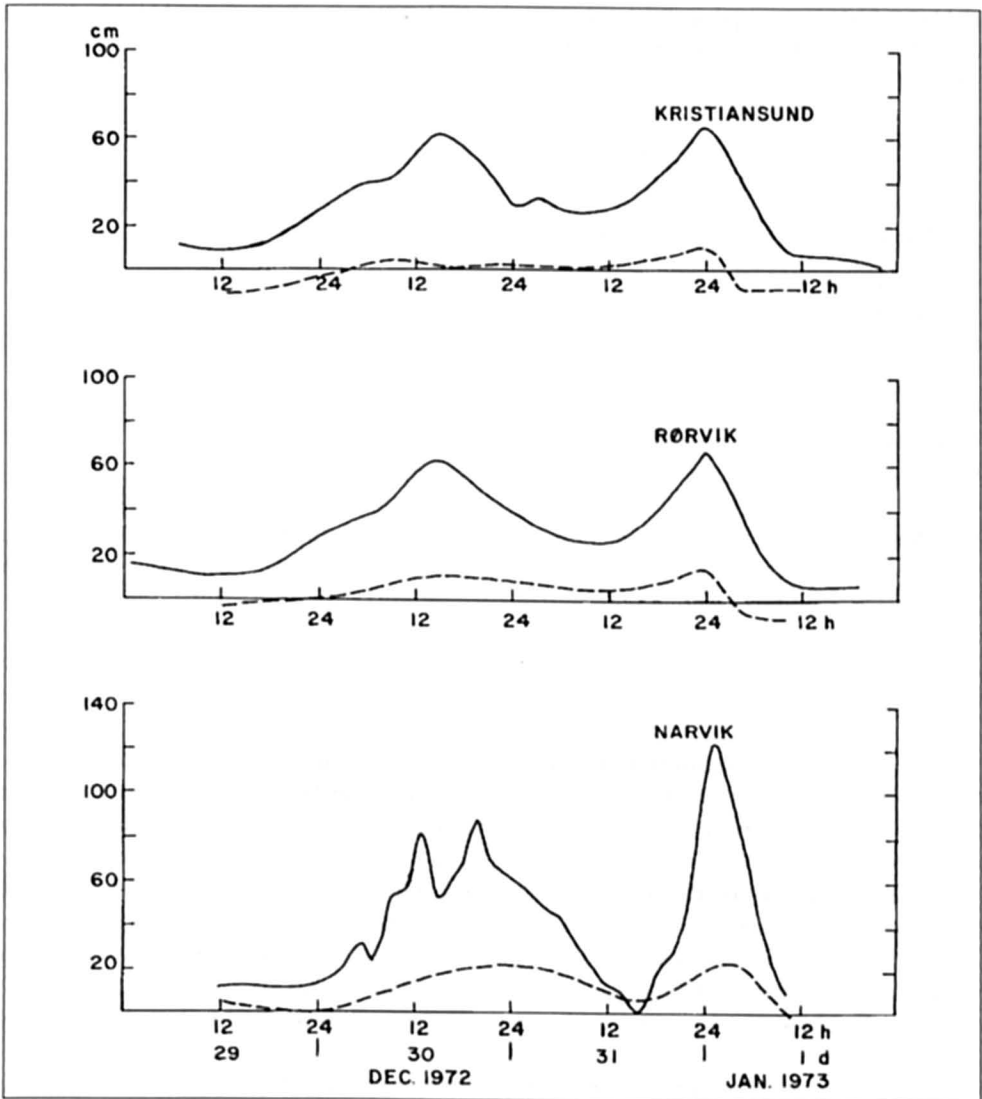


Fig. 7.27: Observed storm surges on the west coast of Norway during December 29, 1972–January 1, 1973 (solid line). Broken line shows the theoretical surge due to the atmospheric pressure gradient only (GJEVIK and ROED, 1974)

Table 7.7: Peak storm surge amplitudes at certain locations on the West coast of Norway for the surge of Nov. 2, 1971 (GJEVIK and ROED, 1974)

Location	Observed peak surge (m)
Alesund	0.40
Heimsjø	0.75*
Trondheim	1.00
Sandnessjøen	1.20
Hammerfest	0.40
Tromsø	0.50

\* This value does not agree with that given by MARTINSEN et al. (1979). See Table 7.8.

Table 7.8: Comparison of observed and calculated peak surge amplitudes on the west coast of Norway for the surge of Nov. 2, 1971 (MARTINSEN et al., 1979)

Location	Observed	Computed
Kristiansund	0.7	0.98
Heimsjø	1.0	1.08
Rorvik	1.4	1.40
Sandnessjøen	1.2	1.47
Tromsø	0.5	0.65

MARTINSEN et al. (1979) developed a numerical model to simulate storm surges along the west coast of Norway. The observed surges at five locations and those calculated from the numerical model including bottom stress are compared in Table 7.8.

### 7.3.2 Baltic Sea

Storm surge investigations in the Baltic Sea are numerous. They extend from the early part of the 20th century by KRÜGER (1910) to BAERENS and HUPFER (1994). Therefore not all available references can be summarized here. The following discussions follows closely STIGGE (1999).

**Special hydrodynamic conditions:** The Baltic Sea extends between latitudes 54 and 66 in the central area of the circumpolar low pressure zone of the northern hemisphere. Relative to the surface area of this marginal sea, the entrances to the North Sea have very small cross sections, so that only long-period oscillations of North Sea water levels propagate undamped into the Baltic. In its southwestern parts, the semi-diurnal tides are reduced to amplitudes of just 10 cm, and towards the central Baltic they disappear almost completely. Because of its enclosed geographical situation and elongated basin shape, the Baltic Sea tends to produce surface seiches with periods ranging from 26 to 39 hours, depending on the type of forcing of all contributing sea areas. Storm surges are triggered by changes in the wind fields above these areas. Strong southwesterly winds cause high water levels on its northern, and low levels on its southern coasts, with water flowing in through the Straits of Denmark increasing the water volume. A change in the wind direction to north/north-east causes high water levels in the southern Baltic, in which case the potential energy of water masses, which had been pushed north, may produce an additional impact. Both at the northeastern and southwestern end points of the Baltic Sea's longitudinal axis, peak high water values exceeding 3 m above MSL may occur. Storm surges may cause considerable damage along the coastlines, so that adequate coastal protection has to be provided. On the other hand, both storm surges and preventive protection measures may impair the functionality of technical structures. Under environmental protection and landscape preservation aspects, regular flooding of land areas is even indispensable to create a habitat for the highly specific, vulnerable flora and fauna of the salt marshes, which deserve special protection.

**Sustainable coastal development:** Sustainable coastal development in this context means to create a balance between coastal defence and environmental protection. Since 1974, the 9 countries bordering the Baltic have been co-operating within the framework of the Convention on the Protection of the Marine Environment of the Baltic Sea (or Helsinki Convention, according to its venue). Owing to the Baltic Sea's economic and ecological relevance to Northern Europe, it is one of the most intensively investigated marginal seas of the world. In Germany alone, 251 coastal research projects were officially recorded between 1990 and 1996, and the trend is upward. Internet search leads to a large number of national marine research institutes, shipping and environmental authorities, storm surge forecasting services, and to almost all universities in the area. Water level and storm surge forecasting for the Baltic Sea today is based mostly on operational hydrodynamic models using output data of the meteorological Europe model, but also statistical methods are used. HELCOM recommendations may be interpreted and implemented differently depending on local conditions. Both climate and sea level fluctuations as well as people's traditional ways of coping with nature's forces play a role in this respect. Near the oscillation nodes, i.e. near the center of the Baltic's longitudinal axis, storm surges of course do not reach the same high levels as at the end points. Since local coastal defence measures are based on past experience, the dykes built in such areas are generally lower. The problem that has to be dealt with in the different areas thus is identical: local and temporary aspects must be considered in the investigation of storm surge scenarios. The secular coastal dynamics of the Baltic (land gain in the north, land losses in the south) and the different local impacts of land/sea interactions (abrasion and accumulation coasts) require primarily the acceptance of natural processes, and human intervention should only come second.

**Climate and sea level fluctuations:** Since the last ice age, after the melting of glacial ice on Fennoscandia, the North Skandinavian landmasses have risen 80–90 cm per century. At the same time, a tilting motion of the Earth's crust has caused a 10–20 cm subsidence of the German Baltic coast per century. However, this fact only partly explains the increasing number of storm surges observed in the 20th century. Detailed investigations of storm surge occurrences have revealed correlation with characteristic atmospheric circulation patterns and certain parameters of the circumpolar low pressure zone (North Atlantic oscillation). Storm surges in the Baltic Sea thus also serve as an interesting indicator of climate developments in Central and Northern Europe. Numerous astronomical tides, primarily those having very long periods, have been identified in the mean sea levels of the Baltic. A significant cycle of 10–11 years has been found which is related to solar activity. However, as the changes observed in the parameters of the circumpolar low-pressure zone are extremely small, this causal relationship is still considered to be an unsatisfactorily proven despite the informative studies of CURRIE (1981) and LABITZKE and VAN LOON (1988). A different interpretation is rather unlikely, though, considering the fact that the phases of the 10–11 a signal measured at all Baltic gauges differ by about 130° between the northern and southern Baltic areas. The climate signal even exhibits a phase difference of about 170° in this respect. A counter-running trend like this, which could also be interpreted as a variable longitudinal tilt in the water surface, can only mean that the cause is an internal phenomenon of the Baltic region, which is not based primarily on hydrodynamic characteristics of the North Atlantic. Periods attributable to the latter (e.g. the Saros period, or half-period of moon apse-line cycle) only exhibit minor phase differences between the northern and southern Baltic Sea levels. The high correlation between wind fields in the Baltic and water levels in the time window of high and low water occurrences confirms this interpretation.

**Scenarios and statistics:** The physical processes and causes of storm surges in the Baltic will continue unchanged also in the future. The travel time of gravity waves is bound to a mean Baltic Sea depth of some 55 meters, so that even a hypothetical rise or fall of the mean sea level by one meter would not cause major changes in the natural periods of the Baltic. Forcing of storm surges depends, among other factors, on changes in wind direction and speed per space or time unit. For example, higher increase rates in a scenario of rapidly tracking low-pressure zones would be compensated partly by the shorter period available for integration of the water levels until high water stand. A preferred method for predicting regional trends during storm surges does not exist presently. Flood protection measures are based generally on the highest water levels on record and take into account regional sea level trends. In this context, the climate scenarios developed by the IPCC are undoubtedly relevant. However, with regard to the functionality of port facilities or initiatives of environmental protection organisations to protect salt marshes in the area, i.e. wherever a certain acceptance of storm surge events may be assumed, statistical methods are preferred in assessing the probability of flooding. Although they clearly indicate an increase in the number of small and medium-size flood events in the 20th century, they do not show significant increases in the high water crest values. Also statistically significant data beyond the scatter of measurements, which might confirm an acceleration of sea level rise in the 20th century, have not been found. Because of the Baltic's own dynamics, an analysis of its storm surge climate should be based rather on weather scenarios than on water level data.

### *Sweden*

BERGSTEN (1955) studied the relationship between winds and the water levels on the coasts of Sweden. He stated (p. 32-133):

Generally, the water level in the South Baltic rises when the winds are northerly, and falls when they are southerly ... The consequence is that on the south coasts of Skane and Blekinge offshore winds will raise the water level, and winds from the sea will reduce it ... Another consequence is that the water level in the Sound and the Belts will be greatly changed in height; e.g., SW gales are blowing, as these will lower the water level in the South Baltic, and raise it on the west coast. The difference between the levels in the South Baltic and the west coast may in extreme cases be as much as a couple of meters. As far as the Sound is concerned, the difference is concentrated on the very short distance from Limhamn to Klagshamn, where a submarine bank runs from the Swedish to the Danish side, constituting the boundary between the Baltic and the western seas. North-easterly gales reverse these conditions.

The surges at five locations on the Baltic coast of Sweden for the storm surge of January 2-5, 1954, are shown in 7.28. This surge was generated by a northerly gale. The surge at Björn on January 3 is particularly interesting because it shows that the Aland archipelago acts as a strong barrier to the southward flow of water.

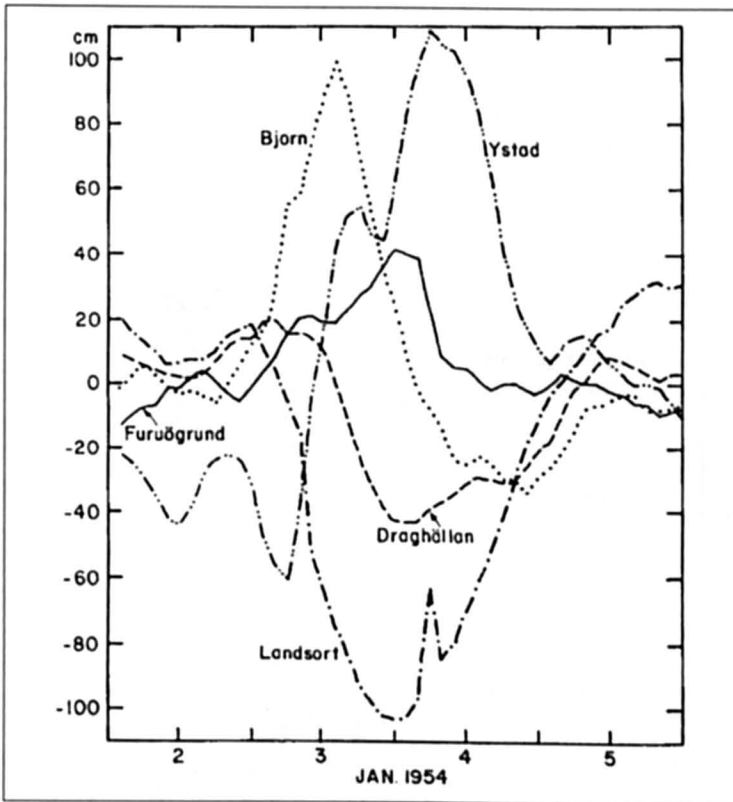


Fig. 7.28: Observed storm surges on the Baltic Sea coast of Sweden during January 2–5, 1954 (BERGSTEN, 1955)

### Denmark

Denmark is attacked by storm surges at both the east and west coasts, i.e. from the Baltic Sea and the North Sea.

EGEDAL (1957) examined the storm surges at Randers on the east coast of Jutland. Depressions traveling over Jutland from the west cause north-northeasterly winds, which generate surges on the east coast of Jutland. Another area where surges are generated by such a weather system is the Island of Funen (Fyn). EGEDAL remarked that as far as storm surges are concerned, there are similarities between the east coast of Jutland and the east coast of the United Kingdom.

RINGE-JORGENSEN (1958) studied the storm surges along the North Sea coast of Denmark. The tidal amplitude varies from about 1.5 m near the Danish-German boundary to about 0.4 m at Thyboron. This study suggested that a meteorological situation similar to that of January 31–February 2, 1953, event could cause surges with amplitudes up to 3.4 m at Harlingen (Holland) and only about 1 m at Hanstholm (50 km north of Thyboron). The influence of the Norwegian Ditch appears to prevent the occurrence of very large amplitude surges at Thyboron but permits the occurrence of a large number of moderate surges.

LACOUR (1917a) studied the storm surge of January 15–16, 1916. He presented tables of the surge amplitudes at 46 locations at every hour from 12:00 on the 15th to 00:00 on the 17th. He also showed several diagrams of winds, currents and the water level at various times. Peak surges up to 1.9 m occurred. The distribution of the storm surge heights at 06:00 January 16, 1916, is given in Fig. 7.29.

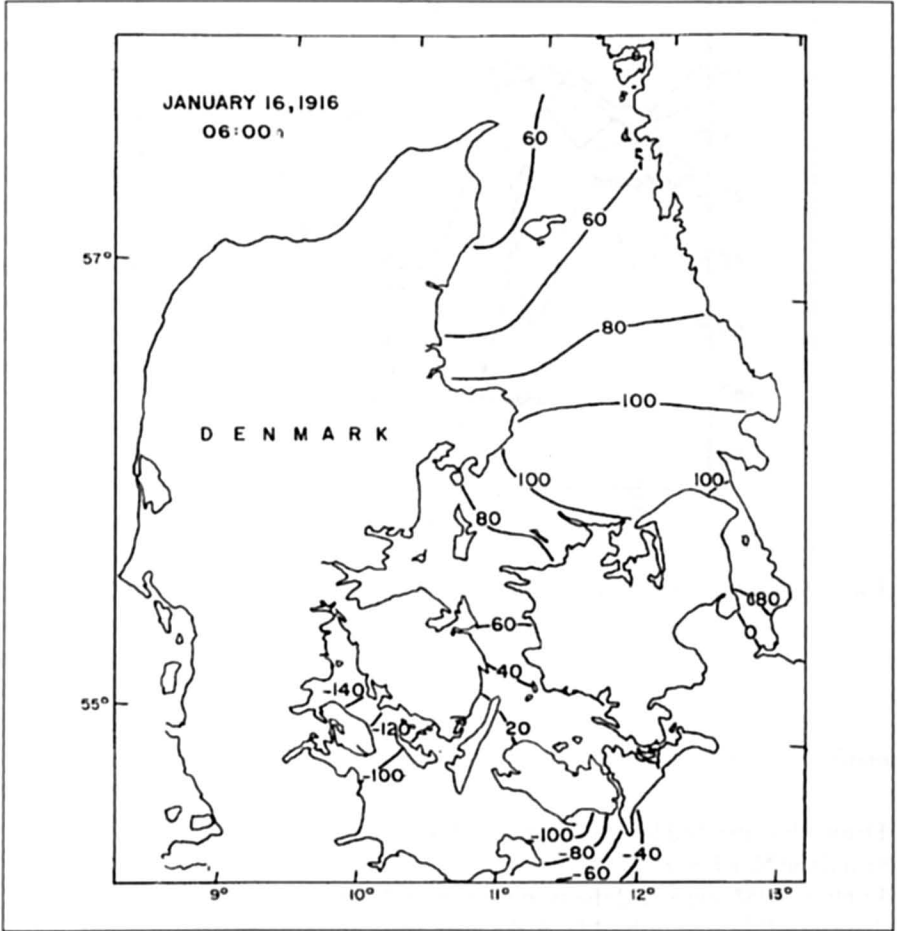


Fig. 7.29: Storm surge amplitudes along the east coast of Denmark at 06:00 on January 16, 1916 (LACOUR, 1932)

## 7.3.3 Irish Sea

In section 5.1.2 the meteorological situations leading to storm surges in the Irish Sea were discussed. The storm surge at Liverpool during December 29, 1921, to January 2, 1922, and the pressure data are shown in Fig. 7.30. CRESWELL (1929) presented storm surge amplitudes at Holyhead, Belfast, Fleetwood and Preston for the surge of October 20–24, 1928. These range from 1 ft 7 in. (48 cm) to 4 ft 7 in. (140 cm). However, a surge on October 29, 1927, had amplitudes of 7 ft 8 in. (2.34 m) at Fleetwood and 10 ft 2 in. (3.1 m) at Preston. For this event, the amplitudes at Holyhead and Belfast were 3 ft 4 in. (1.04 m) and 3 ft 2 in. (0.97 m), respectively.

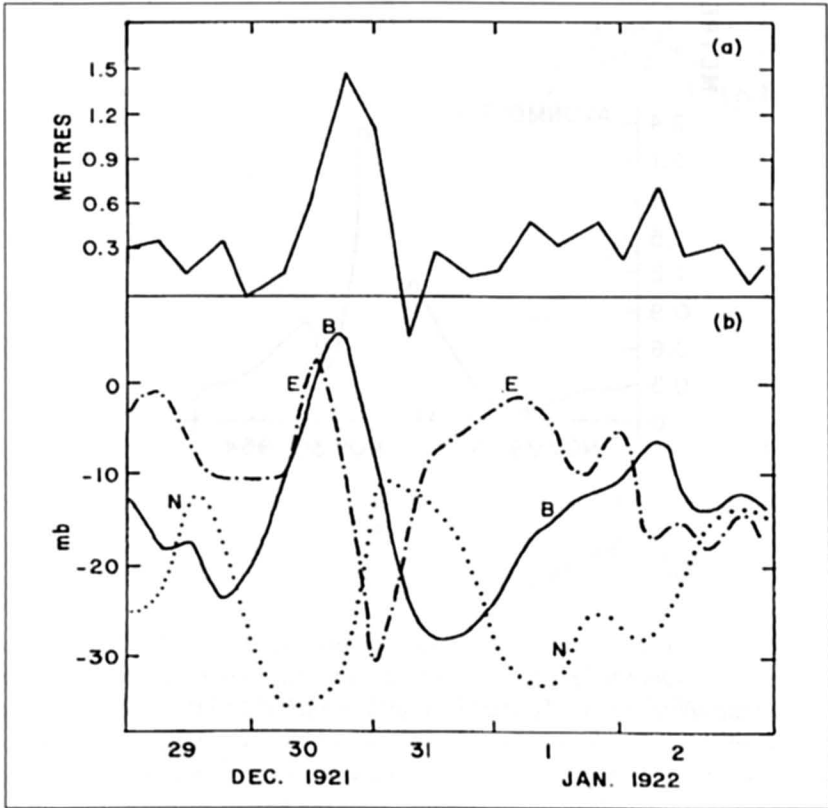


Fig. 7.30: (a) Storm surge at Liverpool, U.K., during December 29, 1921–January 2, 1922. (b) Curve B shows the fall of the atmospheric pressure at Liverpool; curves E and N, respectively, denote the east and north pressure gradients (millibars per 800 km) (DOODSON and DINES, 1929)

During the storm surge event of January 31, 1957, the surge amplitude at Liverpool reached a peak value of 3 ft whereas another event on February 4, 1957, produced a surge with amplitude of 5.8 ft (1.76 m). Another surge event of January 11–12, 1962, produced surges up to 5.5 ft (1.68 m) at Liverpool and up to 6.5 ft (1.98 m) at Avonmouth. The surges at Milfordhaven and Avonmouth during November 29–30, 1954, are shown in Fig. 7.31.

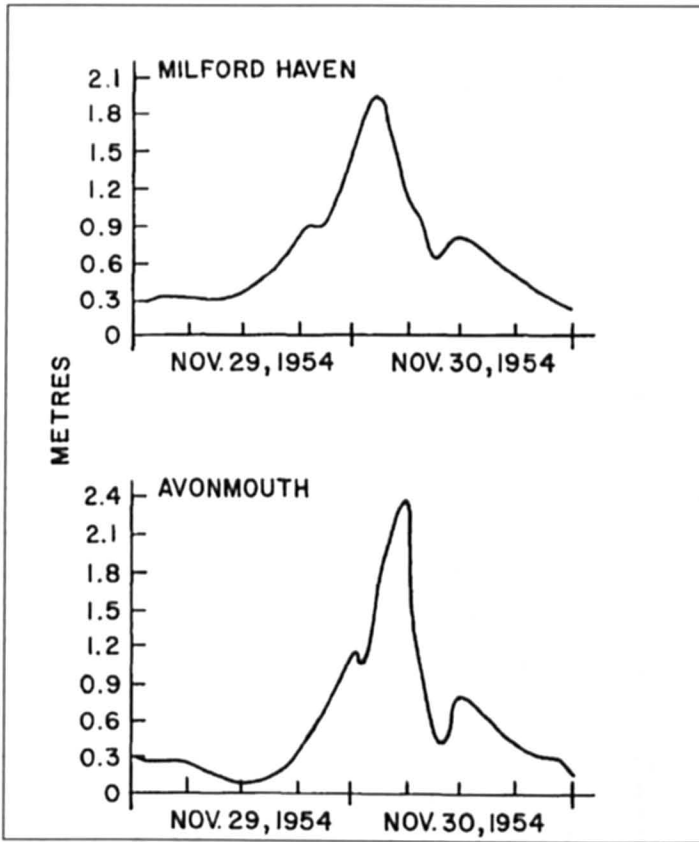


Fig. 7.31: Storm surges at Milford Haven and Avonmouth, U.K., during November 29–30, 1954 (HEAPS, 1967)

CORKAN (1952) mentioned that localized northerly winds over the Irish Sea would lower the water level everywhere in this water body, with the minimum decrease occurring at Liverpool. Strong southerly winds near the southern entrance to the Georges Channel will produce only small surges at locations such as Cork and Newlyn. After several hours, the general level rises in the Irish Sea. On the other hand, when a depression exists south of Ireland (with strong southerly winds blowing steadily) over the Bay of Biscay, surges up to 1–2 ft (0.3–0.6 m) could occur inside the region bordered by a hypothetical line joining Cork to Newlyn.

HEAPS and JONES (1975) simulated the storm surge in the Irish Sea for the event of January 10–18, 1965, using a two-and-a-half-dimensional model. The surge profiles at several locations in the Irish Sea (observed and computed) are shown in Fig. 7.32. The horizontal distribution of the storm surge heights at two different times is given in Fig. 7.33.

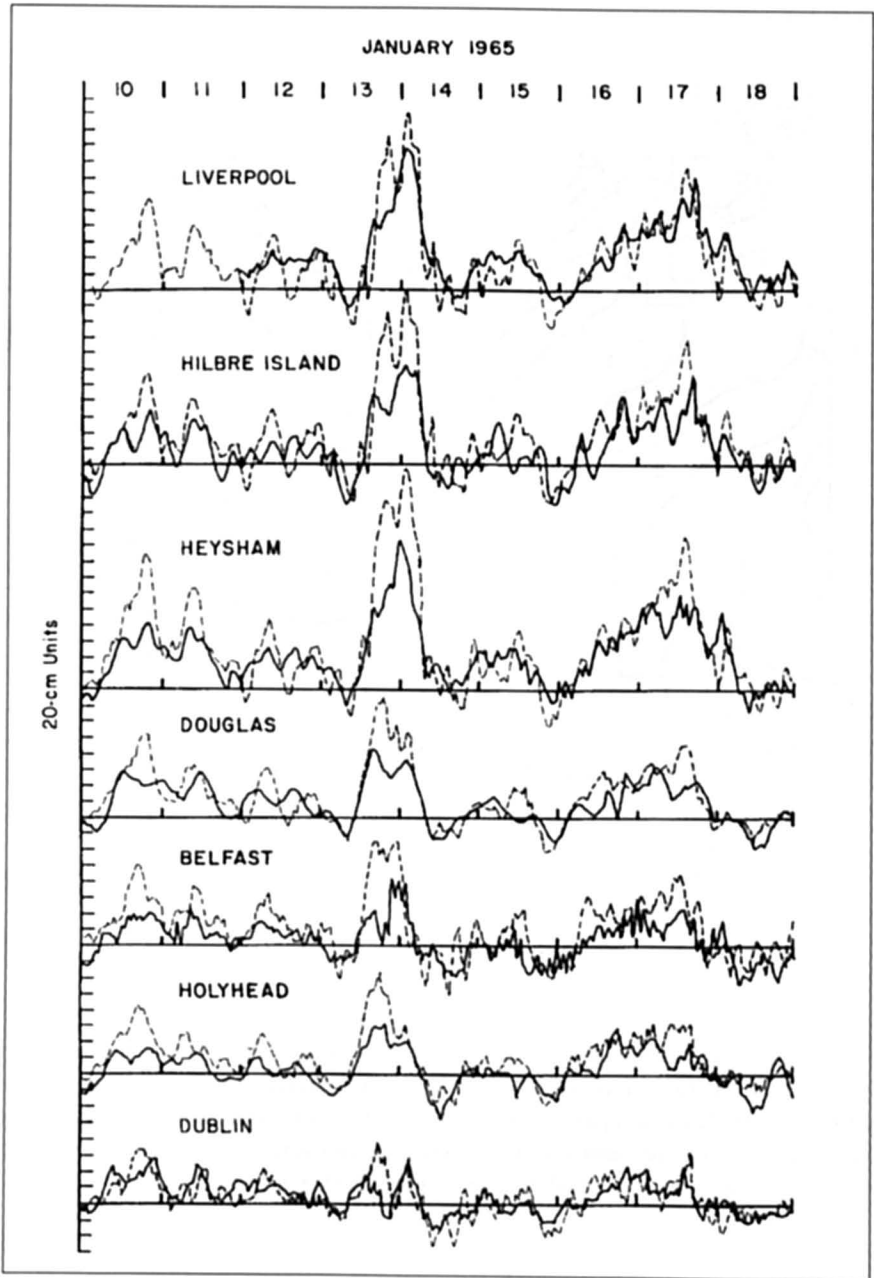


Fig. 7.32: Storm surges at various locations around the Irish Sea during January 10-19, 1965 (One unit = 20 cm along the ordinate) (HEAPS and JONES, 1975)

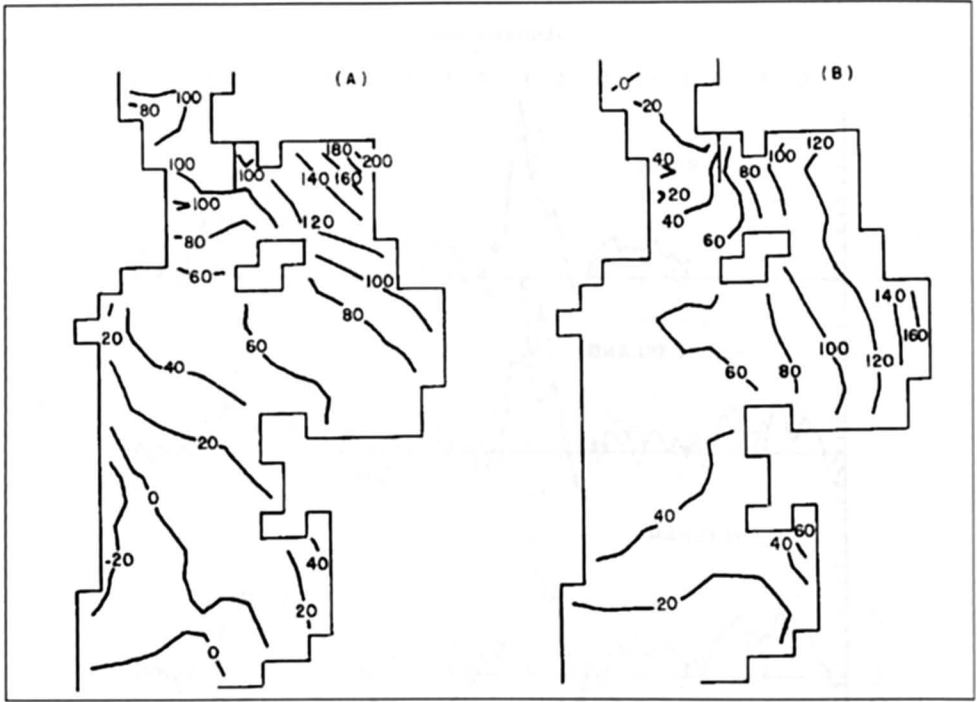


Fig. 7.33: Distribution of storm surge heights (centimeters) in the Irish Sea on January 14, 1965, at (A) 00:00 and (B) 04:00 (HEAPS and JONES, 1975)

HEAPS and JONES (1979) also simulated the storm surges in the Irish Sea for the events of November 11–15, 1977, and January 2–3, 1976, and compared these with the event of January 13–17, 1965. They paid particular attention to the time of occurrence of the peak surge relative to the times of high and low water. The tide and surge (computed and observed) at Liverpool and at Workington are shown in 7.34 and 7.35, respectively.

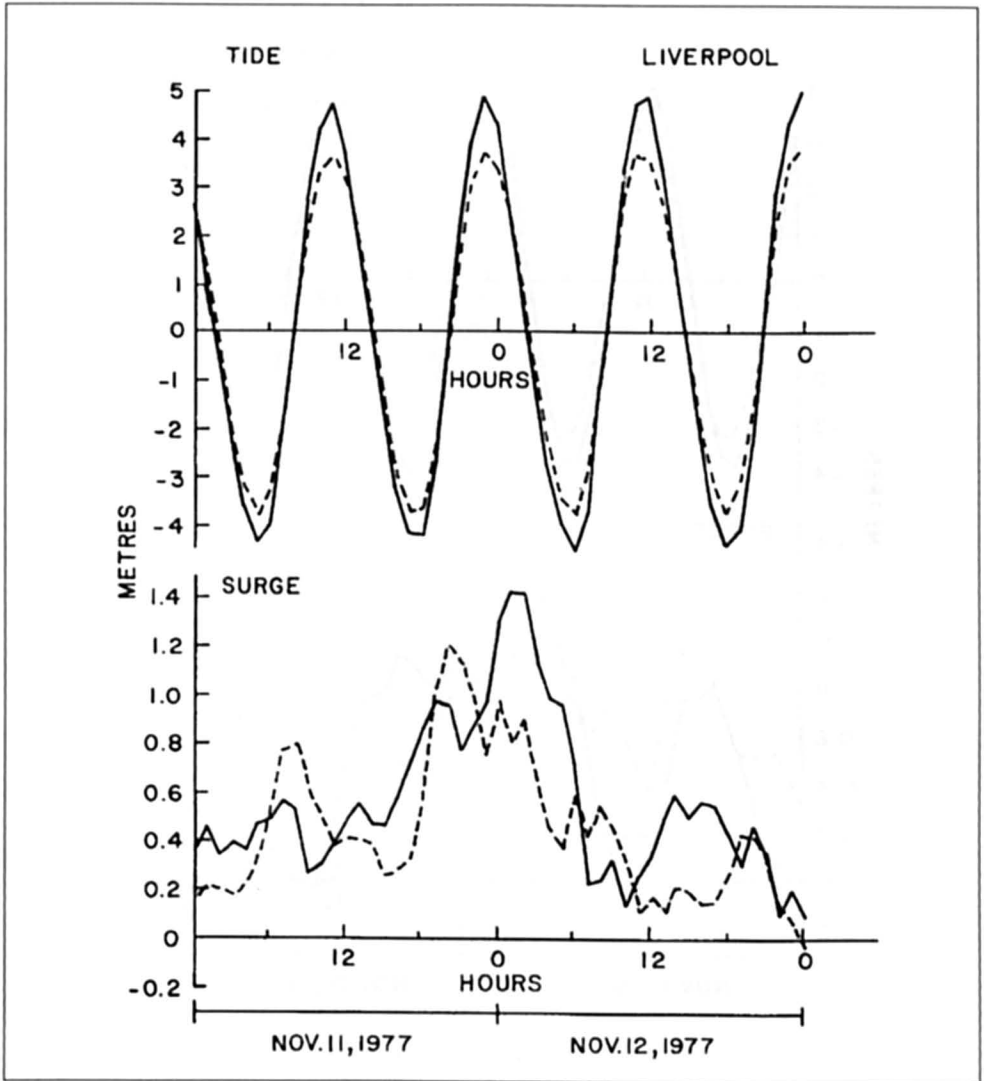


Fig. 7.34: Top: observed (solid line) and computed (broken line) tide at Liverpool during November 11-12, 1977. Bottom: observed (solid line) and computed (broken line) surge at Liverpool for the same period (HEAPS and JONES, 1979)

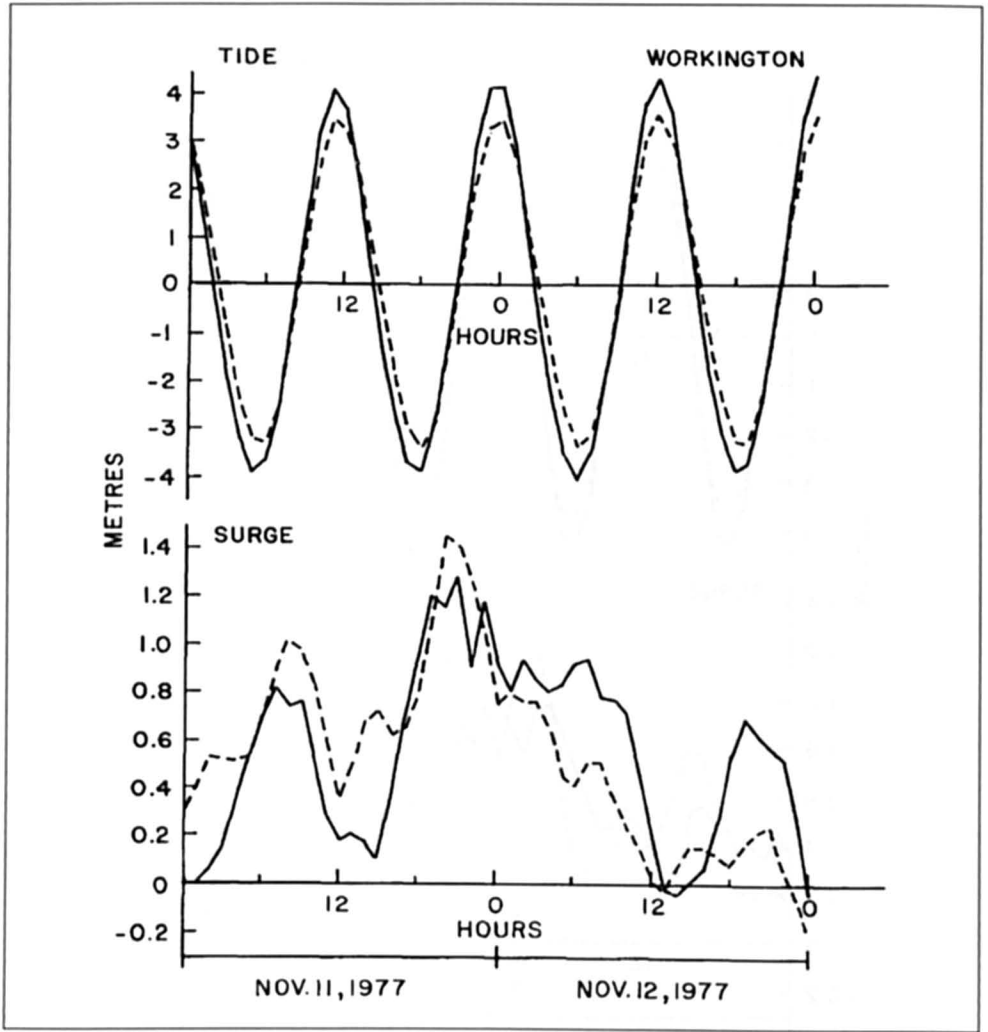


Fig. 7.35: Tide and storm surge at Workington, U.K. See Fig. 7.34 for explanation (HEAPS and JONES, 1979)

## 7.3.4 Mediterranean Sea

*France*

The North Sea coast of France was discussed earlier. Here, the Atlantic and Mediterranean Sea coasts of France will be considered.

FABRY (1909) studied the surge near Marseille (on the Mediterranean Sea coast of France) of June 15, 1909. The surge amplitude was between 0.4 and 0.8 m and an earthquake might have caused this, making this water level oscillation a tsunami rather than a storm surge. Some water level oscillations can occur in this region due to landslides.

CREPON (1974) studied water level oscillations on the Mediterranean coast of France. Note that in this area the tidal range is rather small (less than 1 m). Crepon applied his analytical theory to study the water levels at Sète located at the Mediterranean coast of France. Here, the continental shelf is about 100 km wide with a water depth of 90 m and there are no significant orographic influences on the wind field. The observed and computed water levels at this location for the period January–March 1969 are compared in 7.36. Some storm surge effects can be seen around the following dates: January 3–4, February 17–22, February 27, and March 21–23. It is interesting to note that the calculated water levels are systematically lower than the observed values.

LACOUR (1917b) studied the storm surges at Brest (on the Atlantic coast of France) for the period 1861–1905. It appears that no significant surges occurred. One may conclude that storm surges are probably not significant in France except on the North Sea coast.

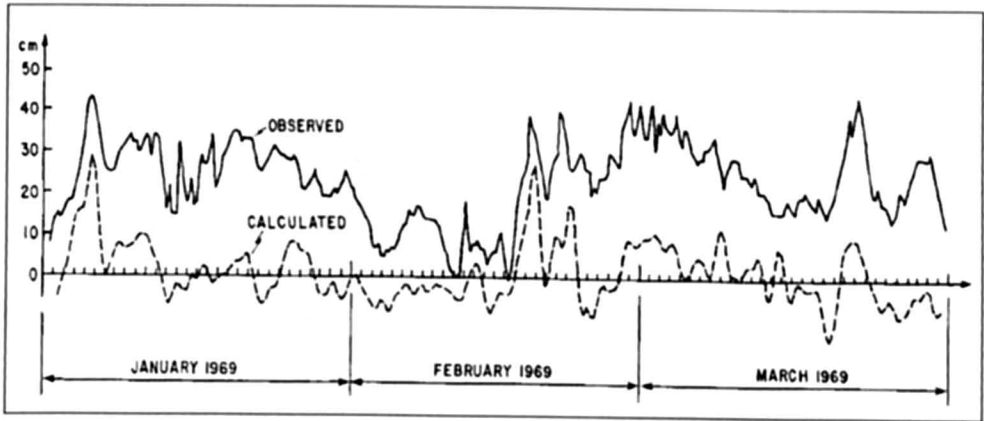


Fig. 7.36: Observed and calculated water levels at Sète (on the Mediterranean coast of France) for the period January–March 1969 (CREPON, 1974)

*Israel*

STRIEM (1974) studied the storm surges at Ashdod at the Mediterranean coast of Israel using the data for a 6yr period (1965–70). The tide here is mainly semidiurnal with a range of less than 1 m. The data for this study were selected whenever the daily mean sea level exceeded the average level by at least 20 cm and when there was a storm present.

STRIEM (1974) used the term “storm surge” to denote the changes in sea level at Ashdod during a period of several days due to storms in the eastern part of the Mediterranean Sea and

the term "storm set-up" to denote the rapid changes in the water level during a few hours. Three examples of these storm set-ups are shown in 7.37.

The six largest positive storm surges at Ashdod during the period of this study are summarized in Table 7.9a. The six largest negative storm surges at Ashdod are listed in Table 7.9b. The factors that cause the sea level to rise and fall at Ashdod are summarized in Tables 7.10 and 7.11, respectively. It was found that the storm surges at Ashdod basically are gradual changes in the daily mean sea level and that these changes could be linearly correlated with daily mean values of wind wave heights and wind velocities at the shore.

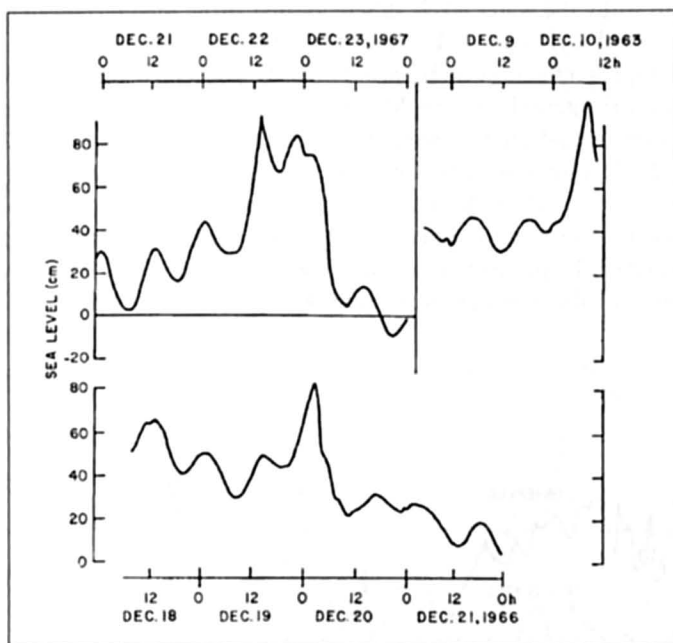


Fig. 7.37: Storm surges at Ashdod, Israel. Examples are shown of rapid changes. Top left: December 21–23, 1967; top right: December 9–10, 1963; bottom: December 19–21, 1966 (STRIEM, 1974)

Table 7.9a: Six largest positive storm surges at Ashdod, Israel, during 1965–70 (STRIEM, 1974)

Date	Amplitude of surge (cm)
Dec. 10, 1963	100
Dec. 22, 1967	93
Dec. 20, 1966	83
Feb. 5, 1965	63
Mar. 26, 1967	63
Jan. 14, 1968	63

Table 7.9b: Six largest negative storm surges at Ashdod, Israel, during 1965–70 (STRIEM, 1974)

Date	Amplitude of surge (cm)
Jan. 29, 1964	51
Mar. 24, 1966	46
Mar. 26, 1968	45
Feb. 12, 1968	42
Oct. 16, 1970	41
Apr. 12, 1968	40

Table 7.10: Factors contributing to the rise of sea level at Ashdod, Israel (STRIEM, 1974)

Factor	Time of occurrence	Approx. maximum rise of sea level (cm)
(a) High of spring tides	Vernal equinox	+ 26
(b) High of the seasonal fluctuation	Midsummer	+ 10
(c) High annual mean sea level		+ 7
(d) Rise due to daily inequality of the tides		+ 5
Total of effects not due to wind		+ 48
(e) Storm surges	Winter	+ 40
(f) Storm set-up	Winter	+ 40

Table 7.11: Factors contributing to the lowering of sea level at Ashdod, Israel (STRIEM, 1974)

Factor	Time of occurrence	Approx. maximum fall in sea level (cm)
(a) Extreme low of spring tides	Vernal equinox	- 26
(b) Low of the seasonal fluctuation	End of spring	- 10
(c) Low of annual levels		- 6
(d) Lowering due to daily inequality of the tides		- 5
Total of effects not due to wind		- 47
(e) Lowering due to eastern (offshore) winds (or down-surge after onshore storms)		- 15 (or - 30)
Possible lowering due to occurrence of all factors		- 62 (or -77)

### *Egypt*

Storm surges occur in the Suez Canal and also at the Mediterranean coast of Egypt. MURTY and ELSABH (1981) studied the storm surges at Port Said at the northern end of the Suez Canal and at Port Suez at the southern end of the canal using the data for 1966.

Table 7.12: Number of occasions (treating each hourly value as one case) when positive and negative storm surges at Port Said, Egypt, exceeded prescribed amplitudes in 1966

State of tide	Surge height (cm)									
	10	20	30	40	50	60	70	80	90	100
Positive surges										
Low tide	253	189	90	28	9	5	1	1	1	1
Rising tide	236	137	51	10	1	0	0	0	0	0
High tide	237	131	44	2	0	0	0	0	0	0
Falling tide	246	175	82	26	6	2	1	0	0	0
Negative surges										
Low tide	19	7	3	2	0	0	0	0	0	0
Rising tide	16	9	3	2	1	1	0	0	0	0
High tide	12	5	1	1	1	1	1	1	1	1
Falling tide	13	5	0	0	0	0	0	0	0	0

The length of the Suez Canal is about 175 km and the average depth is 15 m. At Port Said the tide is co-oscillating with the eastern part of the Mediterranean Sea and has an amplitude of 25 cm. At Port Suez the Red Sea tidal influence is felt and has an amplitude of 75 cm. Based on these features the Suez Canal can be classified into a long estuary, in the Proudman sense (discussed earlier under Tide-Surge Interaction in the North Sea and in the St. Lawrence Estuary).

Treating each hourly surge value as one case, the number of occasions when positive and negative surges exceeded prescribed values at Port Said and Port Suez is given in Tables 7.12 and 7.13, respectively. Earlier, it was seen that PROUDMAN's theory (1957) suggested that for a long estuary, for a tide of progressive wave type, maximum surges are associated predominantly with low tide (or rising tide), and for a tide of standing wave type, maximum surges are associated predominantly with high tide (or falling tide). Observations for 1966 showed that the theoretical results of PROUDMAN, when interpreted for the Suez Canal, agreed with the observations at Port Said but not with those at Port Suez.

Table 7.13: Number of occasions (treating each hourly value as one case) when positive and negative storm surges at Port Suez, Egypt, exceeded prescribed amplitudes for positive surges and 10–90 cm for negative surges in 1966

State of tide	Surge height (cm)													
	10	20	30	40	50	60	70	80	90	100	110	120	130	140
Positive surges														
Low tide	172	111	75	44	32	16	8	3	3	3	3	3	2	1
Rising tide	191	110	76	38	13	7	6	6	3	1	0	0	0	0
High tide	121	57	18	5	2	1	1	1	1	0	0	0	0	0
Falling tide	174	107	50	34	27	23	10	3	0	0	0	0	0	0
Negative surges														
Low tide	84	66	46	32	16	11	3	0	0					
Rising tide	104	69	45	45	14	21	1	0	0					
High tide	117	69	59	49	40	24	6	0	0					
Falling tide	113	84	55	27	38	9	9	2	1					

### 7.3.5 European Part of the Atlantic Ocean

Storm surges at the Atlantic coast of France have been described before. Storm surges can also occur at the northern part of the Atlantic coast of Portugal (MORAIS and ABECASIS, 1975). The tidal range in this area is about 3–8 m and wind waves up to 13 m can occur here. A surge during January 16–17, 1973, did considerable damage in the Leixoes Harbour. The damage was severe because the surge occurred at the time of spring tide. The center of a low pressure system passed over Leixoes and its exceptionally long duration of 24 h generated very large wind waves.

In the surge record, waves with periods between 4 and 40 min attained significant amplitudes. Leixoes Harbour exhibits a seiche with a 4-min period, which was amplified by resonance. There is evidence of the occurrence of a Helmholtz mode type motion also.

Storm surges occurred again in January and February 1974 but the damage was minimal.

### 7.3.6 Adriatic Sea

In Italy, storm surges occur along the Ligurian Sea coast, the Tyrrhenian Sea coast, and the Adriatic Sea coast. On February 18, 1955, a cyclone caused great damage to the breakwater in Genoa Harbour (GRIMALDI, 1955; D'ARRIGO, 1955). Strong winds from the southwest-generated wind waves with greater than 7-m amplitudes and possibly also a storm surge. Some of the water level problems in the Ligurian Sea associated with weather systems were discussed in section 5.1.2. Northeastern Italy is a region where storm surges occur. BONDESAN et al. (1995) investigated the effect of global change on sea surges and stated that the frequency would increase.

The city of Venice is located at a lagoon off the Adriatic Sea and less than 1 m above the mean sea level. Hence, storm surges with amplitudes less than even 1 m cause serious flooding problems in Venice. To add to the problem, the openings between the sea and the lagoon are more extensive now (due to dredging) than before, which allows the storm surge from the sea to travel unimpeded. In addition, in the twentieth century the city subsided by 20 cm.

Storm surges occur quite frequently in this area (TOMASIN and FRASETTO, 1979), for example, in the years 1966, 1967 and 1972. The storm surge season lasts from November to February and occasionally to April. The first two normal modes of the Adriatic Sea have periods quite close to the diurnal and semidiurnal tides. The tidal range is 25–80 cm, the tide being forced by the Mediterranean Sea. There appears to be no interaction between the tide and the surge.

TOMASIN and FRASETTO (1979) studied the surge of April 21–22, 1967 (Fig. 7.38). What makes the problem more complicated is a seiche with a period of about 1 d that can be excited by weather systems. Such a seiche during February 16–20, 1967, is shown in Fig. 7.39. Observed and computed surges at Venice for February 12, 1972, are shown in Fig. 7.40. In the fall of 1982, major storm surges occurred at Venice and Trieste causing considerable damage.

In 1975 the Italian government devised a plan to reduce the effects of tides and storm surges at Venice by constructing barriers to narrow the entrances to the Venice lagoon (VITTORI and TAMPIERI, 1979).

The commune of Venice operates a statistical forecast model. ADAMI and NOLI (1992) describe this model and present an alternative modelling tool, which has been tested by the Danish Hydraulic Institute. "It was found that the existence of reliable air pressure predictions could increase the forecast horizon of reliable storm surge prediction from 3 to 24 hours."

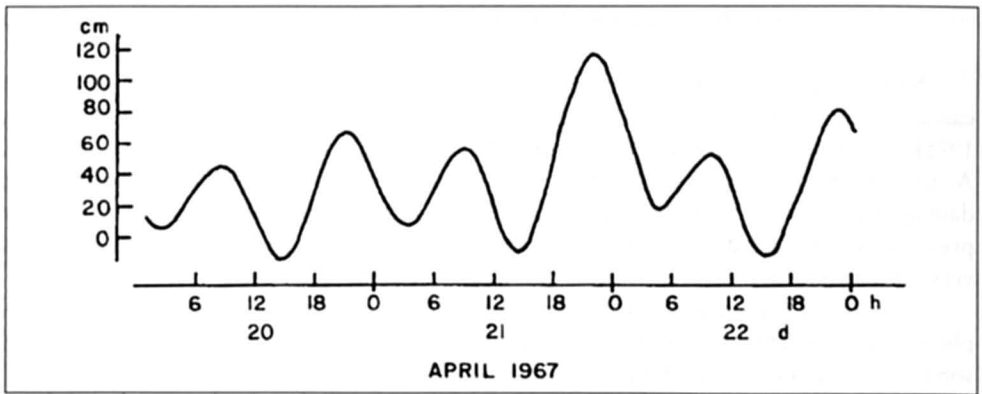


Fig. 7.38: Recorded water level (tide plus surge) at Venice, Italy, during April 20–22, 1967. Time is GMT – 1 (TOMASIN and FRASETTO, 1980)

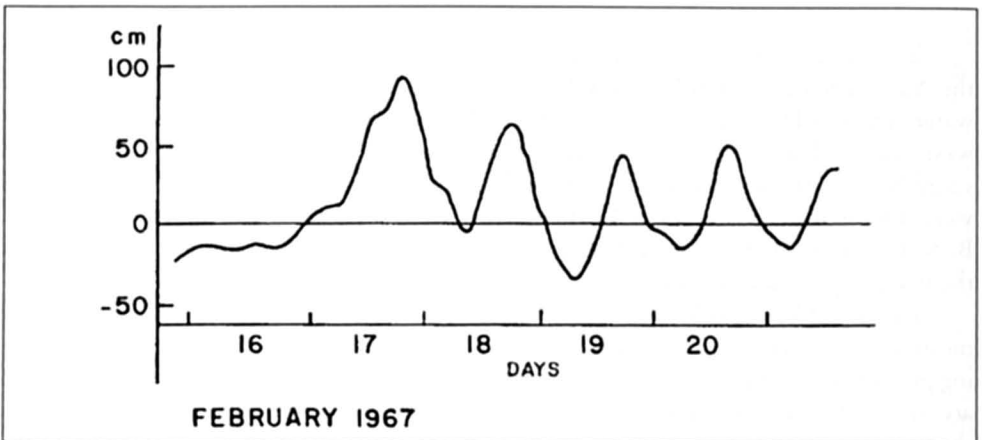


Fig. 7.39: Seiche at Venice, Italy, with a period of approximately 24 h (TOMASIN and FRASETTO, 1979)

STRAVISI (1972) used a one-dimensional numerical model to simulate hypothetical storm surges in the Adriatic Sea. Storm surge amplitudes at two different times are shown in Fig. 41. ADAMI and NOLI (1992) also carried out research on a forecasting system with a hydrodynamic model for the Adriatic. The Danish Hydraulic Institute calibrated a 2D model to reproduce tidal phenomena and seiching. To calibrate the storm surges at least seven historical surge events were simulated with storm winds and air pressures. With good meteorological data storm surge prognosis was very good for forecast up to 5 days.

For the Northern Adriatic Sea MAZARELLA and PALUMBO (1991) took into consideration the seasonal, 11-yr. and secular signals, which are more significant and several times larger than those in the mean sea level for the computation of the storm surge development and mean sea level rise. They stated that analyses of sea level maxima adjusted for such time variations, gives a more adequate and realistic basis for making predictions on the occurrence of damaging storm surges. Data from the gauges at Venice (1924–1970) and Trieste (1944–1988) have been investigated. After using the extension of the annual maxima approach from earlier work for calculation of the occurrence of extreme events calculated non-cycle

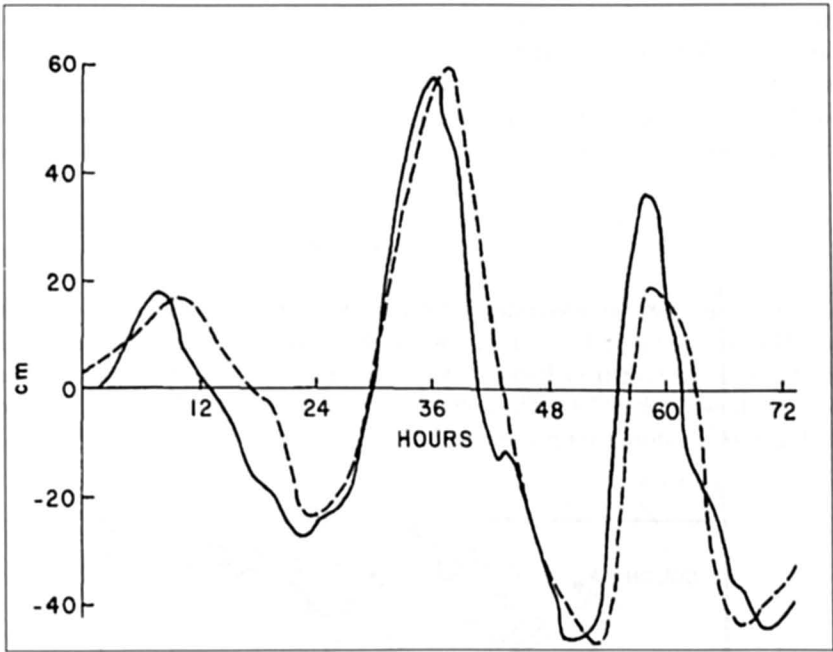


Fig. 7.40: Computed (broken line) and observed (solid line) surges at Venice during February 12-15, 1972. Time is hours from the starting time of 03:00 (GMT) on February 12, 1972 (TOMASIN and FRASETTO, 1979)

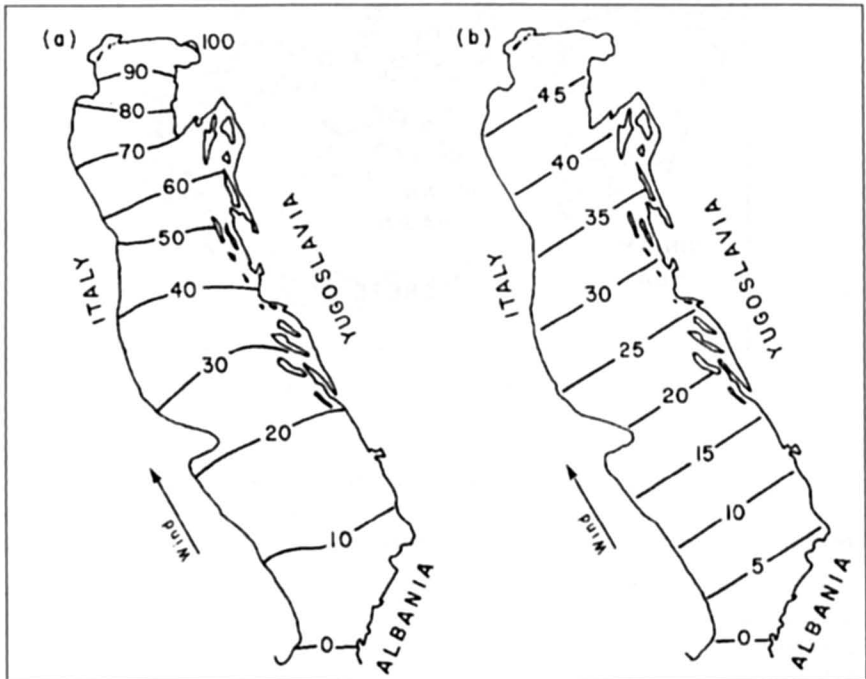


Fig. 7.41: Distribution of the amplitudes (centimeters) of a hypothetical storm surge in the Adriatic Sea at (a) 10 h and (b) 11 h after the start of wind stress application (STRAVISI, 1972)

variations of yearly SL mean and SL max, cycle variations seasonal and 11 yr. Waves have been carried out. MAZARELLA and PALUMBO (1991) summarised their results by stating that "the estimate of the return period obtained by means of the monthly maxima (filtered from seasonal, biennial and longer term non-stationary) is more robust against historical outliers than the analysis of annual maxima."

### 7.3.7 Aegean Sea

WILDING et al. (1980) studied tides and storm surges in the northwestern part of the Aegean Sea. The geography of this area is shown in Fig. 7.42. The tides are rather small in this water body, as can be seen from Table 7.13. The surges during August 20–23, 1975, at three locations are shown in Fig. 7.43. The power spectrum of half-hourly water level records is given in Fig. 7.44. Predominant periods of 2.68 and 2.40 h can be seen.



Fig. 7.42: Geography of the Aegean Sea (WILDING et al., 1980)

Table 7.14: Tides in the Aegean Sea (WILDING et al., 1980)

Location	Mean spring range (cm)	Mean neap range (cm)
Port Salonica	32.4	9.6
Saint Trias	29.0	6.6
Krini	29.6	4.4
Whaniona	29.4	5.0
Kayoura	29.0	4.6

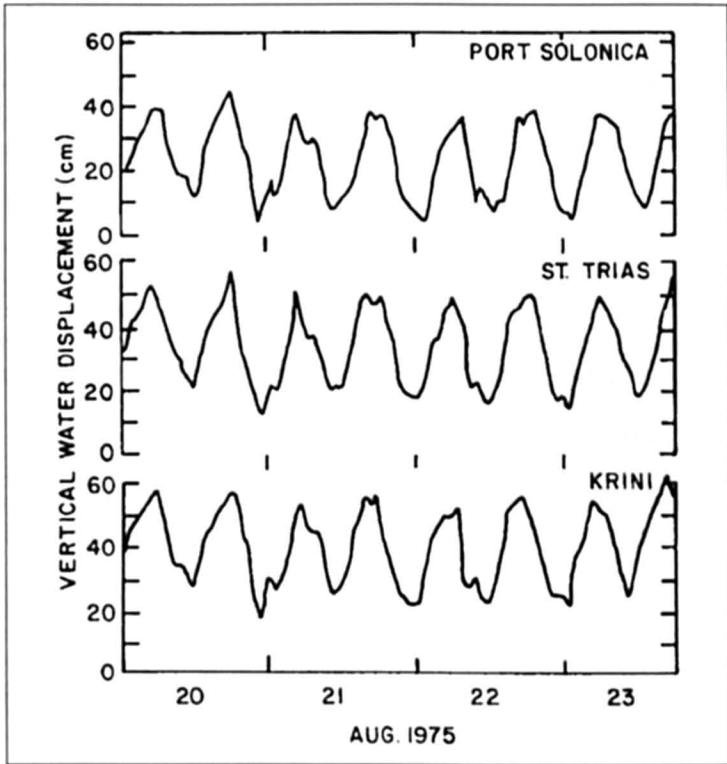


Fig. 7.43: Water level oscillations during August 20–23, 1975, at three locations in the Aegean Sea (WILDING et al., 1980)

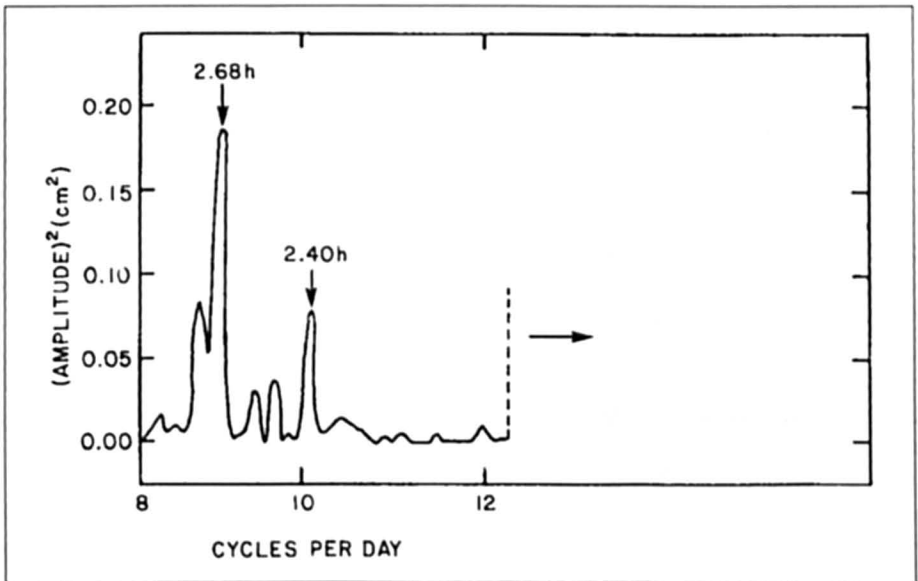


Fig. 7.44: Power spectrum of half-hourly water level data at Port Solonica (Aegean Sea) (WILDING et al., 1980)

## 7.3.8 Black Sea, the Okhotsk Sea and the Pacific

Moderate storm surges occur in the Black Sea, the Okhotsk Sea, the Pacific coast of Russia, the East Siberian Sea, and the Chukchi Sea. Large surges (up to 6 m in amplitude) can occur in Lake Baikal. Winds from north of this lake can produce surges that sometimes take only a few minutes to develop.

Earlier, the work of LAPPO and ROZHDESTVENSKIY (1977, 1979) was discussed in which they considered the lag of storm surges with reference to the atmospheric systems. Their work covered the northwest part of the Pacific Ocean in general and the Pacific coast of Russia near the Kurile Islands in particular. They considered the contribution of the static surge to the total water level deviation and developed the important concept of the hysteresis loop (Fig. 6.123). The lag between the atmospheric forcing and the storm surge could be anywhere between 5 and 18 h on this part of the Russia coast.

KOWALIK and POLYAKOV (1998) studied the tides in the Sea of Okhotsk. This is a region of large tidal sea level oscillations and strong tidal currents. The oscillation reaches 13 m in Penzhinskaya Guba. GORDAY et al. (1991) investigated extreme parameters of tsunamis in the region of Kuril-Kamchatka Trench and the Sea of Okhotsk using numerical simulation results.

MUSTAFIN (1969) studied the storm surges in the East Siberian and Chukchi seas with the particular aim of predicting the surges at Cape Schmidt. Based on 192 cases during the summer period (July–October) for 1951–55, in which the surges at Cape Schmidt and in Ambarchik Inlet exceeded 30 cm (both positive and negative surges), he prepared the following regression relationships:

$$\Delta h_{\text{Schm}} = a_1 \Delta p_1 \cos \alpha_1 + a_2 \Delta p_2 \cos \alpha_2 + a_3 \Delta h_{\text{Amp}} \quad (7.1)$$

$$R = 0.94 \pm 0.001, \quad \Sigma = 21$$

$$\Delta h_{\text{Schm}} = a_4 \Delta h_{\text{Amp}} \quad (7.2)$$

$$R = 0.90 \pm 0.01, \quad \Sigma = 26$$

$$\Delta h_{\text{Schm}} = a_5 \Delta p_1 \cos \alpha_1 + a_6 \Delta h_{\text{Amp}} b_1 \quad (7.3)$$

$$R = 0.93 \pm 0.004, \quad \Sigma = 23$$

$$\Delta h_{\text{Schm}} = a_7 \Delta p_2 \cos \alpha_2 + a_8 \Delta h_{\text{Amp}} b_3 \quad (7.4)$$

$$R = 0.92 \pm 0.007, \quad \Sigma = 24$$

$$\Delta h_{\text{Schm}} = a_9 \Delta p_1 \cos \alpha_1 + a_{10} \Delta p_2 \cos \alpha_2 + b_4 \quad (7.5)$$

$$R = 0.88 \pm 0.01, \quad \Sigma = 29 \quad (7.6)$$

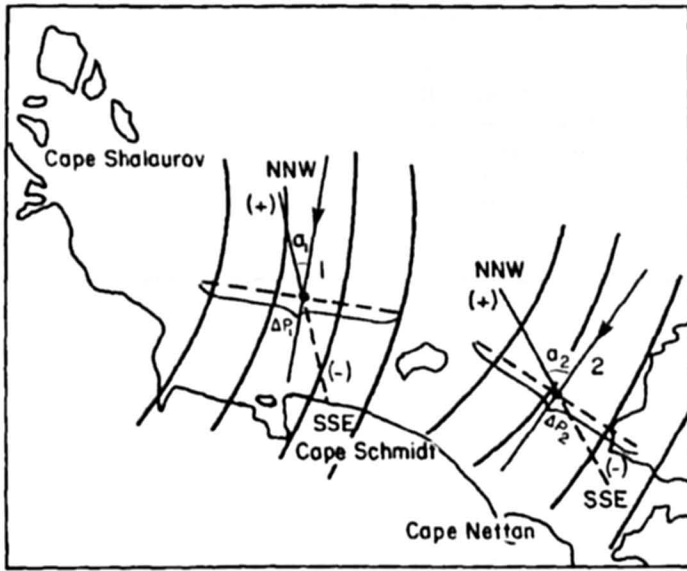


Fig. 7.45. Determination of the quantities  $\Delta p_1$ , and  $\Delta p_2$  and the wind current direction from the isobars at points 1 and 2 (see eq. 7.1–7.6).  $a_1$  and  $a_2$  are the angles between the wind current direction (arrows) and the effective refluxing-fluxing direction north-northwest to south-southeast. The angles are acute and determine positive components (+) of  $\Delta p_1$ , and  $\Delta p_2$  at the time of sea level fluxing motions and negative components (-) at the time of sea level refluxing wind directions (MUSTAFIN, 1969)

where,  $\Delta h_{Schm}$  is the deviation (centimeters) of the no periodic factor in the sea level at Cape Schmidt from the mean annual navigational level, precalculated with an average forewarning period of 12–13 h upward (+) and downward (-);  $\Delta h_{Abm}$  is the deviation (centimeters) of the actual sea level in Ambarchik Bay from the mean annual navigational level upward (+) and downward (-);  $\Delta p_1$ , and  $\Delta p_2$  are the respective pressure differences (millibars) at points 1 and 2 at a distance of 600 km (6 cm on a 1 : 10,000,000 scale map) along lines perpendicular to the isobaric trend (Fig. 7.45 of this chapter and Fig. 7 of MUSTAFIN, 1969);  $a_1$  and  $a_2$  are the angles between the wind direction along the isobars and the line running north-northwest and south-southeast (Fig. 7.45 of this chapter and Fig. 7 of MUSTAFIN (1969));  $a_1, \dots, a_{10}$  are constants;  $b_1, \dots, b_4$  are free terms;  $R$  and  $r$  are multiple and partial correlation coefficients and their probable errors; and  $\Sigma$  is the mean square root error (centimeters) of the regression equation.

Parameters  $\Delta p_1$ ,  $\Delta p_2$ ,  $a_1$ ,  $a_2$ , etc., needed here are determined as shown in Fig. 7.45. One of the interesting features of this study is that, in contrast with the universally used technique of determining the atmospheric pressure gradients along constant directions, here, these gradients are calculated along variable directions but at pre-selected locations in the water body.

MUSTAFIN's (1969) study was done for nine locations on the Siberian coast. Since knowing the water level at one location in advance might help the prediction at other locations, MUSTAFIN (1969) tabulated the correlation coefficients for the water levels between these stations. These are shown in Table 7.15. On this coast, the surges appear to lag the meteorological forcing by about 12 or 13 h.

Table 7.15: Correlation coefficients between the storm surges at various locations on the East Siberian Sea and Chuckchi Sea coasts (MUSTAFIN, 1969)

	Cape Shalau- Rov	Ambar- chik Inlet	Rau- Chua	Pevek	Cape Billings	Cape Schmidt	Cape Vanka- rem	Koly- uchin Island	Cape Nettan
Cape Shalaurov	1	0.86	0.83	0.85	0.82	0.75	0.70	0.84	0.77
Ambarchik Inlet		1	0.95	0.97	0.79	0.80	0.74	0.83	0.70
Rau-Chua			1	0.97	0.88	0.87	0.86	0.80	0.74
Pevek				1	0.85	0.90	0.67	0.81	0.85
Cape Billings					1	0.86	0.83	0.71	0.77
Cape Schmidt						1	0.84	0.84	0.91
Cape Vankarem							1	0.78	0.81
Kolyuchin Island								1	0.85
Cape Nettan									1

### 7.3.9 Storm Surge Forecasting

Storm surge forecasting and quick dissemination of warnings are of high importance for people living at coastlines and tidal rivers behind the dykes. This addresses the demand, that a storm tide forecasting method must satisfy the highest level of scientific standards that can be reached. Methods that are developed by hindcasting 5 to 10 special storm tides are not serious enough. Investigations show that we have to consider many more different surge types. The description follows closely IHP-OHP (IHP-OHP, SIEFERT and MURTY, 1991), and also based on CHRISTIANSEN and SIEFERT (1979), SIEFERT (1980).

The following examples are designed to give a survey of the state of present-day practice-orientated storm surge research and its application. Regional and supraregional systems will be mentioned in this connection.

#### *The English East Coast*

Following the storm surge of Jan. 31/Feb. 1, 1953, leaving behind on the English east coast 300 victims and 24.000 destroyed homes, a research group came to the decision that a warning system for high storm surges between Northhumerland and Kent should be established and investigations be made simultaneously as to whether such system should also cover the Channel, the Bristol Channel and the Irish Sea. Assuming that surges during the neap tide might be neglected, the warning service decided that storm surge prediction will be made only during spring tide. But since at certain locations on the east coast the height differences between spring and neap tides are insignificant so that a surge during neap tide can cause damage, the warning service must operate independent of the type of surge prevailing.

Storm surges on the English east coast develop from the North to the South. First indications as to potential storm surges can be obtained at the first arrival of tidal waves in the North Sea in the region of the Shetland Islands, partly even near the Hebrides. The forecasting system has been set up accordingly. One tries to recognize the storm surges, if possible, already far away in the north and to determine the height at the reference gauges using wind forecasts. Reference gauges are Stornoway/Hebrides, Wick, and Aberdeen.

From the northern tip of Scotland (John o'Groats) the tidal wave needs about 4 h to reach the English border and then another 9 h to reach the Thames. It is, of course, an advantage that such storm surges at the early stage of inaccurate forecasts first reach almost unpopulated coasts in less need of protection. Actual forecasts are being made only for the English east coast, which is subdivided into 5 divisions with one reference gauge, each Fig. 7.46.

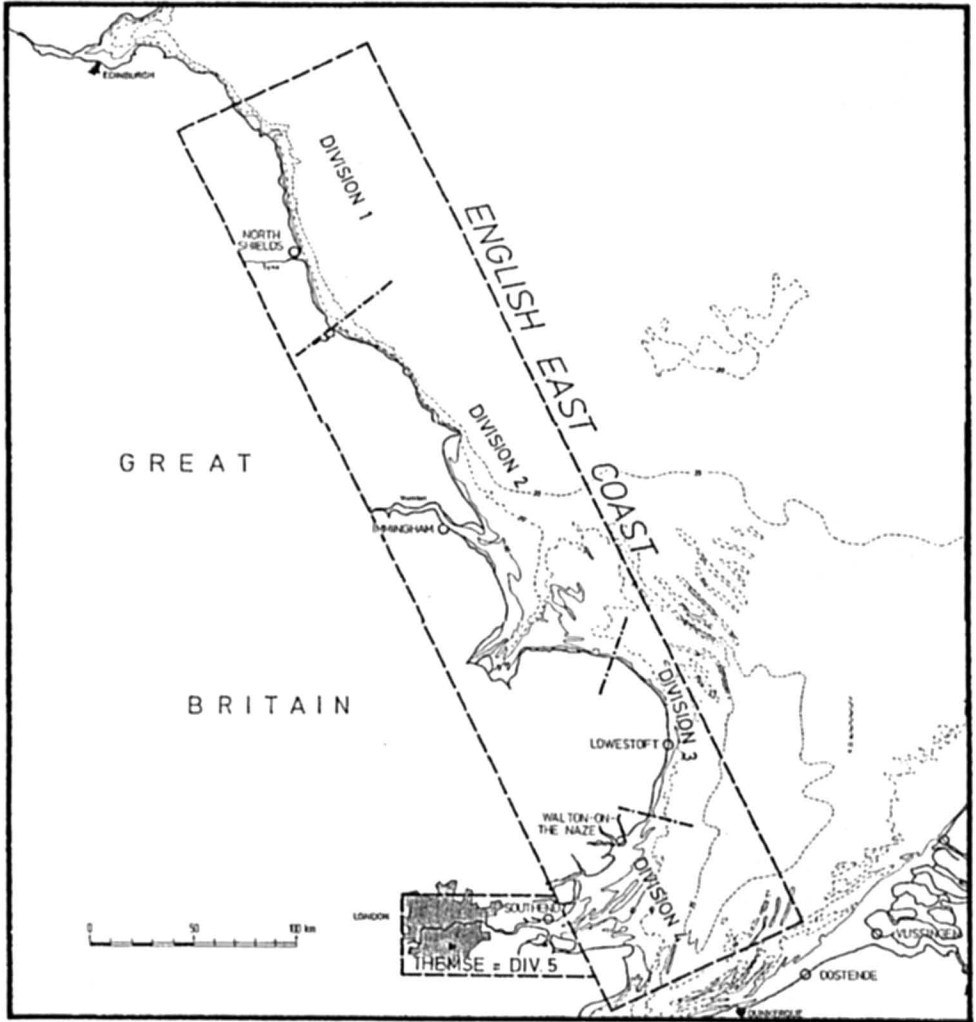


Fig. 7.46: Forecast area English east coast

Whether in the future more attention must also be given to the adjacent Scottish east coast in the north, will be decided in the course of further development in the field of oil exploration. For each reference gauge a "critical level", was fixed. If it is exceeded, certain areas will be flooded. If there is danger that this level will be reached, a warning is issued.

A first early warning (alert) can be given 12 h before HW. The second bulletin i. e. confirmation or withdrawal of the warning, is given 4 h prior to HW. Then, if required, the expected HHW level is pronounced. In the case of warnings for Div. 5 (Thames), a "London Flood Room" is taken over by the Greater London Council. There, the HHW for London is determined using the HHW forecast for Southend and the  $Q_0$  discharge. To set off in time such a procedure in London, the 2nd warning is given as early as 6 h prior to HHW Southend.

The "storm surge season" on the English east coast extends from the end of August to 30 April. On average, that means 100 "alerts", 20 real warnings and 5 critical level reports.

There is a number of empirical correlations based on statistically secured regressions between the water levels at the reference gauges (see above), the wind and the water levels at the Stornoway, Wick and Aberdeen gauges, among which the best suited are selected in each case. The mean error is  $\pm 0.2$  m, individual deviations reaching 0.6 m. For Division 1 e. (Fig. 7.46), the equation reads as follows:

0.75.	(11 HW - MHW Wick)	4 h earlier
+ 0.003.	(320° comp. of the surface wind Fair Isle)	11 h earlier
+ 0.002.	(30° comp. of the geostrophic wind between Scotland and Southern Norway)	6 h earlier
<hr/>		
+ 0.14 m		
<hr/>		
= HHW - MHW North Shields		

The main problems are at present:

- empiric approaches are based on only a few major storm surges (as these occur only seldom),
- dynamic wind effects are not taken into consideration,
- the interactions of tidal waves and waves due to wind stress are not taken into account, astronomical tide forecasts are inaccurate.

### *The Western Schelde*

Storm surge forecasts for the Western Schelde are of great importance in particular for the port of Antwerp (about 80 km upstream of the mouth) with its numerous exposed installations. Therefore, extensive analyses were also made for this region after the storm surge of Feb. 1, 1953. It was thus found, inter alia, that northwest winds are the most dangerous winds. As a result of investigations made over many years a forecasting method was presented which, in principle, is based on a correlation of the HHW at Oostende and that at Antwerp (Fig. 7.47).

HWs occur at Oostende little less than 3 h earlier than at Antwerp. As this time period is too short for a reasonable forecast the Oostende HHWs are calculated about 2 h in advance.

These calculations are based, just as those for the Oostende-Antwerp correlations, on empirical estimates. The method is as follows:

$$\begin{aligned}
 & \text{extrapolation wind stress Oostende by 2 h} \rightarrow \text{HHW}_{\text{Oos}} \\
 & + \text{difference } \text{MHW}_{\text{Ant}} - \text{MHW}_{\text{Oos}} \\
 & + \text{wind according to direction and force off the coast} \\
 & \hline
 & = \text{HHW Antwerp}
 \end{aligned}$$

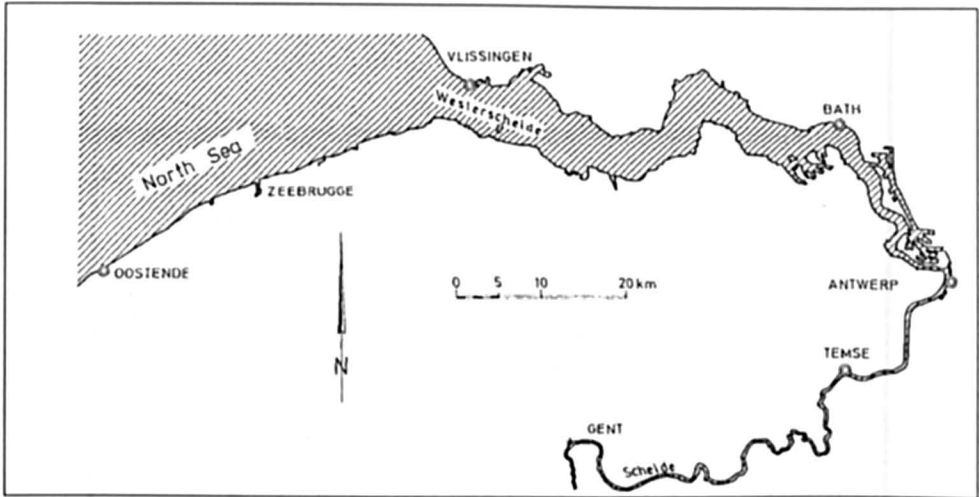


Fig. 7.47: Forecast area Western Schelde

### *The Dutch Coast*

The theoretical principles for the methods applied in the Netherlands originated in the 1950s WEENINK and GROEN (1958). Their results have been tested in many practical applications.

For the stations of Vlissingen, Hoek van Holland, Den Helder, Harlingen, and Delfzijl (Fig. 7.48), the Koninklijk Nederlands Meteorologisch Instituut, (KNMI), publishes prognoses for the high water level due to meteorological causes. During a storm surge the "Stormvloedwaarschuwingsdienst" in The Hague determines the exact heights at the above stations and decides based on  $Q_0$  and the predicted values whether warnings should be issued.

For the forecasting of water levels, correlations between HHWs of various places are needed. For this purpose, reference curves have been put together. Where the prevailing volumes of discharge have an influence on the rise, they have been covered by the statistical correlations.

As a supplement to this forecasting service, regional water level forecasts are also carried. Such forecasts are made on the basis of surge curves. For this purpose, data from a network of gauges, which have been in operation for several years for other purposes, are also relied upon. They are recorded via remote transmission in a central recording room. Every 5 minutes the water levels are recorded on punched tapes, analog recorders and a printer.

On the Dutch coast, too, one tries to use the possibilities offered by mathematical models for storm surge forecasts.

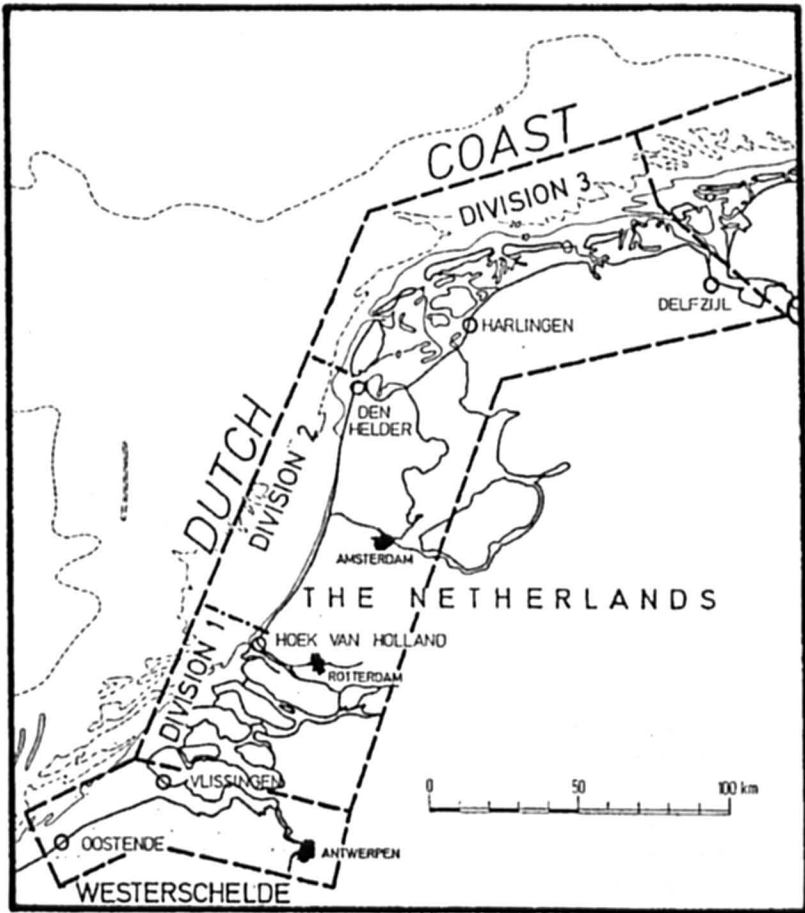


Fig. 7.48: Forecast area Dutch coast

### *Inner German Bight*

Many forecasting methods often yield unsatisfactory results as they are based on weather forecasts and these weather forecasts – mainly wind speed and wind direction evolution – are not accurate enough.

The other reason for unsatisfactory predictions are the methods themselves. Usually only the peaks of storm tides are taken into consideration, representing only single points on a curve. Characteristics of tide and surge curves are not developed, and tide/surge interactions are not evaluated.

To exclude such difficulties a storm tide forecasting method should be developed

1. by analysing storm surge curves of storm tides over the last 50 years at several tide gauges on the coastline. A storm surge is defined as the difference between storm and mean tidal water level.
2. by taking into consideration as many wind data as are available;
3. by using only exact (not predicted) tide and wind data.

Fig. 7.49 shows the situation at the German North Sea coast.

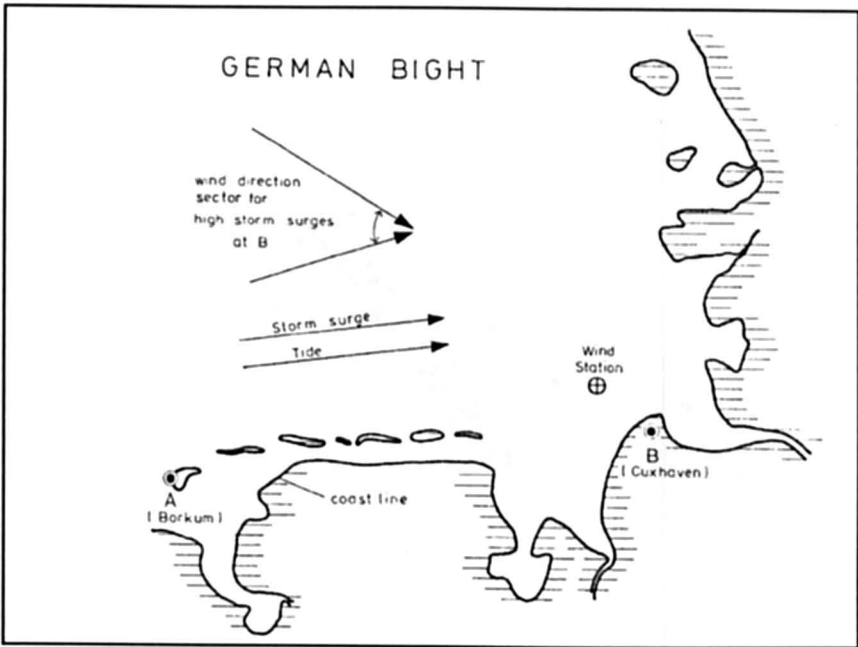


Fig. 7.49: Tide gauge locations A and B in the German Bight

In the German Bight the astronomical tide progresses in an anticlockwise direction. The winds during storm surge events come from west, as does the storm surge. Therefore, a forecast for a point B on this coastline needs information from a location westward of it (gauge A at the island of Borkum). This gauge A is the so-called input gauge for the forecast gauge B. However water level information merely from an input gauge is not sufficient.

Further investigations showed that an explanation for the outliers 7.50 can be given if wind speed and wind direction development within the last 3 hours before high tide at A (Borkum) are taken into account. The wind development in this 3-hour interval (about 3 hours before the expected high water level at B) is the best indicator for what will happen with water level changes in the following 3 hours after high tide at A. So about 3 hours before high tide at B no further wind information is needed to forecast the highest level at B. These conditions are in agreement with results at the Dutch and British coasts.

The high water level at B ( $H_B$ ) can be roughly calculated by a simple linear formula:

$$H_B = 1.2 H_A + \Delta V + \Delta R - 80 \text{ cm} \quad (7.7)$$

where,  $1.2 \cdot H_A - 80 \text{ cm}$  gives the trend of HW level comparison at A and Fig. 7.49 and  $\Delta V$  (Fig. 7.51) and  $\Delta R$  (Fig. 7.52) are the partial contributions to wind speed and wind direction developments respectively within 3 hours before forecasting time.

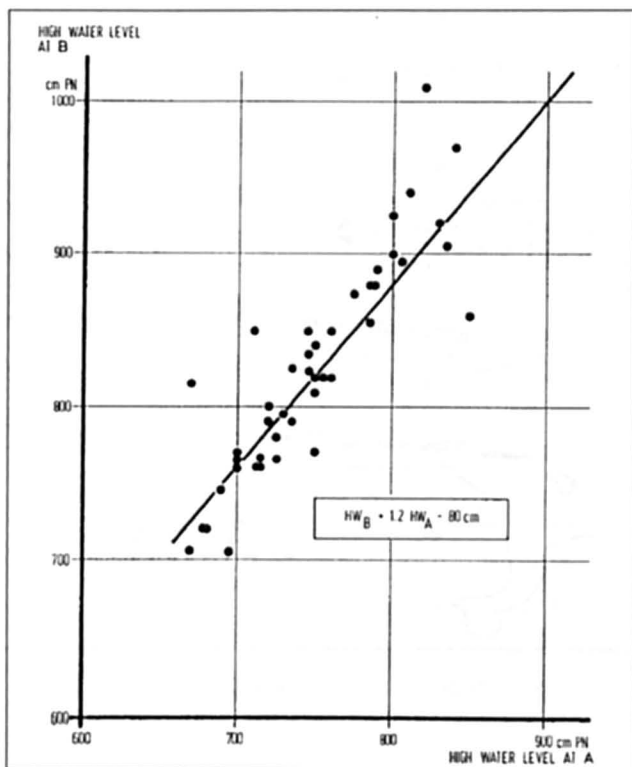


Fig. 7.50: Comparison of high water levels at A and B

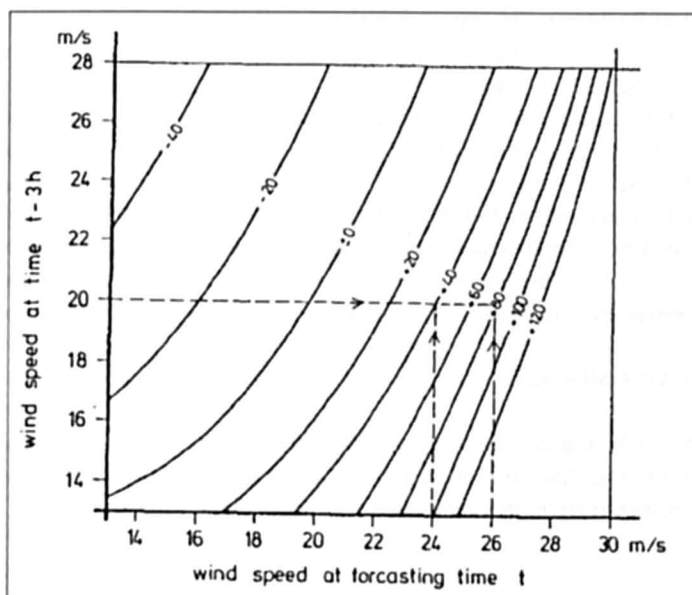


Fig. 7.51: Wind speed development value  $\Delta V$  in cm

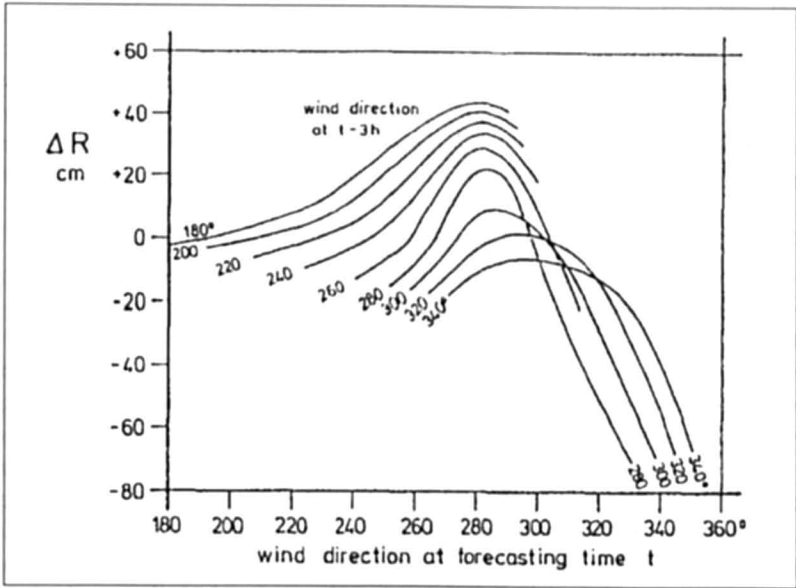


Fig. 7.52: Wind direction development value  $\Delta R$

The wind data is needed with a resolution of 1 m/s in speed and 10° in direction. The example in Fig. 7.52 demonstrates the necessity of exact wind speed data. A change in wind speed from 20 to 24 m/s over the 3 hours interval gives a positive value of  $\Delta V = + 40$  cm. A change of only 2 m/s (to 26 m/s) doubles this to  $\Delta V = + 80$  cm.

Fig. 7.52 shows that highest values for wind direction developments are given by changes from other directions to 280° which is the most effective wind direction for high storm surges at Cuxhaven. Direction changes further northward result in high negative values, up to  $\Delta R$  80 cm.

In a second step the forecasted high water levels at B can be modified. This possibility is given by analysing the surge curves at A and B (Fig. 7.53).

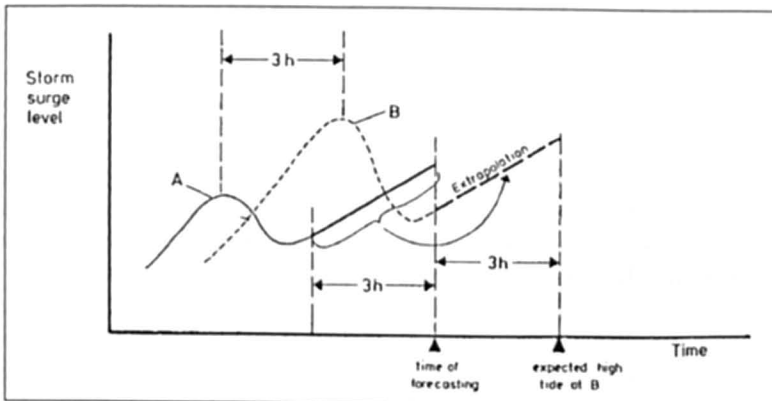


Fig. 7.53: Extrapolation of storm surge curve B by the shape of curve A

This prediction method has been used for the calculation of the high water level in Hamburg using the predicted water level at Cuxhaven + a constant 110 cm. Long-term monitoring shows that this amount must be differentiated more accurately, because fareway and embankments improvement measures at the Elbe River have changed storm surge issue in the Elbe estuary. Since 1996 high water level differences • HTHW between Cuxhaven and Hamburg have been attributed to a class of high surges with • H 0130 cm (FERK, 1999).

The German Hydrographic Service (formerly DHO now BSH) in Hamburg has been charged by a law mandated with the task to inform traffic in the German Bight on anticipated water levels. The empirical-statistical method used is applied in a more simple form for about 50 years.

For the computed surge a distinction is made between local effects (i.e. German Bight) and distant effects. The value of greatest influence is unquestionably the wind (surge approximately proportional to the square of the wind velocity; the greatest surge value is reached after a 3 h influence). Then follow the static atmospheric pressure (the effect is practically spontaneous), the change of atmospheric pressure with time (in case of rapid changes in the pressure free waves up to 1 m height are generated), water temperature and temperature difference air-water (the colder it is and the greater the difference, the stronger the wind effect). In the BSH a mathematical model is being developed covering the influences in their entirety in an overall approach.

Water level forecasts are broadcast twice a day and cover the entire German North Sea coast (Fig. 7.50). Neither the tidal curves nor the times of the onset of peak levels are determined by only rises in such levels (as a measure between anticipated HHW and precalculated astronomical HW). Meteorological details obtained from the German Weather Service.

Because of the uncertainty of the forecasts, water levels are indicated at 25 cm intervals up to a surge height of 1.2 m and thereafter at 50 cm intervals. In the case of a storm surge, the warnings are of use not only for navigation but also for agencies and administrative offices along the coast and tidal rivers.

In the case of anticipated high wind velocities, the BSH needs forecasts on the direction, speed and time of onset of the wind over the North Sea. On the basis of the method applied by the BSH forecasts of sufficient accuracy are possible only if, in addition, the forecast and occurrence of meteorological input data are accurate and external surges are recognized early enough off the English east coast. Only then the first 12 hour forecasts are usable, otherwise only later data are more accurate. But even then there is room for improvements since wind forecasts are made only roughly in units on the Beaufort scale.

### *Danish Southwest Coast*

Although the land behind the Danish tidal flats south of Esbjerg (Fig. 7.54), as the northernmost part of the Dutch-German tidal flat, is only relatively sparsely populated, attempts have been made during the last few years to increase the safety of the population in addition to reinforcing the old dykes by applying storm tide forecasting procedures.

The procedure was developed following the statistical evaluation of water levels measured over six years and allows computation at any time of the tidal cycle of the water levels for the forthcoming 1, 2, and 3 h. Forecasts for a maximum period of 3 h are sufficient to find out in time when an endangered dyke might break at the earliest and then perhaps to evacuate the population concerned which takes almost 2 h.

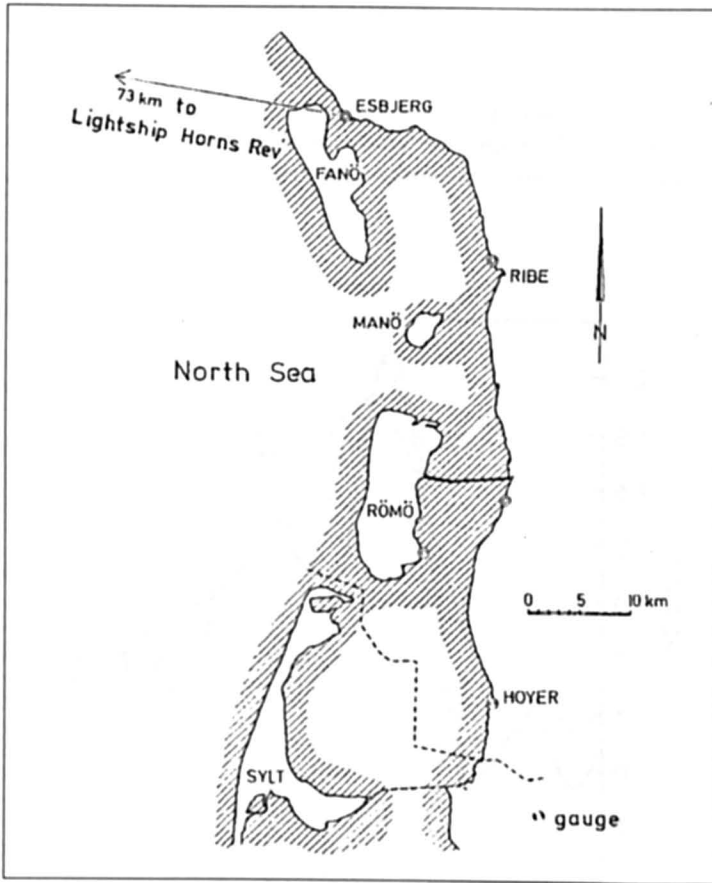


Fig. 7.54: Forecast area Danish Southwest coast

The programmed procedure has been in practice since 1970. It is based on hourly water level data from the Esbjerg and Hoyer gauges for which it was developed (Fig. 7.54) and on 3-hourly data of wind velocity, wind direction, and atmospheric pressure from a lightship off the coast. The 95 % confidence intervals are

- ± 20 cm for a forecast period of 1 h.
- ± 35 cm for a forecast period of 2 h.
- ± 45 cm for a forecast period of 3 h.

As during the storm surge of Jan. 03, 1976, the data flow was interrupted because the public telephone system was blocked, independent systems were rented in the meantime. Although the accuracy mentioned meets the requirements, it is planned to supplement the 3 h model in the next few years by a hydrodynamic 12 h model for the North Sea.

### 7.3.10 Modeling

#### North Sea

Following the 1953 disastrous storm surge, several numerical models for the North Sea and Thames Estuary were developed. Results from a linear model and a nonlinear model are compared with the observed surge at Southend of February 16–17, 1962, in Fig. 7.55.

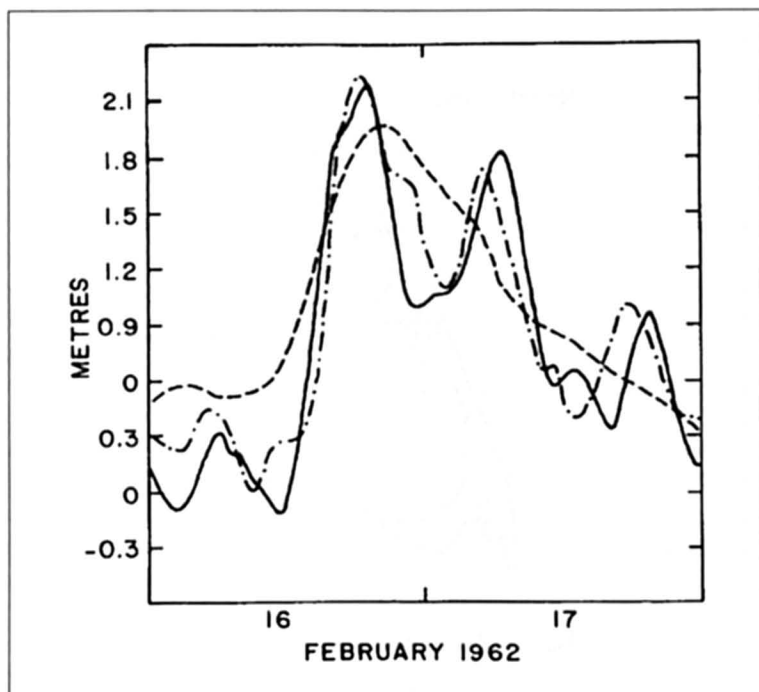


Fig. 7.55: Comparison of observed and computed surges at Southend, U.K., during February 16–17, 1962. Solid line, observed surge; broken line, computed surge using a linear model; dashed-dotted line, computed surge using a nonlinear model (ROSSITER, 1971)

Certain models have already been considered for the North Sea in different sections. ISHIGURO (1976a) showed through electronic analog models that atmospheric pressure gradient generated surges are important in the North Sea (Table 7.16). ISHIGURO (1976b) gave diagrams of estimated peak surges for different wind speeds. Contours of surge height for a wind speed of 36 m/s are illustrated in Fig. 7.56.

DAVIES and FLATHER (1977) computed the storm surge in the North Sea for the case of April 1–6, 1973, using several different numerical models. The features of these models are summarized in Table 7.17 and terms errors at various locations for these models are listed in Table 7.18.

Table 7.16: Comparison of the amplitudes of pressure gradient generated and wind stress generated surges in the North Sea. (ISHIGURO, 1976a)

Wind direction (degrees)	Wind duration (h)	Wind speed (m s <sup>-1</sup> )	Pressure-gradient (mb 100 km <sup>-1</sup> )	Pressure generated surge Y <sub>p</sub> (cm)	Wind generated surge Y <sub>w</sub> (cm)	Y <sub>p</sub> / Y <sub>w</sub> (%)
22	30	10	2.3	8	33	24
		20	4.5	16	130	12
		30	6.7	23	293	8
		40	9.0	32	520	6
112	10	10	2.3	10	15	67
		20	4.5	20	60	33
		30	6.4	30	135	22
		40	9.0	40	240	17

Table 7.17: Features of the different models for the North Sea used in the simulation of the storm surge of Apr. 1-6, 1973. (DAVIES and FLATHER, 1977)

Calculation	Model	Open boundary condition Surge input	Tidal input
a	Shelf	Radiation Hydrostatic	None
b	North Sea	Elevation specified Hydrostatic	None
c	Shelf	Radiation Hydrostatic	M <sub>2</sub> + S <sub>2</sub>
d	North Sea	Elevation specified Hydrostatic	M <sub>2</sub> + S <sub>2</sub>
e	North Sea	Elevation specified from calculation c + observations from Wick	M <sub>2</sub> + S <sub>2</sub>

Table 7.18: Root-mean-square errors (cm) for calculations using models a to e (see Table 7.17) for the storm surge of Apr. 2-6, 1973. (DAVIES and FLATHER, 1977)

Port	a	b	c	d	e
Wick	18.1	12.6	13.5	12.6	0.0
Aberdeen	20.3	13.7	15.9	13.3	10.9
North Shields	22.5	17.7	17.0	16.6	16.3
Inner Dowsing	26.9	27.5	21.2	27.1	25.2
Immingham	26.6	25.6	19.5	20.8	18.2
Lowestoft	29.8	28.5	25.0	27.5	25.3
Walton-on-Naze	34.3	31.2	27.2	29.0	26.8
Southend	42.9	38.6	33.9	35.1	33.0
Ostende	36.1	34.0	25.1	30.3	26.7
Ijrnuiden	42.3	40.6	34.6	35.4	33.3
Terschelling	32.3	31.8	27.2	27.3	26.4
Cuxhaven	48.0	45.0	37.4	40.2	38.4
Esbjerg	32.6	29.0	23.3	24.11	21.2

PRANDLE and WOLF (1978a, 1978b) used parallel numerical models to study the modification of the tide due to surge and vice versa in the southern part of the North Sea. The tide and the surge before and after interaction for the case of October 19, 1970, are shown in Fig. 7.57. The interactions at Lowestoft and Southend for the event of January 31–February 1, 1953, are presented in Fig. 7.58 and 7.59, respectively. The contours of the interaction in the southern part of the North Sea are displayed in Fig. 7.60.

FLATHER (1980) summarized the status of a real-time storm surge prediction scheme for the North Sea. In this scheme, the meteorological forcing terms are obtained in real time as output of a 10-level primitive equation atmospheric model. In the storm surge model, a coarse model covers the whole of the Northwest European continental shelf. Models with finer resolution for the southern bight, eastern part of the English Channel, and the Thames Estuary are being developed. The contours of the surge at 03:00 GMT on January 12, 1978, are shown in Fig. 7.61.

VRIES et. al. (1995) compares 2D storm surge models applied to North Sea, Aegean and the Adriatic. They stated that the differences between the North Sea models are less than 10 cm, storm surges are underestimated by up to 50 cm, which indicates that improvement has to be found in the surface drag relations and not in the difference between the models. For the Mediterranean Sea the comparison shows differences of 35 cm with the observed level, which is due to the meteorological input inaccuracies.

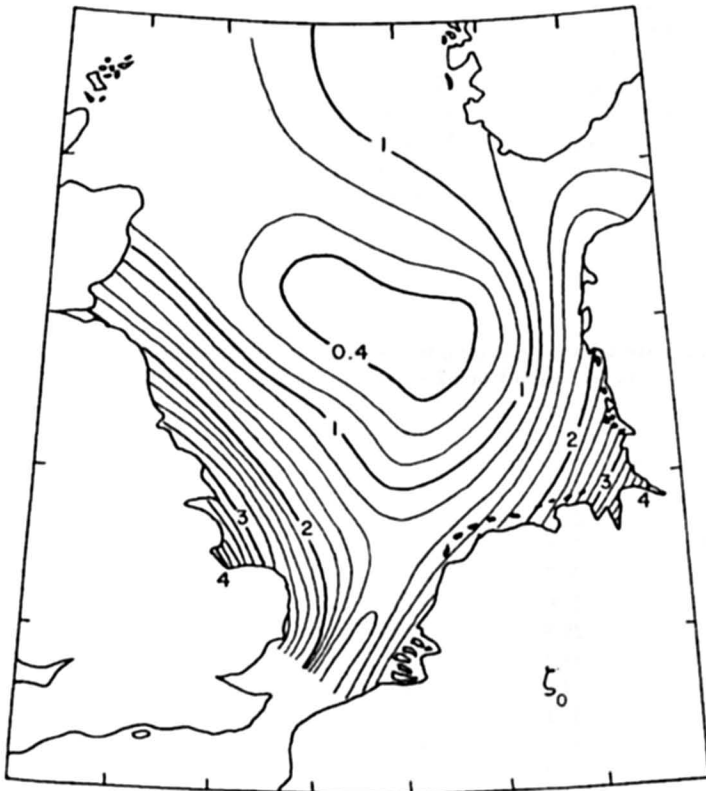


Fig. 7.56: Storm surge heights in the North Sea for a wind speed of 36 m·s<sup>-1</sup> blowing for 10 h. (ISHIGURO, 1976b)

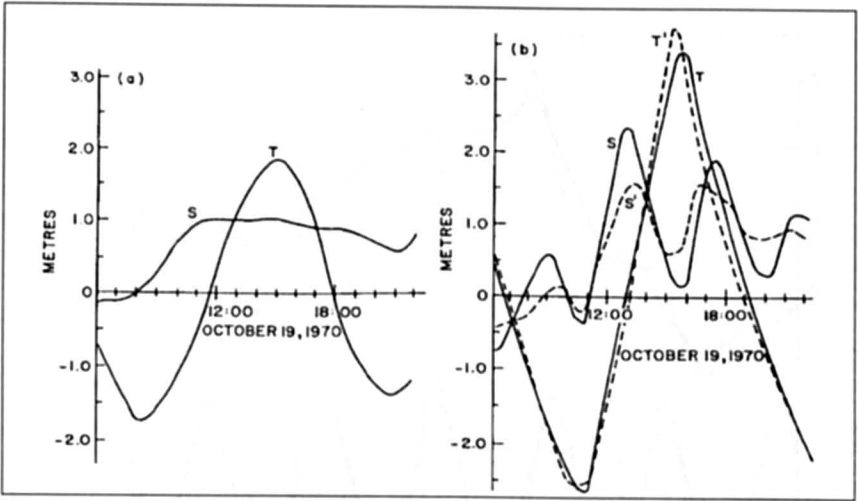


Fig. 7.57: Tide-surge interaction at (a) Walton-Margate (mouth of the model) and (b) Tower Pier. T, tide; S, surge; T', tide modified due to interaction with surge. S', surge modified due to interaction with tide. (PRANDLE and WOLF, 1978b)

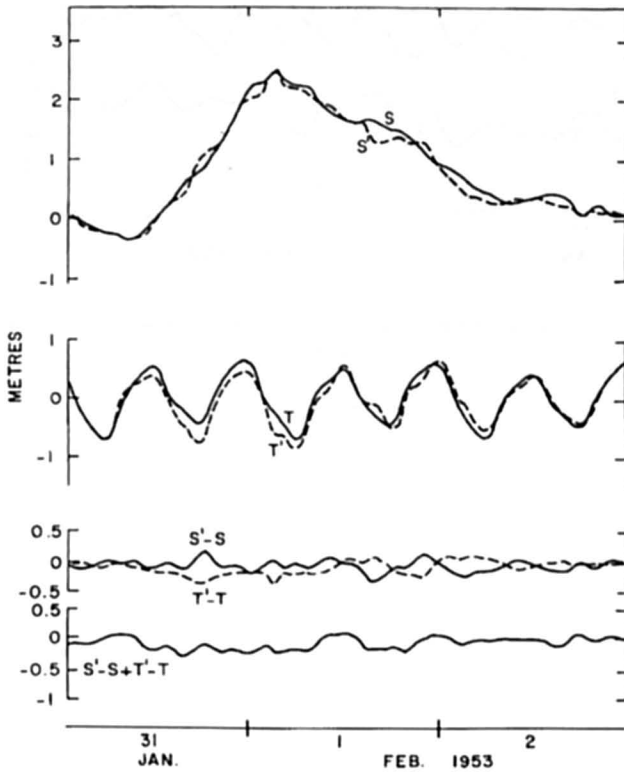


Fig. 7.58: Tide-surge interaction at Lowestoft, U.K. See Fig. 7.47 for explanation. (PRANDLE and WOLF, 1978b)

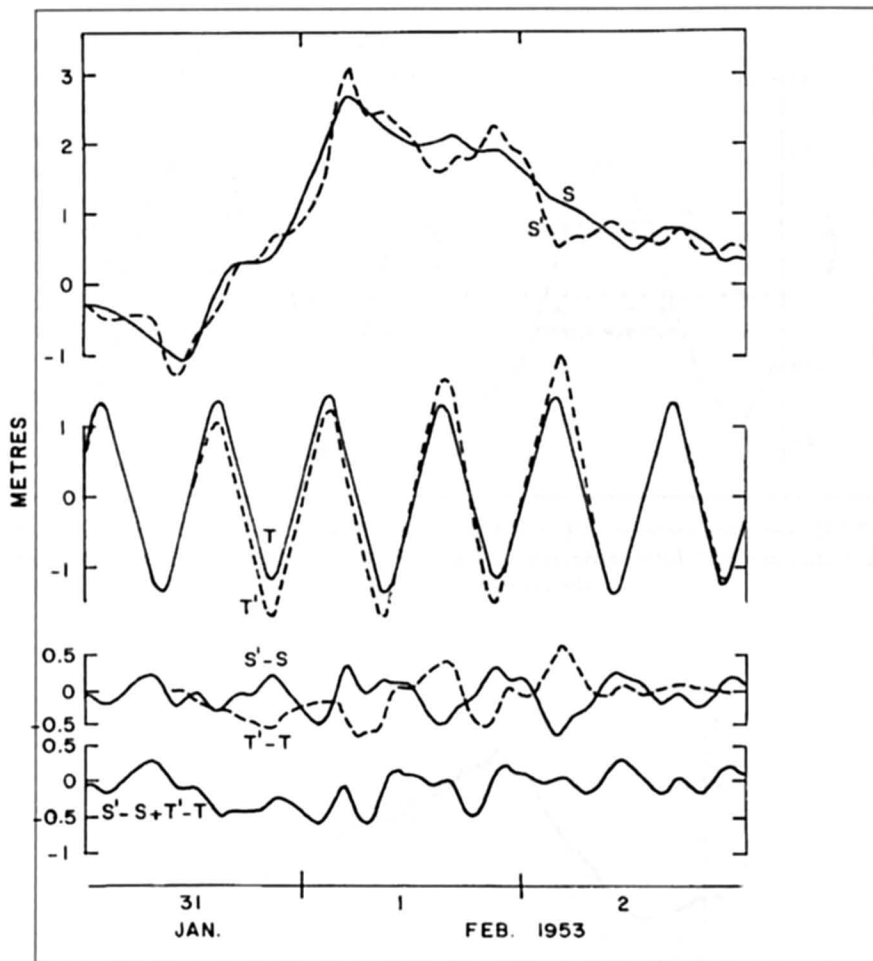


Fig. 7.59: Tide-surge interaction at Southend, U.K. See Fig. 7.57 for explanation.  
(PRANDLE and WOLF, 1978b)

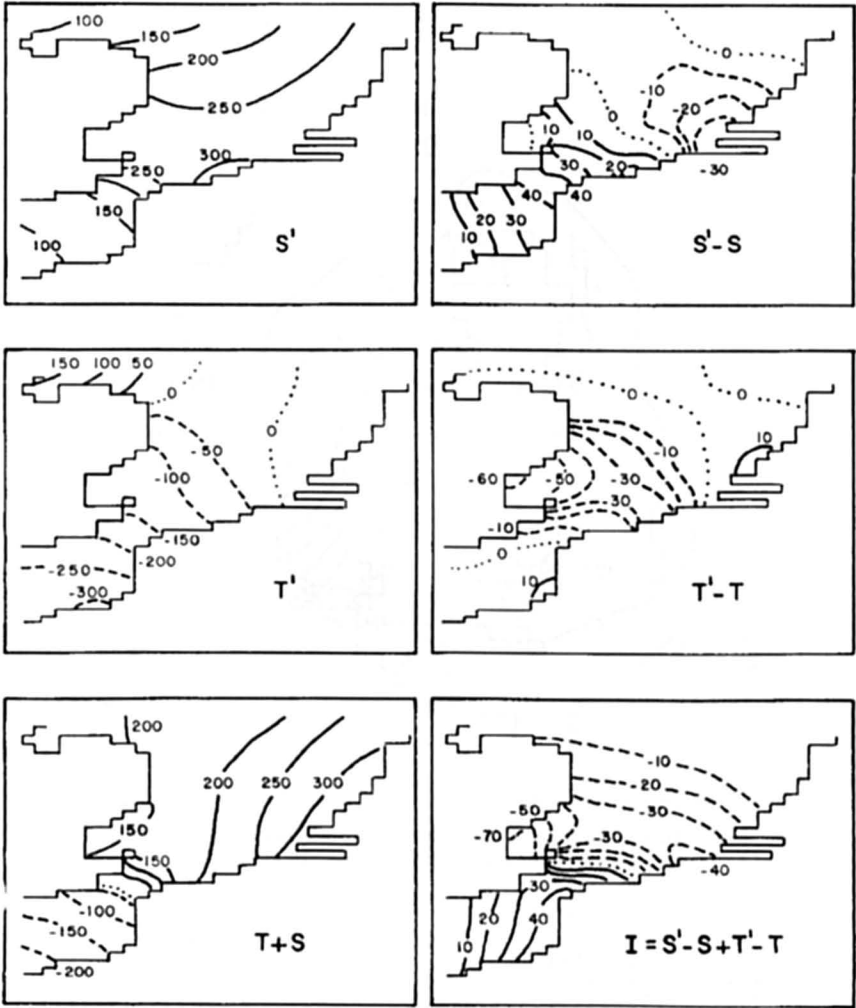


Fig. 7.60: Tide-surge interaction distribution (centimetres) in the southern part of the North Sea. (PRANDLE and WOLF, 1978b)

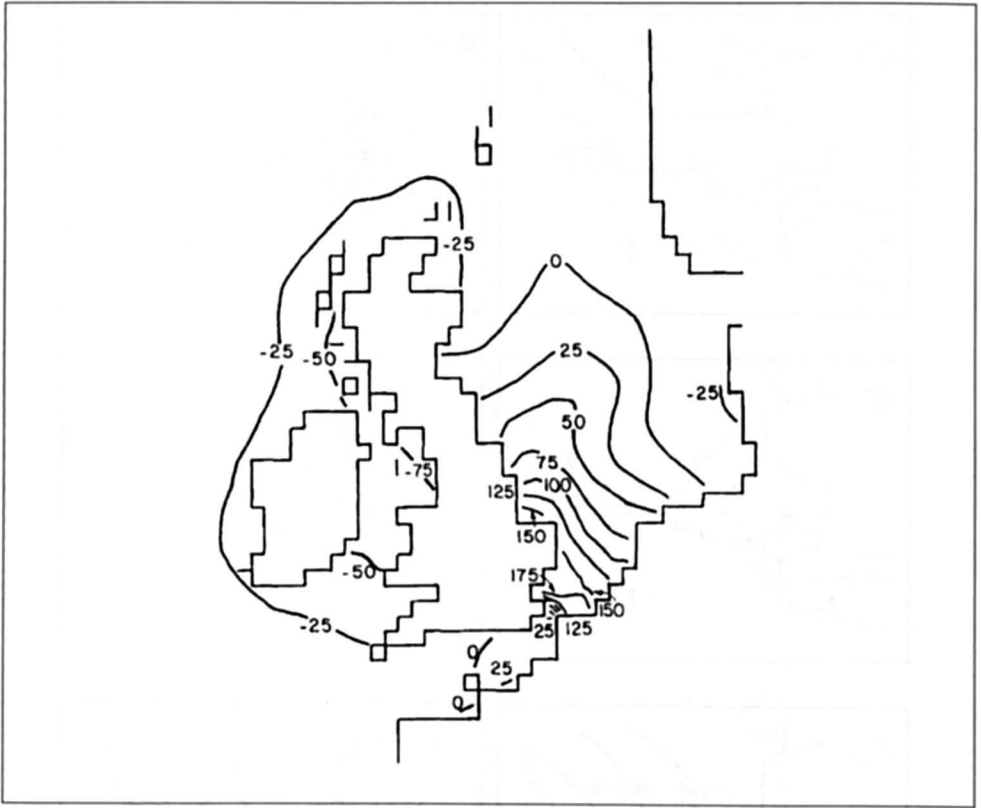


Fig. 7.61: Spatial distribution of surge elevation (centimetres) at 03:00 (GMT) on January 12, 1978, in the northwest continental shelf of Europe. (FLATHER, 1980)

### *A North Sea model*

This chapter follows closely IHP-OHP 1987 and based on RODENHUIS et al. (1978), HAVNOE et al. (1983) and SIEFERT et al. (1987).

The emphasis in hydrographic conditions is often on waves. However, for several important problems, knowledge of currents is also essential. During the past, the technique of simulating currents and surface elevations in sea areas by computer has developed into an accepted engineering method. However, to obtain details of currents, the computations must be made on a high resolution grid. The model presented here permits the use of detailed resolution in selected areas, with the main circulation in the North Sea described on a much coarser grid. With the main grid established for the entire North Sea, the model can be focused on different local areas. Its generality makes refocusing simply a matter of providing the programme with the coordinates for the new local area and its bathymetry.

The model uses the full non-linear equations of nearly horizontal flow, which are solved by implicit, time-centred, finite difference scheme. The effects of wind stresses, Coriolis forces, and bed friction are included. Moreover, such nonlinear equations of shallow water and interaction between tide and storm surges. The System 21 has a high degree of accuracy. This has been demonstrated in practical applications e.g. RODENHUIS et al. (1978).

To provide details for resolving complicated areas, the change of resolution for the North Sea model is shown in Figs 7.62 and 7.63. The grid 1 with low resolution is named  $SD_0$ ; the grid 2 of high resolution is named  $SD_1$ ; and the higher resolution of nested grid 3 is named  $SD_2$  – i. e., subdomains 0, 1, and 2, respectively. In low resolution 1 ( $SD_0$ ), several grids of finer mesh size can be selected at higher resolution 2 ( $SD_1$ ). The mesh size is one-third the original resolution 1. In a nested grid of high resolution 2 ( $SD_1$ ), again several grids of finer mesh size can be selected at higher resolution 3 ( $SD_2$ ). The reduction in mesh size relative to nested grid  $SD_1$  is again onethird; relative to nested grid  $SD_0$  it is one-ninth. For the North Sea model, this means a refinement from 10 nautical miles in resolution 1 to 1.1 nautical miles in resolution 3. There is no principal restriction for further reduction to higher resolution 4 or 5.

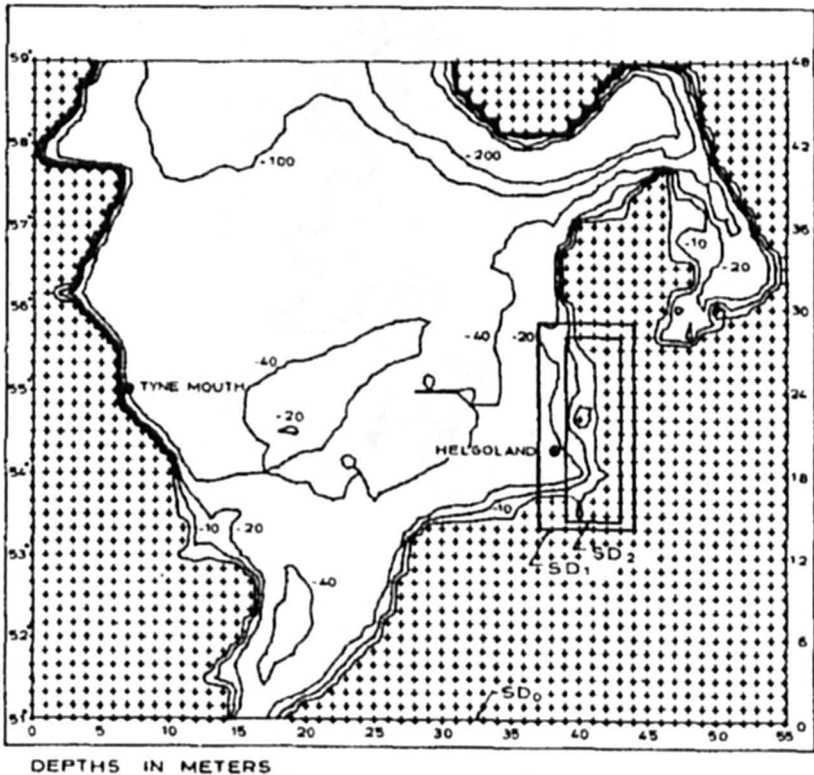


Fig. 7.62: North Sea model with main domain in Scale 1

$SD_0$ : Mesh size = 18 km, gridpoints: 2.640

$SD_1$ : Mesh size = 6 km, gridpoints: 945

$SD_2$ : Mesh size = 2 km, gridpoints: 4.428

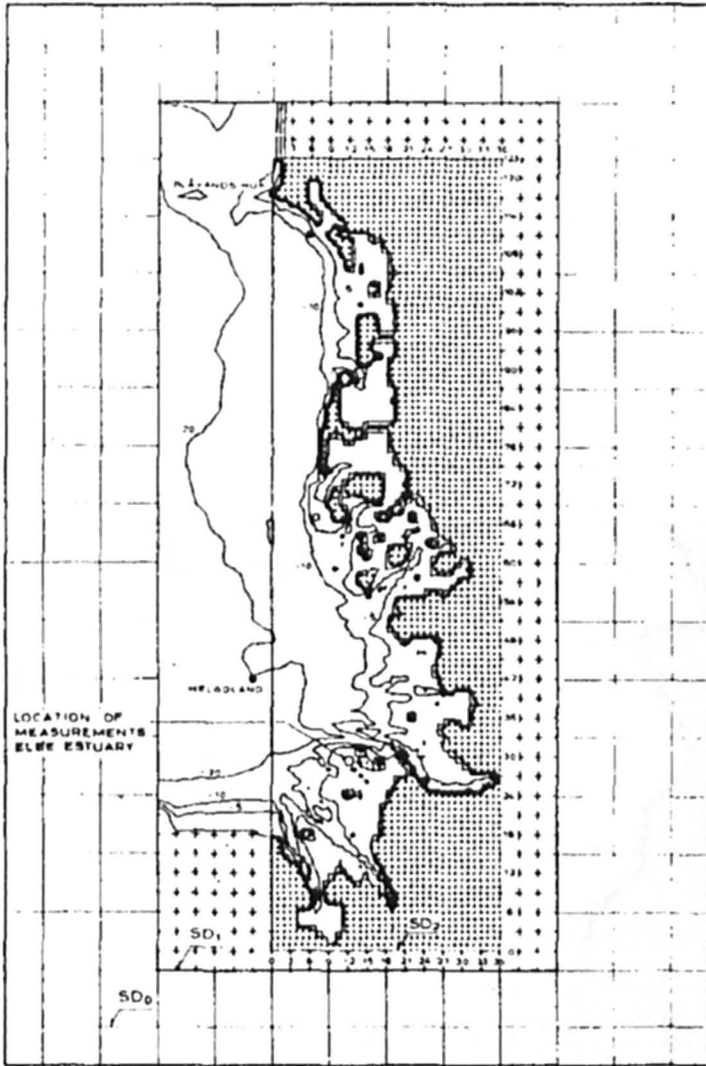


Fig. 7.63: North Sea model with subdomains in Scales 1 and 2

Computations are made simultaneously on all grids. When computing simultaneously, information also can travel from the fine grid to the coarse grid – the conditions in the fine grid can influence the results in the coarse grid.

The model was considered for a storm surge warning system for the Danish west coast and for intended computations of currents in connection with the hydraulic investigations and preliminary design of a gas pipeline that will be brought ashore on the west coast.

The model is set up as follows: The bathymetry of the entire North Sea from Stavanger to the Orkney Islands in the north and Dover–Calais in the south is described on an rectangular finite difference grid with a mesh size of 10 nautical miles. The Skagerrak and the Kattegat also are included. The bathymetry off the Danish west coast is described on the finest grid with a mesh size of 2 km. This grid permits detailed representation of this area (Fig. 7.63).

The main grid has to be set up only once, while the fine grid can be refocused on different areas of interest. The only dynamic entry data required are water-level variations along the open boundaries between Stavanger and the Orkney Islands, and between Dover and Calais and the time variation of the atmospheric pressure distribution for the area. The boundary data is computed from tidal constants, in fact, as a tidal prediction for each grid point along the open boundary.

The changing meteorological conditions are represented in the hydrodynamic equations by barometric pressure gradients and wind-stress terms. Meteorological observations are available with 3-hour intervals. The isobar map is based, however, mostly on observations on land, and only a few ship observations are available.

In the model, the atmospheric pressure at sea level is specified every 3 hours in each grid point with a mesh size of 60 nautical miles, with the same boundaries as the main hydrodynamical grid. The actual wind speed is calculated from the geostrophic wind speed.

The square root formula is based on measurements in the German Bight. Coefficients depend on the vertical stability (expressed by the air-sea temperature difference), here corresponding to a neutrally stable atmosphere. The wind direction is found by assuming a cross-isobar angle of  $15^\circ$ . Using interpolation of the wind components in space and time, a wind vector is calculated in each grid point in the main grid and subgrids at each time step.

Calibration of the finest grid off the Danish coast is incomplete, but the accuracy of the model's representation in the finest grid (Scale 3) may be illustrated with results from a similar run for the Elbe Estuary. In Fig. 7.64, the computed and recorded tidal variations at a point 15 nautical miles northwest of Cuxhaven are compared. The location is indicated in Fig. 7.63.

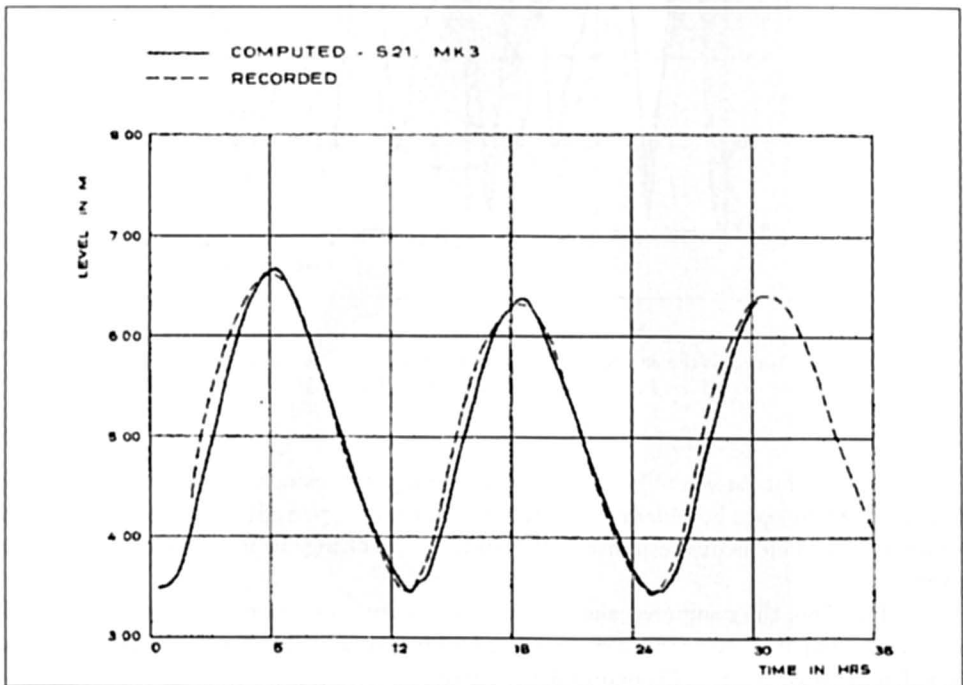


Fig. 7.64: Comparison between recorded and computed tide in Elbe Estuary with subdomain in Scale 3; data source is the Research Group for the Harbour Extension Neuwerk, Hamburg

Note: Location indicated in Fig. 7.63

Again, the computed values agree with the recorded values accurately. Current recordings were made at this location. The computed and recorded currents are compared in Fig. 7.65. The computed current is a depth-averaged current, whereas the recording is at 0.7 m above the seabed in 8 m water. When the velocity profile,  $U_z$  over the vertical is expressed as

$$U_z = K \times Z^{1/n}$$

with  $n = 5$  or  $6$ , and  $K$  some constant, (7.6) a formulation tested in several areas in the North Sea, the relation between mean current,  $U$ , and  $U_{0.7}$  is

$$U_{0.7} = 0.8 U \quad (8.3)$$

As shown in Fig. 7.65 this fits accurately for the computed  $U$  and recorded  $U_{0.7}$ .

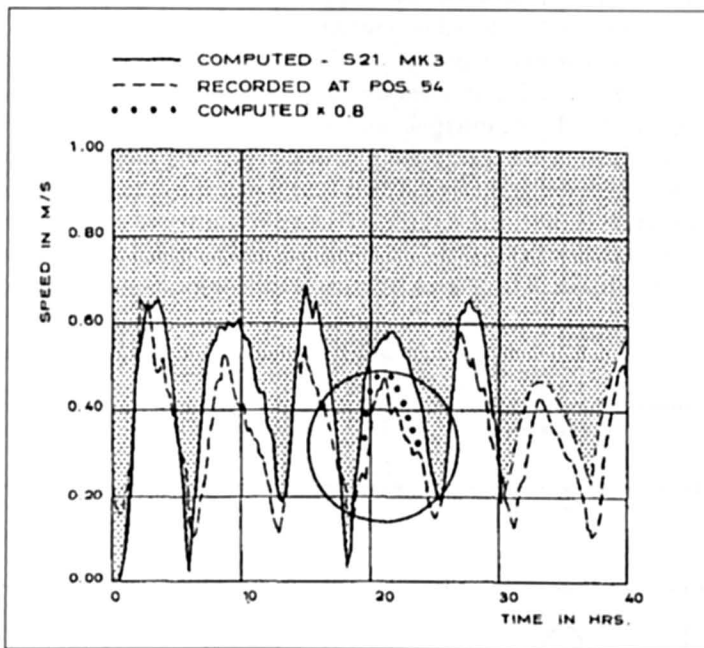


Fig. 7.65: Comparison of recorded with computed current speed in the Elbe Estuary with sub domain in Scale 3; data source is the Research Group for the Harbour Extension 'Neuwerk', Hamburg  
Note: Location indicated in Fig. 7.63

The effect of the storm of Jan. 2-3, 1976, was computed, using the storm field previously described. At the open boundaries, the predicted tide for the period and a pressure surge that results as an instantaneous response of the sea level to a change in atmospheric pressure are given.

In Fig. 7.66, the computed and recorded water-level variations at Helgoland for this period are compared. Note that a storm surge builds up gradually over the initial tidal variation. The error is less than 20 cm on a 3.5 m surge.

Fig. 7.67 illustrates the model's ability to resolve the storm surge inside the bays along the Danish west coast: An instantaneous picture of the sea surface in the form of isolines is compared with recordings at two stations at that moment.

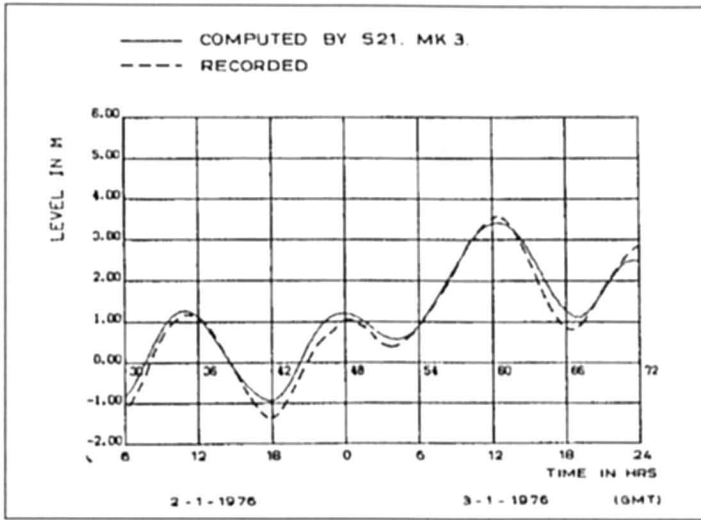


Fig. 7.66: Comparison of recorded with computed storm surge of Jan. 2-3, 1976, at Helgoland with sub domain in Scale 2

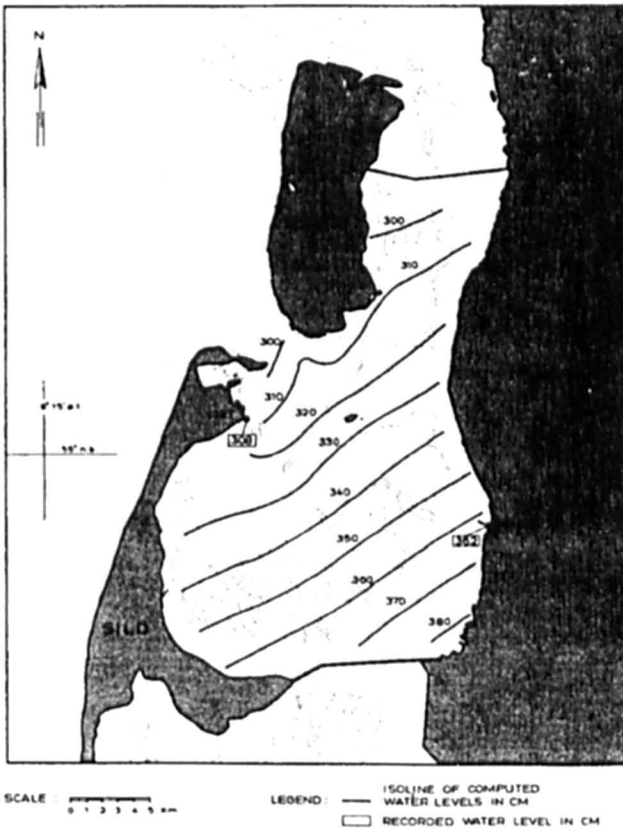


Fig. 7.67: Computed water levels inside a bay on the Danish west coast compared with recordings at two stations on March 1, 1976, 15:00 hours GMT

### *North Sea and Baltic Sea Model*

The Federal Maritime and Hydrographic Agency (BSH) developed an operational model system to calculate currents, water level and dispersion processes. Operational model means that the model produces results daily. The description follows closely a paper of the BSH (1992). The model is a predictive one and is based on forecasts of wind and air pressure supplied by the German Weather Service in Offenbach. Tide prediction, current and water levels are computed nightly for periods up to 36 hours.

The water levels are calculated daily using three nested and interactively coupled grid nets. Towards the German Bight the grid resolution increases. Therefore the interaction between the variable coastline (wadden areas, sand banks and island chains) and offshore areas can be represented. Grid spacing near coastal areas in the German Bight and the western Baltic Sea is 1.8 km; in areas further offshore, it is 10 km while elsewhere in the North Sea and Baltic Sea it is 20 km.

In a three dimensional model the following forcing functions were included: wind, air pressure over North and Baltic Seas, tides, external surge and water discharge from large rivers. The model is a valuable tool for the water level and storm surge warning service at the BSH. It is mainly validated by regular comparison between modelled and measured water levels. In addition the model is occasionally checked using measured currents and drift experiments at sea (BSH, 1992).

### *Baltic Sea*

Earlier the one-dimensional model of SVANSSON and SZARON (1975) for the Baltic Sea was discussed. Observed and computed surges at several locations for the storm surge event of August 15, 1964, are compared in Fig. 7.68.

HENNING (1962) numerically simulated the surge of January 3-4, 1954, in the Baltic Sea. This surge caused maximum elevations of 1.7 m in the western part of the Baltic Sea. The surface weather chart at 06:00 GMT on January 5, 1954, is given in Fig. 7.69. The distributions of the surge heights at two different times are shown in Fig. 7.70 and 7.71. Observed and computed surges at five locations are compared in Fig. 7.72. Some relevant data on this surge are given in Table 7.19.

WROBLEWSKI (1978) used stochastic techniques to simulate the following surges at Nowyport (at the Polish coast of the Baltic Sea): January 17, 1955, February 15, 1962, February 18, 1962, and February 21, 1962. DEMEL (1934) studied the surges of 1930 and 1931 at the Baltic coast of Poland.

KLEVANNY (1994) modeled long wave oscillation in the Baltic Sea. He used wind data from a set of meteorological stations along the Baltic Sea and big Islands. The storm surges of December 30-31, 1975 and February 17-23, 1990 are the basis to compare observed data with surface level oscillations obtained from modelling.

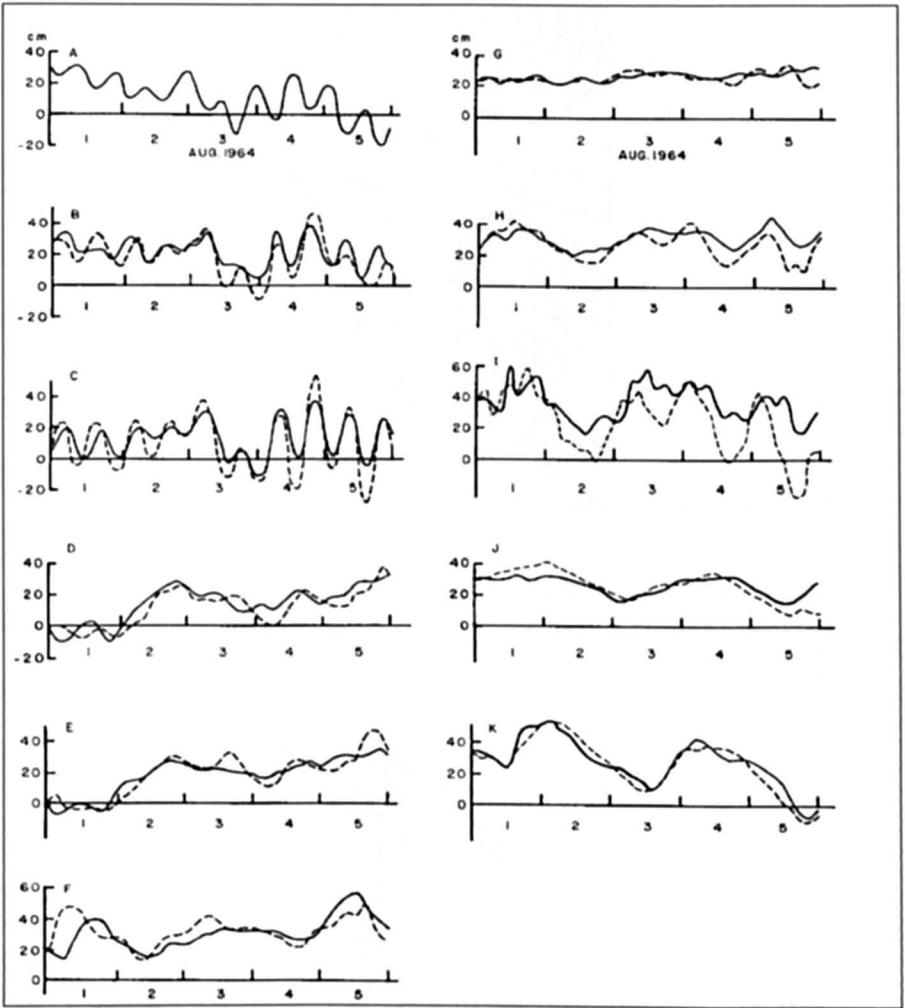


Fig. 7.68: Observed (solid line) and computed (broken line) storm surges at various locations along the Baltic Sea (SVANSSON and SZARON, 1975)

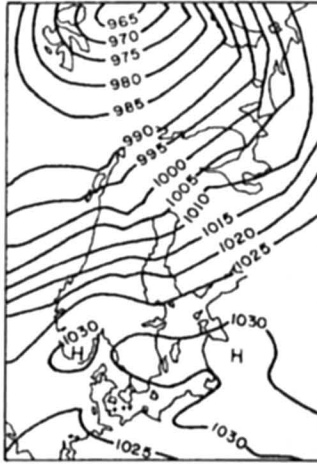


Fig. 7.69: Simplified surface weather chart at 06:00 (GMT) on January 5, 1954, for the Baltic Sea area (HENNING, 1962)

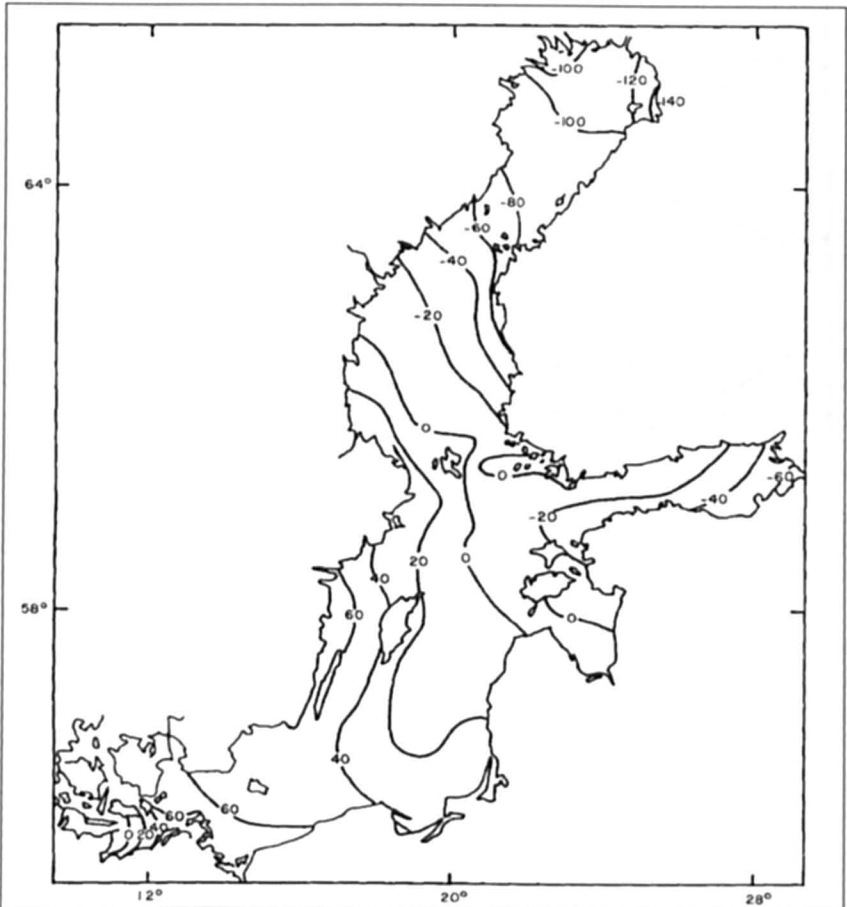


Fig. 7.70: Distribution of storm surge amplitudes (centimeters) in the Baltic Sea at 20:00 (GMT) on January 3, 1954 (HENNING, 1962)

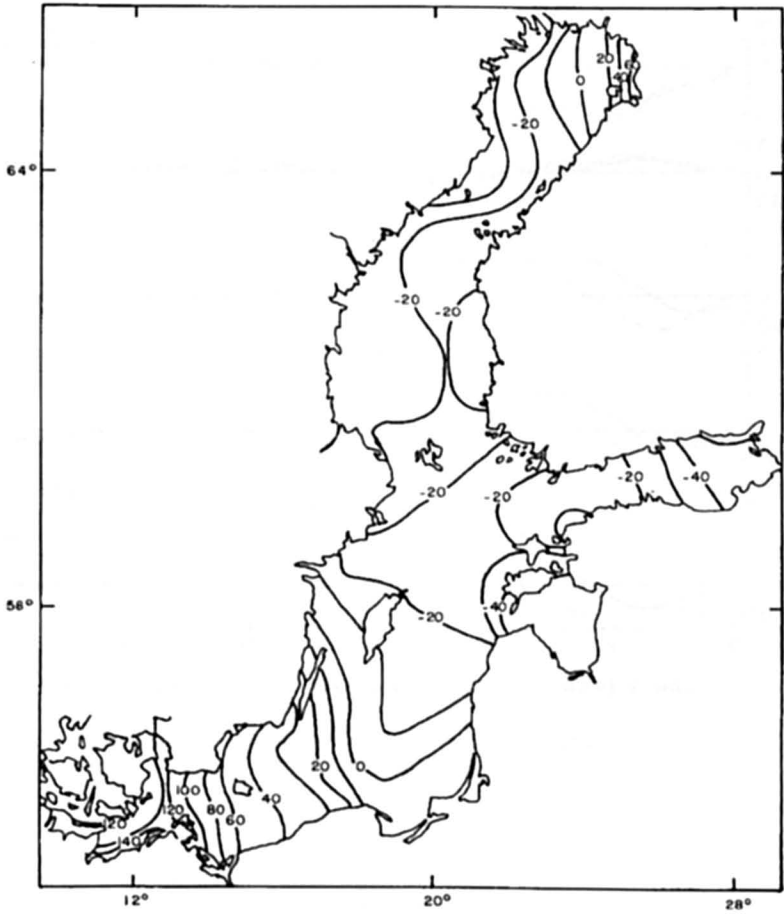


Fig. 7.71: Distribution of storm surge amplitudes (centimeters) in the Baltic Sea at 14:00 (GMT) on January 4, 1954 (HENNING, 1962)

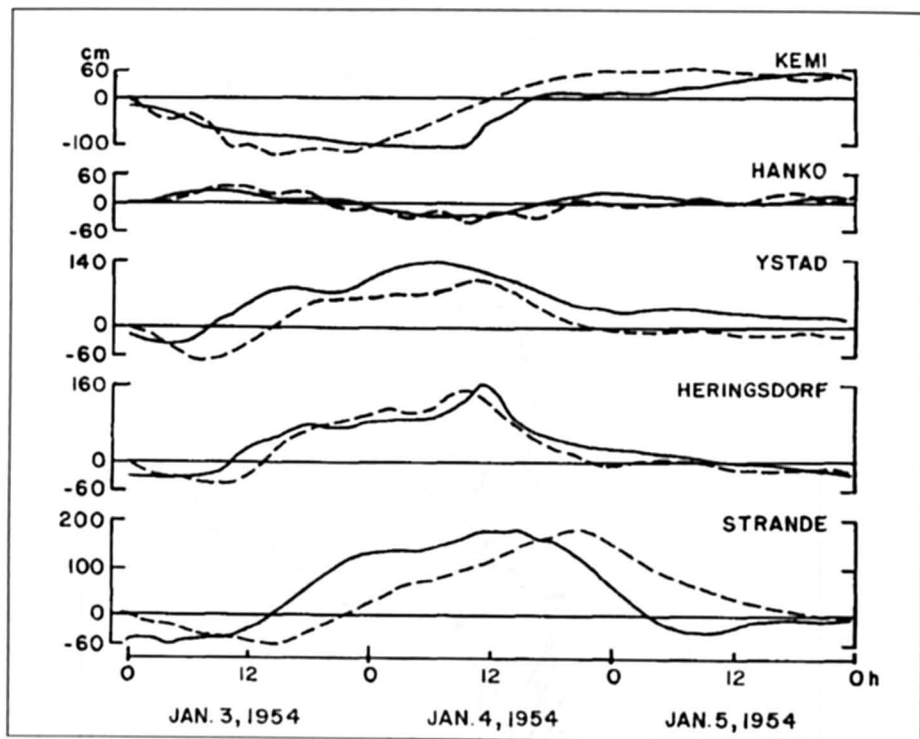


Fig. 7.72: Observed (solid line) and computed (broken line) storm surges in the Baltic Sea during January 3-5, 1954 (HENNING, 1962)

Table 7.19. Comparison between observed and computed storm surges in the Baltic Sea for the event of Jan. 3-4, 1954 (HENNING, 1962)

Water level Gauge	Time of maximum elevation (observed)		Surge (cm)	
	Day	Time (GMT)	Observed	Computed
Degerby	3	8:00	47	52
Landsort	4	0:00	51	77
Kungholmsfort	4	8:00	100	105
Ystad	4	5:00	171	164
Heringsdorf	4	11:00	195	197
Sallnitz	4	11:00	183	171
Kap Arkona	4	10:00	187	193
Daffier Ort	4	12:00	190	195
Warnetminde	4	13:00	224	192
Wismar	4	14:00	291	192
Travernfinde	4	15:00	283	192
Gedser	4	12:00	231	186
Langballigau	4	12:00	236	262
Strande	4	15:00	239	236

## 7.4 Asia

RABINOVICH and SOKOLOVA (1992) produced a catalogue of storm surges for the Russian coast of the Sea of Japan.

Fig. 7.73 shows the locations of the eleven tide gauges whose data have been used to produce this catalogue. Actually out of the eleven stations, Krilyon is located in the Okhotsk Sea, but close to the Boundary with the Sea of Japan and is influenced by surges from the Sea of Japan.

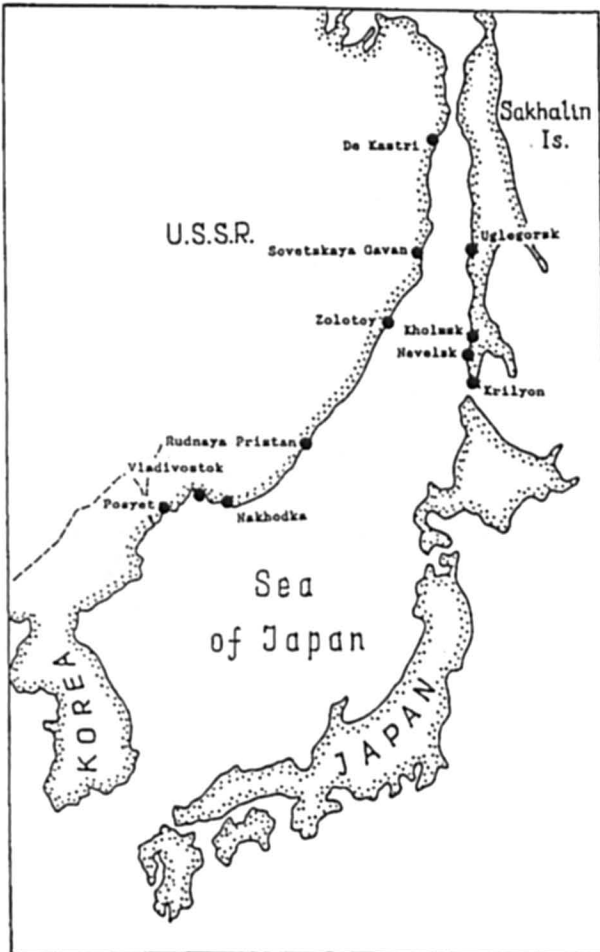


Fig. 7.73: Tide gauge positions (RABINOVICH and SOKOLOVA, 1992)

The residual series (after subtracting predicted tides)  $\zeta(t)$ , where  $t$  is the time, were used to analyse surges. Some simple parameters were chosen to describe each one (Fig. 7.3.2): the maximal height of storm surge  $h_s$ , estimated from mean monthly level  $Z_m$ , and of storm surge plus tide,  $h_{st}$ ; the corresponding moments  $t_s$ ,  $t_{st}$ ; duration of surge  $T_s$  and of its half-height  $T_{s/2}$ ; surge steepness  $\delta = h_s / T_{s/2}$ ; the variance

$$D = \sigma^2 = \frac{1}{T_s} \sum_{t=t_b}^{t=t_e} [\zeta(t) - Z_m]^2 \quad (7.8)$$

where,  $t_b$  is the time of the beginning and  $t_e$  is the end time of the surge; it is supposed that in both moments  $\zeta(t_b) = \zeta(t_e) = Z_m$ .

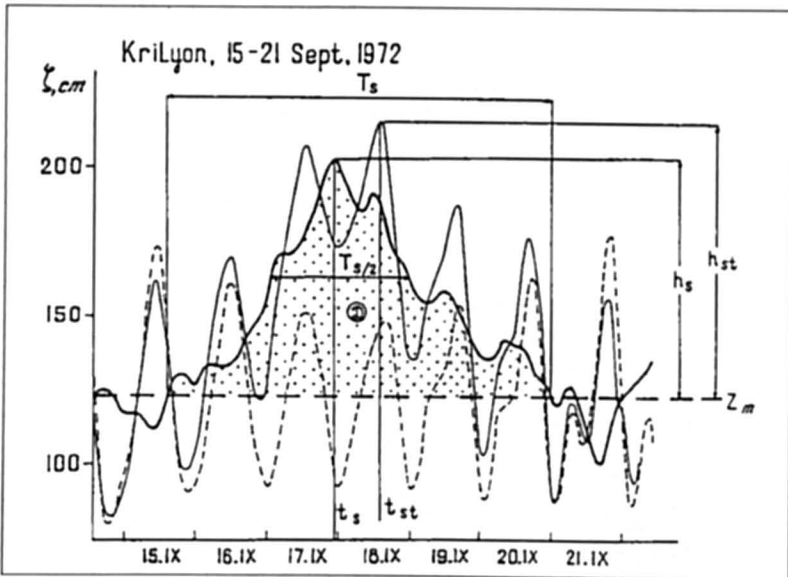


Fig. 7.74: The main parameters of storm surge (RABINOVICH and SOKOLAVA, 1992)

The algorithm of automatic detection of storm surges and calculation of corresponding parameters was used to analyse several years of data. Only the sea-level displacements with  $h_s > Z_{cr} = 25$  cm were examined. A number was given to every surge, which had a height  $h_s \geq 45$  cm at least at one of the 11 stations mentioned above. This numbering system is similar to that used for typhoons: the first two numbers represent year, the other two are sequential numbers (e.g., 7803, 7911, 8001, etc.) As an example, these parameters for the strongest surges at Nevelsk for 1979–91 are presented in Table 7.20.

Table 7.20: An example of catalogue parameters of several storm surges at Nevelsk (RABINOVICH and SOKOLOVA, 1992)

Station	Year	Number	$t_s$ (day, month, hour)	$h_s$ (cm)	$h_{st}$ (cm) (+t,hr)	$T_s$ (hr)	$T_{s/2}$ (hr)	$\delta$ (cm/hr)	D (cm <sup>2</sup> )
Nevelsk	1979	7901	11.02.17	48.4	84(+2)	49	15	3.22	-
Nevelsk	1979	7902	9.04.18	43.3	85(0)	78	32	1.35	689
Nevelsk	1979	7904	19.08.08	43.7	104(0)	76	43	1.02	408
Nevelsk	1979	7905	20.12.23	48.3	103(-3)	53	28	1.73	858
Nevelsk	1980	8007	13.12.14	36.2	95(0)	75	67	0.69	447
Nevelsk	1981	8101	24.08.06	49.2	115(0)	71	24	2.05	465
Nevelsk	1981	8102	24.10.04	62.6	123(0)	70	43	1.46	1177

It is interesting to compare the parameters of the same surge for different stations to better understand the peculiarities of surge formation. For example, the surge occurring during 20–22 October 1976 was not noticed at the southern mainland stations Posyet, Vladivostok, and Nakhodka ( $h_s < 25$  cm), but was relatively strong on the southwestern coast of Sakhalin Island (Table 7.21).

Table 7.21: The storm surges of October 1976 at different coastal stations.  $t$  = time relative to  $t_s$  of surge's maximum (RABINOVICH and SOKOLOVA, 1992)

Stations	$t_s$ (day, month, hour)	$h_s$ (cm)	$h_{st}$ (cm) (+t,hr)	$T_s$ (hr)	$T_{s/2}$ (hr)	$\delta$ (cm/hr)	D (cm <sup>2</sup> )
Krilyon	21.10.00	38.9	57(+3)	23	10	3.9	619
Nevelsk	21.10.17	61.5	63(0)	51	24	2.6	1190
Kholmok	21.10.16	47.2	50(+2)	46	25	1.9	924
Ulegorsk	21.10.12	49.5	73(-3)	51	27	1.8	880
De-Kastri	21.10.01	34.7	89(-3)	51	7	4.9	267

The processing of tide gauge data makes it possible to obtain statistics of the surges, to estimate their seasonal distribution, and to find the most interesting (dangerous) cases. For these cases at least, but preferably for all, it is useful to define the parameters of the atmospheric processes which forced these surges. The following parameters were fixed at the moment of surge maxima (Fig. 7.75) the atmospheric pressure in the centre of the cyclone  $P_{os}$ ; its velocity  $V_s$  and direction  $\alpha_s$ ; the position of the center relative to the station  $r_s$ ,  $\theta_s$ ; the pressure  $P_s$  and in wind  $W_s$ ,  $\phi_s$  at the station. The parameters for the surge of 20–22 October 1976 are presented in Table 7.22. The cross correlation analysis of the parameters from the first (sea level) and second (meteorological) groups for the number of storm surges may be an effective instrument to look for empirical relations which may be used for a surge forecast.

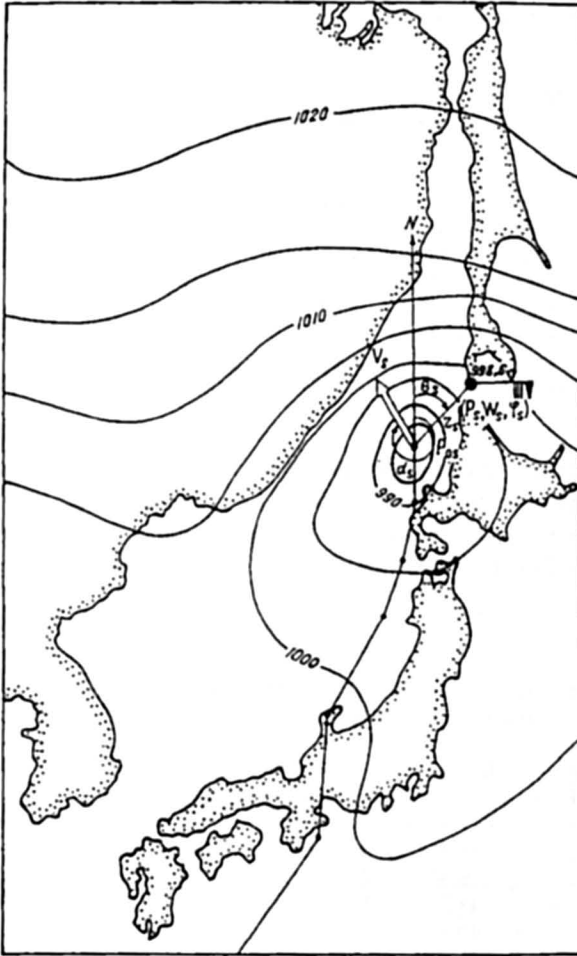


Fig. 7.75: Meteorological parameters of the atmospheric disturbance caused by a storm surge at the Krilyon station (RABINOVICH and SOKOLAVA, 1992)

It is possible also to describe storm surges using regression formulae:

$$\zeta(t) = a_0 + a_1 \cdot P(t) + a_2 \cdot \tau_z(t) + a_3 \cdot \tau_n(t) \quad (7.9a)$$

where,  $a_i$  are regression coefficients;  $P(t) = P_s(t) - 1000$ ;  $P_s(t)$  is the atmospheric pressure at the station in millibars;  $\tau_z(t) = -0.025 \cdot W^2(t) \cdot \sin(\phi(t))$  and  $\tau_n(t) = -0.025 \cdot W^2(t) \cdot \cos(\phi(t))$  are zonal and meridional components of wind stress;  $W(t)$  and  $\phi(t)$  are wind speed and direction at the station. In this case, four coefficients characterize every storm surge. The regression formulae in the form of eq. (7.9a) for the surge of 20–22 October 1976 are given in Table 7.22.

Table 7.22: The main cyclone and meteorological parameters at the maximum of the surge of October 1976 (RABINOVICH and SOKOLOVA, 1992)

Stations	$P_{0s}$ (mb)	$V_s$ (km/h)	$\alpha_s$ (deg)	$\theta_s$ (km)	$r_s$ (mb)	$P_s$ (mb)	$W_s$ (m/s)	$\phi_s$ (deg)	Regression Formulae
Krilyon	980	67	30	60	12	980.7	14	135	$\zeta(t) = 12.16 - 0.87P(0) - 14.34\tau_z(0) + 2.30\tau_n(0)$
Nevelsk	965	41	340	210	726	991.7	19	273	$\zeta(t) = 5.70 - 1.64P(0) + 18.50\tau_z(0) + 5.22\tau_n(0)$
Kholmok	965	41	340	210	670	991.0	21	263	$\zeta(t) = -8.34 - 2.14P(0) + 14.55\tau_z(0) + 1.30\tau_n(0)$
Ulegorsk	965	52	340	225	326	983.8	21	269	$\zeta(t) = -0.76 - 1.66P(0) + 17.50\tau_z(0) + 10.0\tau_n(0)$
De-Kastri	965	79	340	0	780	985.6	7	199	$\zeta(t) = 13.50 - 0.41P(0) - 13.48\tau_z(0) - 6.10\tau_n(0)$

For a better description of individual storm surges, more precise regression formulae may be used:

$$\zeta(t) = a_0 + a_1 \cdot P(t - \Delta t_1) + a_2 \cdot \tau_z(t - \Delta t_2) + a_3 \cdot \tau_n(t - \Delta t_3) \quad (7.9b)$$

where,  $\Delta t_i$  are the corresponding time lags. Three additional parameters are necessary to determine the surge.

## 7.5 Australia

Storm surges on the south coast of Australia occur due to extra tropical cyclones (ETC's). According to VECCHIO (1980) storm surges at Adelaide comprise of a locally generated surge due to the interaction of wind stress with local topography and an external effect arising from the passage of winter depressions across the Great Australian Bight. He cautions that the effects may not be totally independent.

For the positive surge, the local effect contributes about 0.75 m and the external effect adds about another 0.5 m. The 0.75 m of the locally generated surge is made up of about 0.25 m due to the decrease of atmospheric pressure and 0.5 m due to the wind stress.

Between 1948 and 1977, there were 12 surge events in Adelaide. Strong northwest winds prevailing for periods of 24 hours or longer, and associated with deep lows over ocean waters, south of the bight, can generate positive surges up to one meter in amplitude. Along the Adelaide foreshore, the most destructive storm surge of this type occurs when the wind direction rapidly shifts from the northwest to a squally southwesterly, the change in wind direction occurring near the time of maximum tide height. Figs. 7.76 and 7.77 respectively show typical synoptic situations for NW and SE winds at Adelaide.

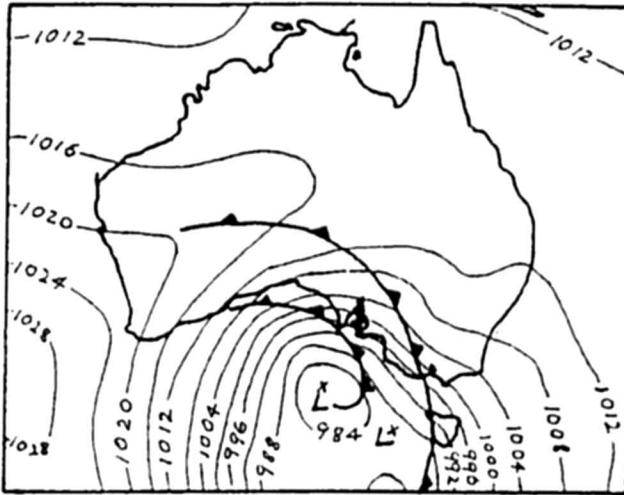


Fig. 7.76: Synoptic chart NW winds at Adelaide (VECCHIO, 1980)

VECCHIO referred to the external component of the surge. MURTY (1995) studied this and showed that surges generated at the southwest coast of Australia propagate eastward along the south coast as far as the Bass Strait. Fig. 7.78 shows the tide gauge locations. One can see from Fig. 7.79 that the surge is quite coherent as it propagates from Hillary's to Port Stanvac (Adelaide) but is not detectable east of Adelaide at Portland. The Bass Strait sets up its own seiches, which can be clearly seen at Lorne, Stony Point and Burnie. Fig. 7.80 shows an event for Nov '94 that is similar to the event of May '94 shown in Fig. 7.79.

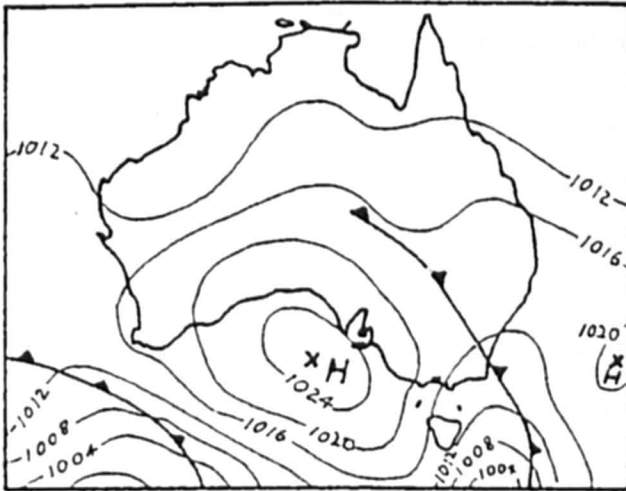
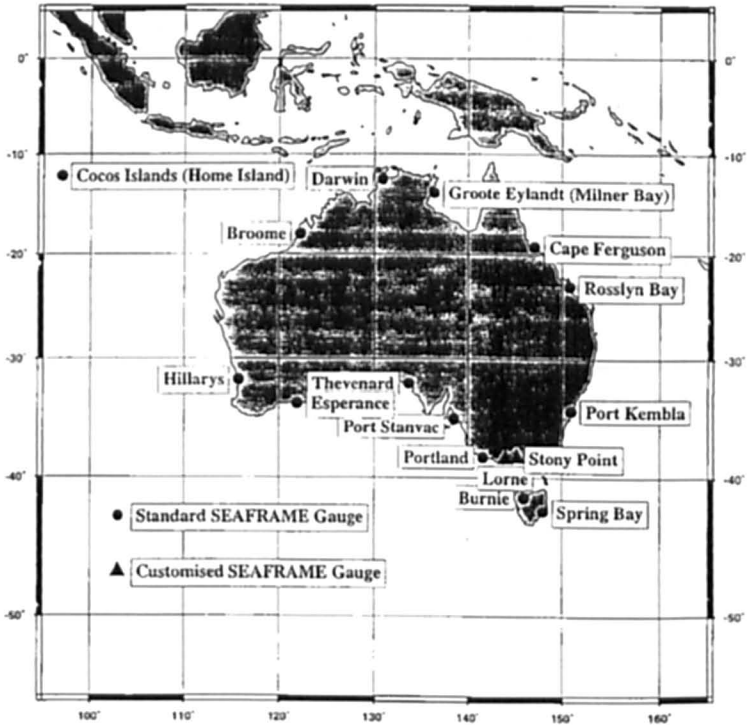


Fig. 7.77: Synoptic chart SE winds at Adelaide (VECCHIO, 1980)

### Australian Baseline Sea Level Monitoring Project - Monitoring Sites



NATIONAL TIDAL FACILITY

Fig. 7.78: Tide gauge positions (MURTY, 1995)

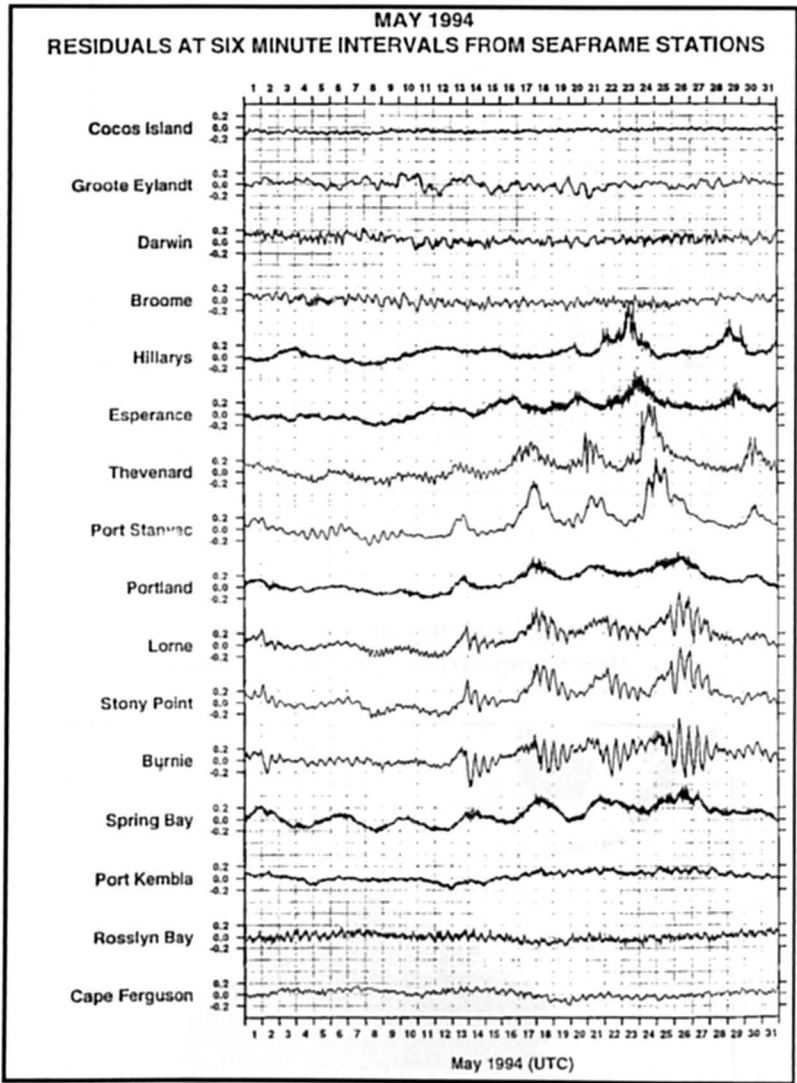


Fig. 7.79: Residuals at six minute intervals from SEAFRAME stations (m) May 1994 (MURTY, 1995)

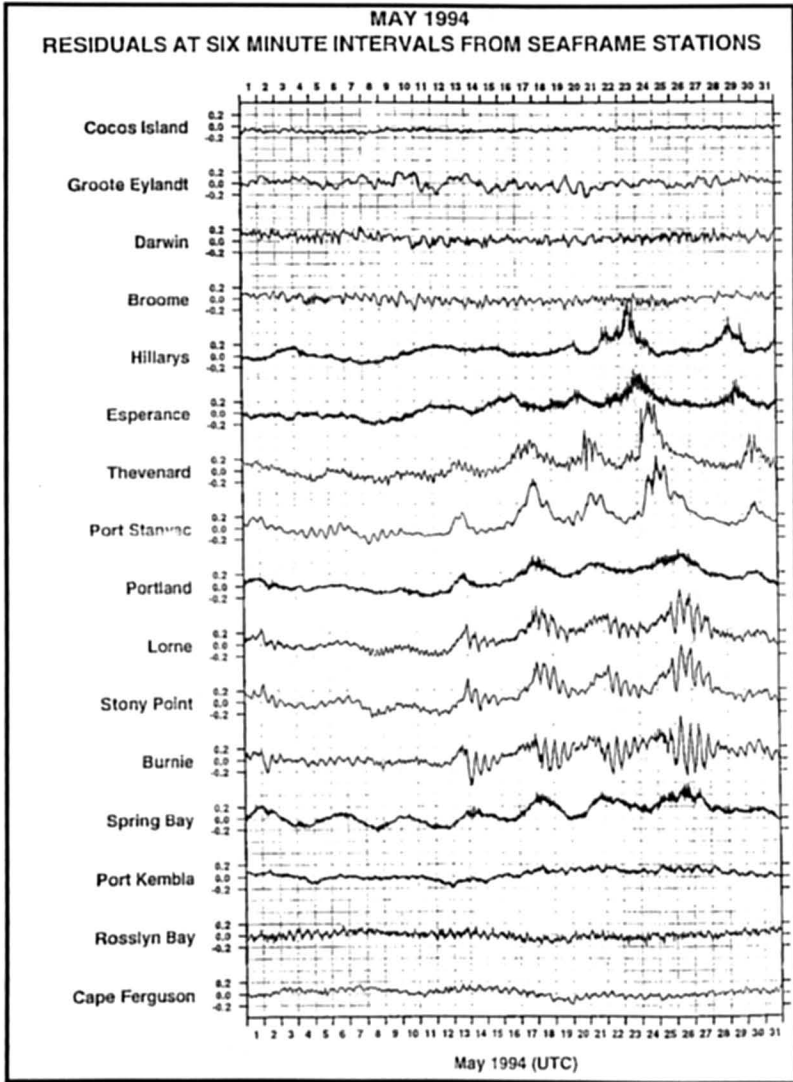


Fig. 7.80: Residuals at six minute intervals from SEAFRAME stations (m) November 1994 (MURTY, 1995)

## 7.6 Oceanic Regions

Some oceanic islands are influenced by a type of weather system known as sub-tropical cyclones, which are similar to tropical cyclones in terms of having a warm core, but otherwise resemble extra-tropical cyclones (HASTENRATH, 1996). SIMPSON (1952) coined the word "sub-tropical cyclone" which was further elaborated by RAMAGE (1971). The subtropical cyclones of the eastern north Pacific during the winter to spring of the Northern Hemisphere are referred to as Kona storms in the Hawaiian Islands. These originate from cut-off lows in the upper level subtropical westerlies.

According to HASTENRATH (1996) the centre of the system is between 400 to 600 hPa (mid-troposphere) and the pressure gradients, winds and convergence increase from the periphery inward. Strong mid-tropospheric convergence is compensated by divergence in the upper troposphere and to a lesser extent in the lower layers. RAMAGE (1971) proposed a conceptual model, which includes an upward and a downward branch within about 500 km from the centre, strong upward motion gives rise to condensation and deep precipitating clouds. Beyond about 500 km from the centre, there is downward motion with dry adiabatic warming extending to the subsidence inversion (HASTENRATH, 1996).

The relatively warm-cored upper branch is energy producing, while kinetic energy dissipation within a weak surface circulation is small, thus favouring the longevity of the system. Development of an eye similar to tropical systems is common. These subtropical cyclones also occur to the southwest of Azores in the Atlantic Ocean.

Over the northern Indian Ocean, a somewhat different type of a subtropical cyclone can occur. These occur during the southwest monsoon (one to two per month) over the northwestern part of the Arabian Sea and occasionally over the northern part of Bay of Bengal and over southern Indochina. According to RAMAGE (1971) the energy exported from the heat low over the South Asian continent is responsible for the origin of these subtropical cyclones. In contrast to the winter subtropical cyclones of the Northern Pacific, those in the monsoon area do dissipate due to the injection of drier air.

It is well known that tropical cyclones get transformed into extratropical cyclones. This extratropical transition (ET) is complex and highly variable process that is currently poorly understood (MALMQUIST, 1999). According to him, the occurrence of ET's also portends the possibility that a single storm system can impact the tropics, midlatitudes and high latitudes. For example, an Atlantic system might track across the Caribbean and the southern part of the U.S.A. as a tropical cyclone and can change to an extratropical cyclone that can strike the New England, States of U.S.A., Canada and Europe. Some new concepts are (1) Maximum Potential Intensity (MPI) of an ET (2) Maximum Potential Extratropical Transition (MPET). These new concepts could be used to produce real time Damage Potential (DP) maps.